INTERNATIONAL FIRE DETECTION
RESEARCH PROJECT

Field Modeling:
Simulating the Effects of HVAC Induced
Air Flow From Various Diffusers and
Returns on Detector Response

TECHNICAL REPORT
Year 4

Prepared by

John H. Klote, P.E., D.Sc.
William D. Davis, Ph.D.
Glenn P. Forney, Ph.D.
Richard W. Bukowski, P.E.
Building & Fire Research Laboratory
National Institute of Standards & Technology

Table of Contents

List of Figures

List of Tables

Simulating the Effects of HVAC Induced Air Flow From Various Diffusers and Returns on Detector Response

John H. Klote
William D. Davis
Glenn P. Forney
Richard W. Bukowski

Abstract

Rapid activation of fire protection systems in response to a growing fire is one of the important factors required to provide for life safety and property protection. Airflow due to the heating, ventilating and air conditioning (HVAC) system can significantly modify the flow of smoke along the ceiling and must be taken into consideration when a particular system is designed. At present, the standards used to guide the design of systems contain very little quantitative information concerning the impact of airflow produced by HVAC systems. This project is part of a multi year, International Fire Detection Research Project sponsored by the National Fire Protection Research Foundation (NFPRF), and it describes the results of the fourth year of the project during which numerical simulations of smoke movement in response to HVAC flows resulting from ceiling mounted slot diffusers, wall mounted slot diffusers, high sidewall diffusers, and ceiling diffusers from which airflow drops to the floor. The design fire used in this study was a medium growth t-squared fire (as defined in the National Fire Alarm Code) with activation to occur prior to the fire reaching a heat release rate of 100 kW (corresponding to 85 seconds of fire growth). The computer model calculated smoke detector activation at 0.021 g/m^3 (0.07 OD/m) using a mass density simulation which was consistent with a 13 °C temperature correlation used during the first two years of the project.

1. Introduction

Rapid activation of fire protection systems in response to a growing fire is one of the important factors required to provide for life safety and property protection. Airflow due to the heating, ventilating and air conditioning (HVAC) system can significantly modify the flow of smoke along the ceiling and must be taken into consideration when a particular system is designed. At present, the standards used to guide the design of systems contain very little quantitative information concerning the impact of airflow produced by HVAC systems.

1

A multi year, International Fire Detection Research Project sponsored by the National Fire Protection Research Foundation (NFPRF) was established to provide quantitative information on the impact of beamed and sloped ceilings, and HVAC flows on the distribution of heat and smoke during a fire. During the first year of the project, validation simulations were made to compare the results of numerical modeling with the experimental data of Heskestad and Delichatsios [1], and additional simulations of smoke movement under level, beamed ceilings were made [2]. In the second year, numerical simulations of smoke movement in response to sloped, beamed ceilings were made [3]. The third year of the project involved numerical simulations of smoke movement in response to HVAC flows resulting from slot diffusers, slot returns and rectangular returns [4].

This report describes the results of the fourth year of the project during which numerical simulations of smoke movement in response to HVAC flows resulting from ceiling mounted slot diffusers, wall mounted slot diffusers, high sidewall diffusers, and ceiling diffusers from which airflow drops to floor. Information about diffuser classification is provided in appendix C. Because of year 3 results unexpectedly showing significant areas of (detector) non-operation in the vicinity of the returns in open plan rooms, modeling of the ceiling returns in year 4 included much more detailed simulation of flows in the plenum space (above the ceiling) to improve confidence in the simulation of flows at these returns. Detector activation was again based on the simulated mass density approach developed in year 3, and additional information about this mass density activation is provided in Appendix B. Simulations of smoke movement including HVAC effects were made for five enclosed rooms and two open plan rooms shown in figure 1 with dimensions listed in table 1.

2. Modeling Approach

The commercially available computational fluid dynamic (CFD) model CFX Flow Solver[1] release 4.1 was used to perform the numerical simulations. This release is an upgrade of release 3.3 which was used for the simulations of the second year of this project. In release 4.1 the only upgraded features relevant to the simulations of this study consist of simplified data input.

A detailed description of computational fluid dynamics modeling is beyond the scope of this report. The non-mathematical descriptions in the following sections are intended to provide an explanation of the assumptions of the simulations and to provide insight for those not familiar with the field. The CFX Flow Solver *User Manual* [5] provides the exact equations and mathematical definitions that apply to these simulations. For more information about CFD modeling, readers are referred to [6][7][8][9][10]. References [11][12][13][14][15] provide general information about fluid dynamics.

2.1 CFD Concept

The CFD modeling consists of dividing the flow field into a collection of small rectangular cells, and determining the flow at each cell by solving numerically the governing conservation equations of fluid dynamics. Boundary conditions are prescribed for walls, floor, ceiling, HVAC supplies, HVAC returns, openings to the outside, and planes of symmetry. For this project, all the CFD simulations were unsteady, using the calculated properties from one time step to calculate those of the next time step. At the start of a simulation, each cell can be set to zero flow conditions or conditions read into the computer from a previous simulation.

---

[*]Previous names for this software are HARWELL FLOW3D and CFDS FLOW3D.

Zero flow conditions consist of zero velocity and ambient pressure and temperature. To generate fire induced flows, heat is released in several control volumes over time.

The governing equations of fluid dynamics describe the motion of fluid throughout the flow field. These equations are: (1) conservation of mass, (2) conservation of momentum and (3) conservation of energy. The mass conservation equation depends on the concept that matter is not created or destroyed for the processes of interest in fluid dynamics. The momentum conservation or the Navier Stokes equations are equivalent to Newton's second law of motion. The energy conservation equation is equivalent to the first law of thermodynamics. In addition to these conservation equations, the ideal gas law relates density, pressure and temperature. The conservation equations are expressed mathematically as a set of simultaneous, non-linear partial differential equations. This set of equations is solved numerically for each cell to simulate the motion of fluid.

2.2 Turbulence

The flow equations alone can be used to simulate the effects of turbulence on a scale larger than that of the cells. However, use of the flow equations alone cannot account for turbulence on a scale smaller than the cells. Turbulence modeling was developed to account for movement and mixing effects inside the cells. In such models a number of empirically developed partial differential equations are added to the flow equations which are solved for each cell and for each time step. Because turbulence models account for turbulent effects inside the cells, the number of cells needed for a particular application can be reduced.

The turbulence model used for this work is the k-ϵ model developed by Launder and Spalding [16]. Information about this model and the specific values of empirical coefficients used for this project are provided in appendix A.

2.3 Heat Transfer to Surfaces

The solid surfaces (walls, floor and ceiling) were considered to be adiabatic. This assumption was evaluated for year 2 of the project, and it was shown that neglecting heat transfer to solid surfaces resulted in negligible variations in activation time (reference 4 figure 11). These calculations were for gypsum wall board. The year 2 report showed that, for wall materials that are nearly insulating, the boundary surface temperatures rose quickly to the gas temperature, reducing heat transfer. The time period over which a parcel of gas was in contact with a solid surface was about two seconds. Thus it was concluded in year 2 that there was no significant difference in activation for detectors located 0.076 m (3 in) below an adiabatic ceiling or one constructed of gypsum wallboard. This approach did not include HVAC jets, but the reasoning can be extended from fire gases to HVAC jets as the jets are of lower temperature.

Radiation effects were not included explicitly in the calculation except that only a fraction of the heat release rate was assumed to contribute to convective heating of smoke and air. The rest of the heat was considered to be radiated away. A radiative fraction of 0.35 was used for all four years of the project.

2.4 Area Modeled and Gridding

A number of grids were needed to represent the seven room sizes and the combinations of HVAC supplies and returns. The total number of grid cells ranged from 11,000 to 37,000. Figure 2 shows typical grids used for a room including a section of plenum. As in the previously reported calculations, the grids have smaller spacing at locations where more flow detail is needed: the fire, the slot diffuser, and the slot returns.

3

The selection of the area modeled for the open plan simulations was influenced by the desire to obtain realistic flow at the edge of the area of interest. In a real open plan room, the ceiling jet of combustion gases and HVAC diffuser jet continue to flow under the ceiling for a considerable distance. The common approach for this type of flow is to have a much larger ceiling area than the area of specific interest, so that the edge effects are away from the area of interest. This same approach was used for the open room simulations as can be observed from figure 1 (c) and (d), and Table 1.

2.5 Initial Conditions

For any time dependent analysis, conditions at the start of the simulation must be defined. The initial velocities need to be established for each cell, and the default condition is zero velocity. This zero velocity condition was used for the mass density calibration simulations of year 3.

For the simulations that included HVAC supplies and returns, the initial conditions describing the flow resulting at every cell are so intricate that the only practical way of determining them is by use of the CFD model itself. Thus, for each room geometry an initial condition simulation was made without a fire but with the same gridding and boundary conditions. The initial condition simulations had zero initial velocity and ran for about 30 seconds, which was sufficient for development of a stable, ambient temperature supply jet up to 3 m (10 ft) from the supply outlet. The velocity and other properties[2] for the computational space were written to a file at the end of the initial condition simulation, and the data in this file was read as the initial conditions for the start of the simulations discussed in this paper.

2.6 Boundary Conditions

In any fluid flow analysis, conditions at the boundaries of the flow field need be defined. For the simulations of this paper, the following boundary conditions were used (1) solid surface, (2) plane of symmetry, (3) velocity at an opening, and (4) pressure at an opening. These conditions remained constant throughout each simulation.

At the solid surfaces (walls, floors and ceilings) the velocity was assumed to be zero. This boundary condition is referred to as the no slip condition. The symmetry boundary can be compared to a mirror in that it is as if the flow in the flow field were reflected by this boundary. As with a solid surface there is no flow through a symmetry boundary, but there can be flow at a symmetry boundary provided that the direction of such flow is in the plane of the boundary.

Both velocity and pressure boundaries can be used where mass is to enter or leave the domain. The domain is the region of space for which the simulation is made. Velocity boundaries are used to define the velocity entering or leaving the domain. For pressure boundaries, the pressure is defined by the user and the CFD model calculates the velocity. Modeling HVAC returns involved both velocity and pressure boundaries as is discussed later.

[**]These other properties consist of temperature, pressure, effective viscosity, kinetic energy of turbulence, and turbulent dissipation rate. For the initial condition simulations of this project, the calculated values of temperature and pressure do not vary much from ambient. The last three properties are particular to the $k\text{-}\epsilon$ model (appendix A).

2.7 Fire

For all of the simulations discussed in this report the fire was the same as the one used for years 2 and 3 of this project. This was a medium growth t-squared fire which was designed to reach 1055 kW (1000 Btu/s) in 275 seconds [17]. A t-squared fire is one that has a heat release rate that increases with the square of time. In year 1, it was shown that the areas in which detectors activate before the fire reaches a specified heat release rate were not sensitive to the specific t-square fire growth rate. Years 1 and 2 examined response to design fires of 100 kW and 1 MW, while in years 3 and 4 design fires were limited to 100 kW which occurs at 84.75 seconds after ignition[3].

The fire was modeled by releasing energy over several grid cells. As in prior years, the number of cells occupied by the fire was varied during the simulation such that the heat release rate per unit volume would not exceed 2.6 kW/m^3 (0.070 Btu/s ft^3). The fire was situated at various locations on the plane of symmetry. To account for radiative losses from the fire to the walls and ceiling, the heat release prescribed for the fire was reduced by 35 % [18].

As with the earlier years, the plume flow includes only the entrained air and does not include the mass released into the flow due to the combustion process. This is consistent with most fire models that assume that such mass release is so small in comparison to the total fire plume flow that this mass release can be neglected.

To study the impact of various fire locations relative to HVAC supplies and returns, this one fire heat release rate was used for all locations. The same fire was used to provide a comparable generation of fire gases for all the simulations. However, this should not be taken to indicate that materials are expected to burn the same way when they are away from walls or near a wall. Because of reradiation from hot walls, it is expected that the same fuel package would burn faster when near a wall than it would away from walls.

2.8 Smoke Generation and Movement

As in year 3, the movement of smoke was simulated by a species mass fraction approach by using the scalar equation feature of the CFD model. This mass concentration calculation can be explained by analogy to water flow visualization by dye injection. To prevent the dye from affecting the water flow, the flow rate of the dye is small in comparison to the water flow. The dye flows downstream and mixes with the water. Downstream of the injection point, the dye can be observed, and dye concentration can be measured. The dye injection rate can be constant or it can vary with time. If the injection rate is multiplied by a constant, the dye concentration at every point in the flow field will by multiplied by that same constant (provided that the injection flow rate is still relatively small).

In the CFD model, the species generation rate corresponds to the dye injection rate, and the mass density of species corresponds to the dye concentration. The species calculation is a perfect idealization of the dye injection experiment in the respect that the species generation rate adds no mass to the flow field. Thus a species calculation has absolutely no impact on the simulated flow field. As with the dye experiment, multiplication of the species generation rate by a constant results in multiplying the mass density at every point

---

[***]For this fire 100 kW is reached at 84.67 seconds. Because the simulation time step was 0.25 seconds, the fire was actually simulated for 84.75 seconds at which the heat release was 100.2 kW.

in the flow field by that same constant. Because this species calculation adds no mass to the flow field, this relationship between species generation and mass density is exact.

The species mass fraction approach is appropriate to simulate the flow of any species provided that the mass generation of the species and the differences in properties (specific heat, thermal conductivity and gas constant) due to the addition of species have an insignificant effect on the fluid flow. Two assumptions that are fundamental to most fire modeling are (1) that the mass released into the flow field due to the combustion process is so small in comparison to the total fire plume flow that this mass release (or mass generation) can be neglected, and (2) that the differences in properties of air and those of the mixture of air and combustion products (mostly CO_2 and water vapor) do not have a significant effect on the flow. By these same assumptions, the species mass fraction approach is appropriate for simulation of the gases and particulates produced by the fire.

It should be noted that the particulate motion simulated does not simulate smoke particle aging (particulate agglomeration and deposition). Appendix B provides further information about smoke generation and mass density.

2.9 HVAC Supplies

The HVAC supplies consisted of slot, troffer diffusers, high sidewall outlets, and group E outlets. The locations of these outlets are shown in figures 3-8. For this project, the slot diffusers are long narrow outlets located on the ceiling or high on the wall from which air blows under the ceiling. The high sidewall outlet of these simulations is a rectangular register from which air blows under the ceiling. A troffer diffuser is a type of slot diffuser located at the side of a ceiling light fixture. Group E outlets are ones located in the ceiling from which air drops toward the floor. The outlets had the following flow rates:

Slot	0.106 m^3/s (225 cfm)
Troffer	0.0236 m^3/s (50 cfm)
High Sidewall	0.318 m^3/s (674 cfm)
Group E Above Computer	0.27 m^3/s (572 cfm)
Group E At Room Edge	0.045 m^3/s (95 cfm)

The open plan room of figure 6 shows 2 slots and 2 troffers in the area of detailed simulation. Because in a building, there would be long rows slots and troffers, the simulation also includes another slot and troffer outside the detailed area of simulation.

As discussed in the year 3 report, HVAC industry design practice assumes diffuser velocities and throw are unaffected by the temperature of the flow for the range of conditions covered by this study. Accordingly, the HVAC flow was selected to be at ambient temperature, and the results are applicable to both heating and cooling. Further information about the supplies is provided in appendix C.

2.10 HVAC Returns

A general HVAC industry design rule is that the location of a return has almost no effect on room air distribution, provided that the supply is not blowing directly into a return. In the beginning of year 3, it was erroneously thought that this rule could be extended to indicate that returns have an insignificant effect on detector activation. Because the industry rule is so strongly and universally held, it was felt that any errors in CFD simulated velocities in the vicinity of the return would not have a significant effect on detector activation. For this reason, in year 3 all returns for enclosed rooms were simulated as pressure boundaries and for open plan rooms as velocity boundaries. However, year 3 results indicated a strong influence of returns on detector activation. Thus more detailed treatment of returns was used in year 4 to evaluate the unexpected results.

As already stated, year 4 returns included simulation of a portion of the plenum space above the ceiling (figure 2). For enclosed rooms the sides of the plenum section (other than the sides that are part of exterior walls or part of the plane of symmetry) are pressure boundaries. For the initial condition simulation, these boundary conditions resulted in the flow out of the return equaling the supply flow. For the fire simulations, the CFD software calculated the return flow accounting for the effects of expansion of gases inside the room due to the fire.

In order to simulate the complicated flows in and out of the large open boundaries of the open plan room [figure 1(c) and (d)], pressure boundaries were needed. However, using pressure boundaries for these large open areas resulted in difficulties concerning use of pressure boundaries for the sides of the plenum section. The pressures assigned to the large open areas and to the plenum sides would need to be such that the desired flows occurred at the HVAC returns. The CFD model could be used to determine such pressures at these boundaries without a fire. However, fire induced pressure changes near the plenum sides could result in significant error in return airflow.

For the open plan simulations, all the sides of the plenum were walls (or part of the plane of symmetry) except for one side which was a velocity boundary. The velocity boundary was chosen as the plenum side farthest from the exterior wall resulting in a plenum flow direction toward the building core. The value assigned to the velocity boundary was such that the average velocity at the return was 2 m/s (400 fpm) for runs 43, 44, 47 and 48. This is the return velocity used for the open plan simulations of year 3. The resulting return flow is approximately equal to the air supplied to the slots and troffers in the total space simulated (including the slot and troffer outside the area of detailed simulation).

To examine the effect of a greater return velocity, runs 45 and 46 increased the return velocities by 50 % to 3 m/s (600 fpm). Such returns with their greater flow can be thought of serving an occupied building space larger than the total space simulated. Since the supplies were not changed the additional net flow into the space came from the open boundaries.

2.11 Uncertainties resulting from sub-model assumptions

In applying the results of these simulations to detection system designs, the impact of assumptions made in the modeling and analysis must be considered. For example, in the first year report, it was shown that the results were relatively insensitive to the assumed growth rate for t-squared fires. The activation times change, but the HRR at activation (the design fire size criterion) is fairly constant. A scaling method to account for different growth rates is provided in Appendix B of this report.

The t-squared fires used were all assumed to involve fuels which burn with a 35 % radiative fraction. Since the production and transport of heat and smoke are highly dependent on the convective heat release rate, different radiative fractions can have a significant effect on activation times. For different radiative fractions, activation times can be scaled in the same manner as for different growth rates, as shown in Appendix B of this report. The scaling will only be valid for activations that depend solely on an interaction with the ceiling jet. If the activation is dependent on the development of a hot layer, scaling will not be applicable.

The mass density activation criteria used for these simulations was developed during year 3. For continuity with years 1 and 2, the criteria were selected to correspond to activation at a 13 °C (23 °F) temperature rise. Because the differential equations for mass concentration are similar to those for heat diffusion with adiabatic walls, it was expected that the activation times calculated by mass density would be the same as those calculated by temperature rise for ambient temperature HVAC flows. The year 3 simulations showed that this expectation was correct (reference 4 figure 40).

The relation between the 13 °C model and the equivalent mass density model depends on the fuel characteristics, the heat of combustion, and the soot yield fraction [19]. Application of these results to fuels with characteristics different than the typical values used in this study can be corrected by scaling. Further, the calculations assumed no significant soot deposition to surfaces or other losses. In other situations, e.g., the smoke passes through grilles or narrow openings, losses of both soot and heat would be higher than assumed here. The model is valid only if it can be shown that the smoke density is diluted primarily by entrained air.

The simulations assumed a smooth ceiling. Years one and two showed that even shallow beams slow the flow and thicken the layer. This effect will also be caused by other obstructions such as decorative moldings or even highly textured ceiling treatments.

Vent flows were modeled with specific flow velocities typical of those encountered in normal installations and systems. Where vent flows are higher due to specific design factors associated with special applications, the areas of non-activation may be larger. Where vent flows are lower than assumed, the areas of non-activation should decrease in size. The term, areas of non-activation, is used to designate regions where smoke detector activation is not expected to occur based on a specific detector sensitivity.

The design fire size selected for smoke detector activation was 100 kW, but the constant response plots were made at 80 s in order to simplify the time scale. This corresponds to a design fire size of 89.3 kW for a medium t-squared fire. If the plots were done at 100 kW (at 84.67 s) the areas of non-activation would be slightly smaller, so the results presented here are conservative.

3. Simulations

Simulations are divided into the following groups: transition study, room with ceiling slot supply, open plan room with ceiling slot supply, room with wall slot supply, room with high sidewall supply, and a computer room. The simulations are summarized in table 2. Figures 3 through 8 show the fire locations and the arrangements of HVAC supplies and returns.

The results of the simulations are shown in figures 9 to 40[4]. Each figure shows activation times at 0.02 m (0.79 in) and 0.05 m (2.0 in) below the ceiling with the intent of providing insight into the activation times of low profile and normal detectors. Differences between simulated results at these positions must be interpreted with caution because the 0.02 m position is calculated in a grid cell adjacent to the ceiling and the 0.05 m position is in the grid cell immediately below that one. The sensitivity of the conclusions to gridding was examined by increasing the number of grid cells at the ceiling for the configuration of run 32 (figure 9) so that there was one empty cell between the 0.02 m position and the ceiling. The spacing of grid cells beneath the ceiling for this calculation was 0.0159 m (0.626 in), 0.0201 m (0.791 in), and 0.0255 m (1.00 in) compared with 0.0373 m (1.47 in) and 0.0466 m (1.83 in) for the earlier calculation. As shown in figure 41, the calculation with the refined grid produced predicted response volumes which agreed to within 0.1 m (0.3 ft) of the position and size of the response volumes of the earlier calculation.

3.1 Transition Simulations

Transition simulations consisted of arrangements of a slot diffuser in open plan rooms and enclosed rooms with open doors shown in figures 3 and 4. These arrangements were selected to allow comparison between the different rooms and were not representative of realistic HVAC conditions.

The transition simulations consisted of runs 32-36 with activation times shown in figures 9-13. The conventions used in these figures are the same as for the other figures of activation time in this report and the report of year 3. For example, figure 9(a) shows the activation time at 0.02 m (0.79 in) below the ceiling. Activation directly above the fire took 35 seconds or less [second darkest area on key in figure 9(c) and 9(d)]. The white space in figure 9(a) is where activation takes 80 seconds or more. The white spaces where activation takes longer than 80 seconds will be referred to as areas of non-activation. The spaces where activation is 80 seconds or less will be referred to as the areas of activation. The range from 20 to 80 seconds was selected to simplify the scales, and these figures show the same trends as ones that go up to the full 84.75 seconds of simulation. At 80 seconds the heat release rate of the fire is 89.3 kW.

The purpose of these simulations was to develop information about the transition between the two very different patterns of non-activation observed in year 3 between enclosed rooms and open plan rooms. In year 3, the non-activation distances in front of the slot supply of the open plan rooms ranged from 1.1 to 3.3 m (3.6 to 10.8 ft), and those in front of the slot supply of the enclosed rooms ranged from 0 to 1 m (0 to 3.3 ft). It was hoped that some intermediate geometry would shed light on the specific conditions under which the non-activation areas increase in size.

3.2 Room With Ceiling Slot Supply

Runs 37-42 (figures 14-19) are in an enclosed room with ceiling slot supply and plenum return. These are reruns of year 3 simulations except that in year 3 the returns were pressure boundaries. The intent of these simulations was to determine the extent to which these different returns influence activation time.

3.3 Open Plan Room With Ceiling Slot Supply

[****]It should be noted that the irregular boundary on figure 9 between the white region (>80 s) and the next region (65 to 80 s) is an artifact of the computational grid. Similar irregular boundaries occur on most of the other activation time plots in this paper.

Six simulations of detector activation were made for an open plan room with ceiling slot supply, troffer supply and plenum return (runs 43-48; figures 20-25). The first two of these were reruns of year 3 simulations except that in year 3 the returns were velocity boundaries. The intent of these simulations was to determine if non-activation areas adjacent to the return in year 3 simulations would occur with better simulations of plenum returns.

3.4 Room With Wall Slot Supply

All the previous simulations have had ceiling mounted slot supplies or ceiling mounted troffer supplies. The effect of flow from a wall mounted slot supply on activation was simulated in an enclosed room with a plenum return (runs 49-52; figures 26-29). The top of these slots were 0.15 m (0.49 ft) below the ceiling on the exterior wall as shown in figure 5 (d). For the first two of these simulations, the discharge velocity from the slot was horizontal. The direction of the discharge velocity of many slot diffusers can be adjusted, so the other two simulations in this group were done with a discharge velocity at a 20° upward angle.

3.5 Room With High Sidewall Supply

Runs 53-56 (figures 30-33) focused on the effect of high sidewall supply diffusers in an enclosed room. This diffuser was 0.600 m (1.97 ft) by 0.259 m (0.850 ft) high with the top located 0.15 m (0.49 ft) below the ceiling on the exterior wall as shown in figure 7. Because the diffuser was located on the plane of symmetry, only half of it was simulated. The first simulation examined the effect of a discharge velocity at an angle of 30° to the side and an angle of 20° upward. The other simulations in this group examined discharge velocities aimed straight across the room with a 20° upward angle. The first three simulations had rectangular ceiling returns that were simulated with plenums.

In addition to being used in commercial buildings, high sidewall supplies are commonly used in hotel and motel rooms. These hotel and motel applications often have the return located low in one of the walls. Run 56 was made to study the effect of locating the return near the floor.

3.6 Computer Room With Downward Airflow

Simulations were conduced for an enclosed computer room with group E supply outlets (runs 57-59; figures 34-36). Some computer manufacturers make equipment intended for installation in rooms where the computer cooling air is supplied to the room through outlets in the ceiling. Figure 8 shows that the room has two computers with two ceiling outlets for computer cooling air and two smaller outlets for space cooling air. However, all simulations assumed ambient temperature air in the HVAC system.

4. Observations Based on the Simulatons

Most of the room simulations resulted in areas of non-activation near the HVAC supplies, and tables 3, 4 and 5 list the distances from the supplies to the area of activation at 0.05 m (2.0 in) below the ceiling[5]. With a few exceptions, the areas of non-activation for a design fire size of 100 kW (89.3 kW actual) at 0.02 and 0.05 m (0.79 and 2.0 in) below the ceiling are the same, and the selection of values 0.05 m (2.0 in) below the ceiling for the tables was to provide information for comparison among simulations.

[*****]Lengths on figures 9-40 can be scaled using the room dimensions listed in table 1.

4.1 Transition Simulations

Observation 1 The enclosed rooms with normal sized doors gave results that were exactly like the fully enclosed rooms. The reason for this is that the door soffit is sufficiently deep to cause a smoke layer to develop. For the unconfined calculations, a smoke layer did not develop. Based on the calculations, it would be expected that rooms with geometries which would cause a smoke layer to develop would produce non-activation regions equivalent to the enclosed room calculations.

4.2 Room With Ceiling Slot Supply

Observation 2 Simulated activation regions for the enclosed rooms with the plenum return are almost identical (varied by at most 0.1 m) to the corresponding year 3 simulations without simulation of plenum space (figures 37-39). This indicates that for these enclosed room simulations, using a pressure boundary to simulate a ceiling return results in the same activation times as simulating a section of plenum above the return.

Observation 3 As observed during year 3 for the enclosed rooms with slot diffusers, the activation times at 0.02 m (0.79 in) below the ceiling are similar to those at 0.05 m (2.0 in) below the ceiling (figures 14-19). The differences in the non-activation distances at these two levels below the ceiling were less than 0.1 m (0.3 ft). Differences in location of the activation regions at these two levels were at most 0.3 m (1.0 ft).

Observation 4 As observed during year 3 for the enclosed rooms with slot diffusers, when a fire is located below or nearly below a return, there is a tendency toward increased non-activation distance in front of the slot diffuser. Examination of runs 40 to 42 illustrates this (table 4; figures 17-19). Run 42 is under the return, and has a greater non-activation distance than similar runs with the fire further from the return (runs 40 and 41). This tendency was observed in other sets of similar simulations in year 3. Hot gases were observed to enter the plenum in run 42 which would reduce the amount of hot gas contributing to the ceiling jet and therefore enhance the effect of the diffuser in producing non-activation areas.

Observation 5 As observed during year 3 for the enclosed rooms with slot diffusers, when a fire is located below or nearly below a return, there is a tendency toward decreased activation layer depth under the ceiling. This is illustrated by run 42, where the return is almost directly over the fire. For this simulation, the depth of activation area under the ceiling is about 0.6 m (2.0 ft) as shown on figure 19(c). Similar simulations (runs 39-40) with fires further from the return had activation depths from 1.0 to 1.7 m (3.3 to 5.6 ft) as shown on figures 16(c), 17(c) and 18(c).

Observation 6 As observed during year 3 for the enclosed rooms with slot diffusers, many of these simulations resulted in areas of non-activation to the side of the diffuser. The largest distance of non-activation on the side was 0.2 m (0.7 ft) for run 37 (table 4; figure 14).

Observation 7 As observed during year 3 for the enclosed rooms with slot diffusers, in many simulations, airflow caused by the HVAC system deflected the plumes during the early stages of development. This effect can be observed in the simulations where the fires that were away from walls [for example run 41; figure 18(d)] where the dark activation region (20 seconds and less) is bent over toward the supply slot.

The air flows calculated as initial conditions consist of the supply jet attached to the ceiling and a low velocity flow towards the supply from the floor and nearly up to the ceiling jet. During the early fire development, the heat generated was carried by the HVAC induced flows and resulted in this pattern of the dark activation region. This pattern also occurred in many year 3 simulations.

4.3 Open Plan Room With Ceiling Slot Supply

Observation 8   As with year 3 simulations of open plan rooms with slot supply, areas of non-activation occurred at some of the returns (runs 43-48; figures 20-25). As previously stated this non-activation was unexpected in year 3. This year's simulations included plenum return, and resulted in similar non-activation adjacent to the return.

Runs 43 and 44 are the same as year 3 runs 26 and 28 respectively, and comparison of figure 40 shows that the simulations are almost the same, except that the non-activation distances around the return are up to 0.2 m (0.7 ft) smaller for the simulations with the plenum return (runs 43 and 44).

Runs 45 and 46 are the same as runs 43 and 44 respectively, except that the average return velocity is 3 m/s (600 fpm) for runs 45 and 46 and 2 m/s (400 fpm) for runs 43 and 44. Comparison of figures 20 with 22 and 21 with 23 shows that this increase in the return velocity resulted in slightly larger non-activation distances of up to 0.2 m (0.7 ft) around the return. Runs 47 and 48 are the same as runs 43 and 44 respectively, except that the slot diffuser is dumping air towards the floor in runs 47 and 48. Non-activation areas occur around the return when air is dumped from the slot supplies (figures 24 and 25).

Observation 9   As observed during year 3 for the open plan rooms with slot diffusers, the activation times in many of the simulations were very similar at 0.05 m (2.0 in) and 0.02 m (0.79 in) below the ceiling. In Runs 43-47 (figures 20-24), activation areas were about the same for both distances below the ceiling [usually within 0.1 m (0.3 ft)]. The exception was run 48 (figure 25) with the fire located away from a supply troffer that was dumping air toward the floor. For this simulation, the non-activation area for the slot closest to the return extended out to 0.5 m (1.6 ft) behind the return at 0.05 m (2.0 in) while at 0.02 m (0.79 in) below the ceiling the non-activation area extended from the return to the supply troffer, a distance of 2.3 m (7.7 ft).

Observation 10   As observed during year 3 with slot diffusers blowing horizontally under the ceiling, the non-activation areas were larger for the open floor plan simulations than they were for the enclosed room simulations. From table 5, the relevant open plan simulations (runs 43-46) have non-activation distances in front of the slots ranging from 1.3 m to 2 m (4.3 ft to 6.6 ft). From table 4, the relevant enclosed plan simulations (runs 37-42 and 49-52) have non-activation distances in front of the slots ranging from 0.0 m to 0.7 m (0.0 ft to 2.3 ft). Thus for the conditions of the simulations of this study, slot diffusers discharging horizontally under the ceiling can be expected to produce larger non-activation areas in open plan rooms than in enclosed rooms.

Observation 11   As observed during year 3 for the open plan rooms with slot diffusers, many of these simulations resulted in areas of non-activation to the side of the diffuser. For most of these simulations, non-activation distance on the side was 0.5 m (1.6 ft) as listed in table 5. These non-activation distances are listed in table 5 to the edge of the area of detailed simulation.

4.4 Room With Wall Slot Supply

Observation 12 For most of the simulations with the wall mounted slot, the non-activation areas near the supply are greater at 0.05 (2.0 in) below the ceiling than at 0.02 m (0.79 in) below the ceiling. This occurs in run 51 (figure 28), but it is most pronounced in runs 49 and 50 (figures 26 and 27) where there is no non-activation area at 0.02 m (0.79 in) below the ceiling while at 0.05 m non-activation regions are located up to 0.4 m (1.3 ft) in front of the supply. For locations away from the supply [0.75 m (2.5 ft) or more], the activation times at these two levels below the ceiling are almost the same.

Observation 13 The effect of having a fire almost below the return was a tendency toward decreased activation layer depth under the ceiling. This can be seen by comparing runs 49 and 50 (figures 26 and 27) and comparing runs 51 and 52 (figures 28 and 29). Enclosed rooms with slot diffusers also had this tendency (observation 5).

Observation 14 A discharge velocity at an upward angle of 20° results in increased non-activation distances in front of the supply. This is most noticeable in run 52 (figure 29) which can be compared to run 50 (figure 27). Run 52 has a much larger non-activation area at 0.05 (2.0 in) below the ceiling than run 50. At 0.02 m (0.79 in) below the ceiling run 52 has a significant non-activation area while run 50 has none. This tendency can also be seen by comparing run 49 with run 51 (with upward discharge angle).

4.5 Room With High Sidewall Supply

Observation 15 The high sidewall diffuser resulted in the largest non-activation distances observed in enclosed rooms in this study. This happened for runs 54, 55 and 56 for which the non-activation distances in front of the diffuser ranged from 1.5 to 4.1 m (4.9 to 13.5 ft).

Observation 16 As with the other enclosed rooms, the effect of having a fire almost below the return was a tendency toward decreased activation layer depth under the ceiling. This can be seen by comparing runs 53 and 54 (figures 30 and 31).

Observation 17 As with the enclosed room with ceiling slots, the effect of having a fire almost below the return was a tendency toward increased non-activation area in front of the supply diffuser. This can be seen by comparing runs 53 and 54 (figures 30 and 31).

Observation 18 As observed for the enclosed rooms with slot diffusers, the activation times at 0.02 m (0.79 in) below the ceiling are very similar to those at 0.05 m (2.0 in) below the ceiling (runs 54-56; figures 31-33). As with the rooms with slot diffuser, the differences in the activation distances at these two levels below the ceiling were generally less than 0.1 m (0.3 ft).

4.6 Computer Room With Downward Airflow

Observation 19 For the computer room with downward airflow, the non-activation areas were located under the supply grills and extended about 0.1 m (0.3 ft) to the sides of the grills (runs 57, 58 and 59; figures 34, 35 and 36; table 4).

Observation 20 As observed for other enclosed rooms in this study, the activation times at 0.02 m (0.79 in) below the ceiling are very similar to those at 0.05 m (2.0 in) below the ceiling (runs 57-59; figures 34-36). As with the rooms with slot diffuser, the differences in the activation distances at these two levels below the ceiling were generally less than 0.1 m (0.3 ft).

5. Summary of Observations

The following observations are applicable to the interaction of detectors with HVAC outlets and returns studied under the conditions of the computer simulations.

Non-activation areas occur at returns of the open plan rooms when the fire is located away from the return. During year 3, non-activation around these returns was unexpected and caused concern about the appropriateness of the simplified return model used for those simulations. Because of this concern, year 4 returns included simulation of a section of plenum above the ceiling. All of the year 3 and 4 simulations of open plan rooms with fires away from the returns had areas of non-activation around the return. Because this important phenomenon has not been studied, appropriate experiments need to be conducted to verify the extent of the non-activation areas predicted by the simulations.

Activation times for the enclosed rooms, including a simulation of the plenum space, are almost identical to the corresponding year 3 simulations which used pressure boundaries.

Non-activation areas exist at the sides of the HVAC supplies for the specific flows studied in this project. All but one of the 28 simulations in year 4 had non-activation areas to the side of the supply, and the non-activation distance from the side of the supply ranged from 0.1 m to 0.5 m (0.3 ft to 1.6 ft). Year 3 simulations resulted in similar side non-activation.

For slot diffusers which discharge under the ceiling, larger non-activation areas can occur in open plan rooms than in the enclosed room of this study. For open plan rooms under these conditions, the non-activation distances in front of the slots ranging from 1.3 m to 2 m (4.3 to 6.6 ft). For enclosed room simulations, the relevant non-activation distances ranged from 0.0 m to 0.7 m ft (0.0 ft to 2.3 ft).

For fires in enclosed rooms under or nearly under the return, the activation depth will be smaller than if the fire had been located away from the return [run pairs: 39, 42; 49, 50; 51, 52; and 53, 54). This was also observed in year 3. This is due to hot gases from the fire plume under the return entering the plenum and not contributing to the smoke in the room.

Non-activation areas in front of the high sidewall diffusers were the largest non-activation distances observed in enclosed rooms in this study. This happened for runs 54, 55 and 56 for which the non-activation distances in front of the diffuser ranged from 1.5 to 4.1 m (4.9 to 13.5 ft). Such large non-activation distances were unexpected, and of particular concern due to the common use of these diffusers in commercial buildings, hotels and motels. Because of the many complex characteristics of such applications, the few simulations of this project that included high sidewall diffusers should only be thought of as an initial look at the effects of these diffusers. Further study of the interaction of detectors and flow from high sidewall diffusers is needed.

Activation times, for most simulations, were very similar at 0.02 m (0.79 in) and 0.05 m (2.0 in) below the ceiling. There were some exceptions, where activation was faster at 0.02 m (0.79 in) than at 0.05 m (2.0 in). As already stated, differences between simulated results at these levels must be interpreted with caution, because the simulated detector locations are in adjacent grid cells. Based on the calculated trends, it is possible that low profile detectors may activate slightly faster than normal detectors for some flow patterns. Additional simulations coupled with experimental verification is required to establish the differences in detector activation with ceiling depth suggested by the present set of simulations.

The HVAC system may not be operating at design conditions when a fire starts. In the last two decades, the vast majority of new commercial buildings have had variable air volume (VAV) systems. A VAV system is an HVAC system that controls temperature in a space by varying the quantity of supply air. When a space is

not occupied, the interior loads are low, and a VAV system will supply less air than the design value. Detection locations should be based on the maximum air flow as the non-activation regions around the supplies will shrink as the rate of air flow is decreased.

6. Discussion

The current edition of the National Fire Alarm Code (NFPA 72) contains limited guidance on the installation of detectors relative to the components of HVAC systems. Section 5-3.6 cautions against the installation of detectors,

"… where air from supply diffusers could dilute smoke before it reaches the detectors. Detectors shall be located to intercept the air flow toward the return air opening(s). This may require additional detectors, since placing detectors only near return air openings may leave the balance of the area with inadequate protection when the air handling system is shut down."

This guidance has led to a "rule of thumb" that detectors should be located no closer than 0.9 meter (3 ft) from a supply register. With the exception of high sidewall diffusers that need more study, this work indicates that this "3 foot rule" is appropriate for the enclosed rooms of this study. It needs to be clear that this three foot exclusion zone should include the ends of slot diffusers as this fact would not be intuitive. For the open plan room, this 3 foot rule seems to break down as the area of non-activation reached 2.0 m (6.6 ft) in front of the diffuser.

In nearly all cases, the activation areas at 0.02 m (0.79 in) and 0.05 m (2.0 in) were very similar, indicating that both standard and the newer low profile sensors may provide similar activation performance. Even under the worst case conditions in the enclosed rooms of this study, sensors of up to 0.3 m (1 ft) in depth should activate.

With the exception of the high sidewall diffusers which need further study, the activation depths for all the simulations in enclosed rooms (table 6) was equal to or greater than 0.3 m (1 ft) indicating that the current rule of locating sensors up to 0.3 m (1 ft) in depth is sufficient for the enclosed rooms of these simulations.

The concept of locating the detectors "near the return air opening" mentioned in the current code does not appear to be supported by this research. In fact the conformation of year 3 observations by the present work indicates that the return type and location is every bit as important to detection system performance as is the supply. Non-activation "near the return air opening" is of particular concern for open plan spaces, but the simulations do not indicate that there is any activation advantage near the return in enclosed rooms.

7. Conclusion

The following conclusions are based on the results of the computer simulations presented in the year 3 report and in this report.

1. **Low Profile and Normal Detectors**: In most of the simulations with forced ventilation, the activation areas at 0.05 (2.0 in) below the ceiling are similar to those at 0.02 m (0.79 in) below the ceiling. However, in some simulations the non-activation areas were somewhat larger at 0.05 (2.0 in) below the ceiling than they were at 0.02 m (0.79 in) below the ceiling. This trend toward similar activation areas at these elevations was observed for simulations with ceiling mounted slots, light troffers, wall slots, high sidewalls and group E outlets. This indicates that for the simulations with forced ventilation

of this project, the activation time of low profile detectors can be the same or slightly faster than that of normal detectors.

2. **Fire Below Return in Enclosed Room**: When a fire is located below or nearly below a return in an enclosed room simulation, there is a tendency toward:

   a.   hot plume gases entering the return,

   b.   decreased depth of activation in the room, and

   c.   increased non-activation distance in front of the slot diffuser.

3. **Non-Activation on Diffuser Side**: Many of the enclosed room and open simulations resulted in areas of non-activation to the side of the diffuser. For the enclosed room simulations, many of these areas of non-activation reached the wall of the room about 0.2 m (0.7 ft) from the diffuser. For open plan simulations, many of these areas of non-activation extended beyond the area of detailed simulation.

4. **Large Non-Activation Areas in Open Plan Rooms**: The non-activation areas were much larger for the open floor plan simulations than they were for the enclosed room simulations (table 7).

5. **Activation Depth Small in Open Plan Rooms**: The activation depths were much smaller for the open floor plan simulations than they were for the enclosed room simulations (table 6).

6. **Non-Activation Areas at Returns in Open Plan Rooms**: Areas of non-activation occurred at the returns in some of the open plan room simulations. This non-activation was unexpected in year 3, but year 4 analysis with detailed plenum return simulations resulted in similar non-activation adjacent to the return.

7. **Non-Activation Dependent on Discharge Angle**: For the wall slot simulations, the non-activation distances in front of the supply was dependent on the upward discharge angle of the air at the diffuser. It is expected that the discharge angle would have a similar impact for high sidewall diffusers. Because the discharge angle can be field adjusted, the diffuser adjustment that can be made by the building operating personnel can have an impact on non-activation near diffusers.

8. **High Sidewall Non-Activation**: The high sidewall diffuser simulations resulted in the largest non-activation distances observed in enclosed rooms in this study. However, considering the small number of these simulations, further study is needed before conclusions can be reached concerning non-activation and sidewall diffusers.

9. **Group E Non-Activation**: For the computer room with downward airflow (group E outlet), the non-activation areas were located under the supply grills and extended about 0.1 m (0.3 ft) to the sides of the grills. The non-activation distances were also about this small for the open plan room simulation with the slot diffuser dumping air downward.

References

[1]   Heskestad, G. and Delichatsios, M.A. Environments of Fire Detectors - Phase I: Effect of Fire Size, Ceiling Height and Materials. Volume I - Measurements (NBS-GCR-77-86), Gaithersburg, MD,

National Bureau of Standards, 1977.

[2]   Forney, G.P., Bukowski, R.W., Davis, W.D. Simulating the effect of flat beamed ceilings on detector and sprinkler response, 1993. Available from the National Fire Protection Association, Batterymarch Park, Quincy, MA.

[3]   Davis, W.D., Forney, G.P., Bukowski, R.W. Simulating the effect of sloped beamed ceilings on detector and sprinkler response, 1994. Available from the National Fire Protection Association, Batterymarch Park, Quincy, MA.

[4]   Klote, J.H., Forney, G.P., Davis, W.D., Bukowski, R.W. Simulating the effect of HVAC induced air flow from slot diffusers on detector response, 1996. Available from the National Fire Protection Association, Batterymarch Park, Quincy, MA.

[5]   CFC Department, AEA Industrial Technology, Harwell Laboratory, Oxfordshire, United Kingdom, CFX Flow Solver: User Manual, October 1995.

[6]   Abbott, M.B. and Basco, D.R. Computational Fluid Dynamics: An Introduction for Engineers, Wiley, New York, NY, 1989.

[7]   Anderson, D.A., Tannehill J.C. and Pletcher, R.H. Computational Fluid Mechanics and Heat Transfer, Hemisphere, New York, NY, 1984.

[8]   Hirsch, C. Numerical Computation of Internal and External Flows, Vol 2: Computational Methods for Inviscid and Viscous Flows, Wiley, New York, NY, 1990.

[9]   Hoffmann, K.A. Computational Fluid Dynamics for Engineers, Engineering Education System, Austin, TX, 1989.

[10]   Kumar, S. Mathematical Modelling of Natural Convection in Fire - A State of the Art Review of the Field Modelling of Variable Density Turbulent Flow, *Fire and Materials*, Vol 7, No 1, pp 1-24, 1983.

[11]   Schetz, J.A. Boundary Layer Analysis, Prentice Hall, Englewood Cliffs, NJ, 1993.

[12]   Schlichting, H. Boundary Layer Theory, 4th ed., Kestin, J. Translator, McGraw, New York, NY, 1960.

[13]   Sherman, F.S. Viscous Flow, McGraw, New York, NY, 1990.

[14]   White, F.M. Viscous Fluid Flow, McGraw, New York, NY, 1974.

[15]   Yuan, S.W. Foundations of Fluid Dynamics, Prentice Hall, Englewood Cliffs, NJ, 1967.

[16]   Launder, B.E. and Spalding, D.B. The numerical computation of turbulent flows, Computer Methods in Applied Mechanics and Engineering, 3: pp. 269-289, 1974.

[17]   NFPA 72, National Fire Alarm Code, National Fire Protection Association, 1993.

[18]   Drysdale, D. *An Introduction to Fire Dynamics*, Wiley, New York, 1985, p 281.

[19]   Mulholland, G. W., Henzel, V., and Babrauskas, V., The effect of scale on smoke emission, Fire
Safety Science - Proceedings of the Second International Symposium, pp. 347-357, 1989.

Table 1.   Room dimensions in meters (feet) for CFD simulations

Plane of Symmetry

Area of Detailed Simulation

B

Wall (See note 3)

Open Boundary

D

A

Open Boundary

C

Open plan room (O)

Plane of Symmetry

Wall (See note 3)

Interior Partition

B

Interior Partition

A

Enclosed room (E)

Notes: 1. *H* is floor to ceiling height.
2. NA is not applicable.
3. Wall is an exterior wall for rooms O2, E3, and E4; it is interior partition for rooms O1, E1, E2 and E5.

Room Type	*A*	*B*	*C*	*D*	*H*
O1	4.6 (15)	4.6 (15)	9.2 (30)	9.2 (30)	2.74 (9.0)
O2	5.5 (18)	3.91 (13)	10.5 (34)	9.09 (30)	2.74 (9.0)
E1	4.6 (15)	4.6 (15)	NA	NA	2.74 (9.0)
E2	4.6 (15)	3.0 (9.8)	NA	NA	2.74 (9.0)
E3	4.6 (15)	1.71 (5.6)	NA	NA	2.74 (9.0)
E4	4.6 (15)	2.56 (8.7)	NA	NA	2.74 (9.0)
E5	6.0 (20)	2.3 (7.5)	NA	NA	2.44 (8.0)

Table 2.   Summary of smoke movement simulations

Run	ID Number	Room[1]	Fire[2]	HVAC[2]	Comments
Transition Study					
32	m19.5196	O1	2	1	Open plan room
33	m23.1028	E1	2	1	Enclosed room with open door
34	m25.13988	E2	2	1	Enclosed room with open door
35	m20.26725	O1	1	2	Open plan room
36	m27.21477	E2	1	2	Enclosed room with open door
Enclosed Room With Ceiling Slot Supply and Plenum[3] Return					
37	m33.7450	E3	1	1	Similar to run 3
38	m35.9175	E3	4	2	Similar to run 10
39	m37.21853	E3	1	3	Similar to run 11
40	m04a.22733	E3	2	3	Similar to run 12
41	m39.25121	E3	3	3	Similar to run 13
42	m06.12496	E3	4	3	Similar to run 11
Open Plan Room With Ceiling Slot Supply, Troffer Supply and Plenum[3] Return					
43	m11.13354	O2	1	2	Similar to run 26
44	m12.26160	O2	3	2	Similar to run 28
45	m14.4275	O2	1	2	Similar to run 43 but return at 3 m/s (600 fpm)
46	m15.10073	O2	3	2	Similar to run 44 but return at 3 m/s (600 fpm)
47	m41.3667	O2	1	2	Similar to run 43 but slot dumps air
48	m42.15672	O2	3	2	Similar to run 44 but slot dumps air
Enclosed Room With Wall Slot Supply and Plenum[3] Return					
49	m08.3767	E3	1	4	Supply discharge horizontal
50	m09.22437	E3	4	4	Supply discharge horizontal
51	m08a.27793	E3	1	4	Supply discharge 20° upward
52	m09a.16316	E3	4	4	Supply discharge 20° upward
Enclosed Room With High Sidewall Supply					
53	m29.16914	E4	1	1	Supply discharge diagonally & 20° upward; plenum[3] return
54	m30.18824	E4	2	1	Supply discharge diagonally & 20° upward; plenum[3] return
55	m44.11711	E4	2	2	Supply discharge across room & 20° upward; plenum[3] return
56	m46.6981	E4	2	3	Supply discharge across room & 20° upward; return at floor
Enclosed Computer Room With Group E[4] Supply					
57	m48.11682	E5	1	1	Supply outlets dump air toward floor
58	m49.25577	E5	2	1	Supply outlets dump air toward floor
59	m50.5402	E5	3	1	Supply outlets dump air toward floor

[1]See table 1 for room dimensions.
[2]See figures 3 through 8 for fire locations and HVAC arrangements.
[3]Simulation of ceiling returns includes a section of plenum 0.75 m (2.46 ft) in depth and extending 2 m (6.56 ft) in all horizontal directions from the return except that extensions do not go beyond the plane of symmetry or the exterior wall.
[4]Group E supply outlets are mounted in the ceiling, and air flows vertically from them toward the floor.

Table 3.   Non-activation distances at 0.05 m (0.20 in) under the ceiling and horizontal
separation between fire and return for transition study simulations

| Run | Fire to Return Separation | | Distances of Non-Activation | | | |
| | m | ft | Slot Front[*] | | Slot Side[‡] | |
			m	ft	m	ft
32	2.4	7.9	0.9	3.0	0.1	0.3
33	2.4	7.9	0.9	3.0	0.1	0.3
34	2.4	7.9	0.9	3.0	0.1	0.3
35	1.1	3.6	0.6	2.0	0.1	0.3
36	1.1	3.6	0.5	1.6	0.1	0.3

[*]Values listed are the greatest distance of non-activation in front of the diffuser and perpendicular to the diffuser length. The front of the slot is taken to be the direction of flow.
[‡]Values listed are largest distance of non-activation on either side of the slot diffuser (or troffer).

Table 4. Non-activation distances at 0.05 m (0.20 in) under the ceiling and horizontal separation between fire and return for enclosed room simulations

Run	Fire to Return Separation		Distances of Non-Activation			
			Diffuser Front[*]		Diffuser Side[‡]	
	m	ft	m	ft	m	ft
37	0.3	1.0	0.6	2.0	0.2	0.7
38	0.3	1.0	0.5	1.6	0.1	0.3
39	4.2	13.8	0.0	0.0	0.0	0.0
40	4.0	13.1	0.2	0.7	0.1	0.3
41	2.0	6.6	0.4	1.3	0.1	0.3
42	0.0	0.0	0.7	2.3	0.1	0.3
49	4.2	13.8	0.4	1.3	0.0	0.0
50	0.0	0.0	0.3	1.0	0.1	0.3
51	4.2	13.8	0.5	1.6	0.1	0.3
52	0.0	0.0	0.5	1.6	0.1	0.3
53	4.2	13.8	0.0	0.0	0.0	0.0
54	0.0	0.0	3.0	9.8	0.3	1.0
55	0.0	0.0	4.1	13.5	0.1	0.3
56	0.0	0.0	1.5	4.9	0.0	0.0
57	NA[§]	NA[§]	NA[§]	NA[§]	0.1	0.3
58	NA[§]	NA[§]	NA[§]	NA[§]	0.1	0.3
59	NA[§]	NA[§]	NA[§]	NA[§]	0.1	0.3

[*]Values listed are the greatest distance of non-activation in front of the diffuser and perpendicular to the diffuser length. The front of the slot is taken to be the direction of flow.
[‡]Values listed are largest distance of non-activation on either side of the slot diffuser.
[§]Not applicable because these diffusers dump air toward the floor.

Table 5.   Non-activation distances at 0.05 m (2.0 in) under the ceiling and horizontal separation between fire and return for open plan room simulations

Run	Fire to Return Separation		Distances of Non-Activation					
			Slot Front*		Slot Side‡		Return§	
	m	ft	m	ft	m	ft	m	ft
43	2.5	8.2	1.3	4.3	0.5	1.6	0.2	0.7
44	2.2	7.2	2.[†]	6.6[†]	0.5	1.6	2.[†]	6.6[†]
45	2.5	8.2	1.3	4.3	0.5	1.6	0.2	0.7
46	2.2	7.2	2.[†]	6.6[†]	0.5	1.5	2.[†]	6.6[†]
47	2.5	8.2	0.1	0.3	0.2	0.7	0.2	0.7
48	2.2	7.2	2.[†]	6.6[†]	0.5	1.6	0.3	1.0

*Values listed are the greatest distance of non-activation in front of the diffuser and perpendicular to the diffuser length. The front of the slot is taken to be the direction of flow except for runs 47 and 48. The slot diffusers dump air toward the floor in runs 47 and 48, and the front direction is taken as the same direction as in the other runs listed above.

‡Values listed are largest distance of non-activation on either side of the slot diffuser.

†The areas of non-activation in front of the slot supply joins another around the return.

§Values listed are the greatest distance of non-activation on any side of the return.

Table 6.   Activation depths[1] from simulations involving HVAC supplies and returns

Run	Room Type[2]	Minimum[3] m	ft	Maximum m	ft	Run	Room Type[2]	Minimum[3] m	ft	Maximum m	ft
3	E3	1.1	3.6	1.1	3.6	32	O1	0.2	0.7	0.3	1.0
4	E3	1.5	4.9	1.7	5.6	33	E1	0.8	2.6	0.9	3.0
5	E3	1.5	4.9	1.5	4.9	34	E2	1.1	3.6	1.3	4.3
6	E3	0.9	3.0	1.5	4.9	35	O1	0.1	0.3	0.3	1.0
7	E3	1.5	4.9	2.0	6.6	36	E2	0.7	2.3	0.9	3.0
8	E3	1.5	4.9	1.7	5.6	37	E3	1.1	3.6	1.1	3.6
9	E3	1.4	4.6	1.5	4.9	38	E3	0.9	3.0	1.1	3.6
10	E3	0.9	3.0	1.1	3.6	39	E3	1.1	3.6	1.3	4.3
11	E3	1.1	3.6	1.3	4.3	40	E3	1.5	4.9	1.7	5.6
12	E3	1.5	4.9	1.7	5.6	41	E3	1.3	4.3	1.7	5.6
13	E3	1.4	4.6	1.7	5.6	42	E3	0.4	1.3	0.9	3.0
14	E3	0.4	1.3	0.5	1.6	43	O2	0.0	0.0	0.2	0.7
15	E4	0.0	0.0	0.7	2.3	44	O2	0.0	0.0	0.2	0.7
16	E4	0.7	2.3	1.1	3.6	45	O2	0.0	0.0	0.2	0.7
17	E4	0.7	2.3	1.3	4.3	46	O2	0.0	0.0	0.2	0.7
18	E4	0.5	1.6	0.9	3.0	47	O2	0.0	0.0	0.3	1.0
19	E4	0.7	2.3	0.9	3.0	48	O2	0.0	0.0	0.2	0.7
20	E4	0.6	2.0	1.3	4.3	49	E3	1.1	3.6	1.3	4.3
21	E4	0.7	2.3	1.1	3.6	50	E3	0.0	0.0	0.7	2.3
22	E4	0.2	0.7	0.7	2.3	51	E3	1.2	3.9	1.3	4.3
23	O2	0.0	0.0	0.2	0.7	52	E3	0.0	0.0	0.7	2.3
24	O2	0.0	0.0	0.2	0.7	53	E4	1.2	3.9	1.2	3.9
25	O2	0.0	0.0	0.1	0.3	54	E4	0.0	0.0	0.2	0.7
26	O2	0.0	0.0	0.2	0.7	55	E4	0.1	0.3	0.6	2.0
27	O2	0.0	0.0	0.4	1.3	56	E4	1.1	3.6	1.5	4.9
28	O2	0.0	0.0	0.2	0.7	57	E5	0.7	2.3	1.3	4.3
29	O2	0.0	0.0	0.2	0.7	58	E5	0.8	2.6	1.5	4.9
30	O2	0.0	0.0	0.2	0.7	59	E5	0.8	2.6	1.5	4.9
31	O2	0.0	0.0	0.0	0.0						

[1]Location of activation depths from the CD plane on figures 3 - 7.
[2]Room types beginning with O are open plan, and those beginning with E are enclosed. Dimensions of the rooms are listed in table 1.
[3]Actvation depths of 0.0 were in front of supply diffuser, except for run 31 were the fire was at the edge of the area of detailed simulation.

Table 7.   Non-activation distances at 0.05 m (0.20 in) under the ceiling and horizontal separation between fire and return for enclosed room simulations

| Diffuser Type | Room Type | Number[†] of Simulations | Maximum Distance of Non-Activation | | | |
| | | | Diffuser Front[*] | | Diffuser Side[‡] | |
			m	ft	m	ft
Ceiling Slot	Open	17	2.0[††]	6.6[††]	0.5	1.6
Light Troffer	Open	15	1.0	3.3	0.6	2.0
Ceiling Slot	Enclosed	29	1.0	3.3	0.2	0.7
Wall Slot	Enclosed	4	0.5	1.6	0.1	0.3
High Sidewall	Enclosed	4	4.1	13.5	0.3	1.0
Group E (Downward Discharge)	Enclosed	3	NA[§]	NA[§]	0.1	0.3

[†]A total of 57 simulations were made that studied HVAC effects on smoke detector activation, and some of the simulations above are included twice because they include more than one type of diffuser.
[*]Values listed are the greatest distance of non-activation in front of the diffuser and perpendicular to the diffuser length. The front of the diffuser is taken to be the direction of flow.
[‡]Values listed are largest distance of non-activation on either side of the diffuser.
[††]The areas of non-activation in front of the slot supply joins another such area around the return.
[§]Not applicable because these diffusers dump air toward the floor.

IP

IP

- - - CP - - -

EW

B

IP

A

(a) Enclosed room

Ceiling

EW

IP

H

Floor

A
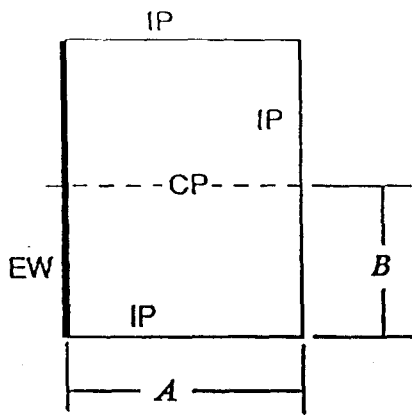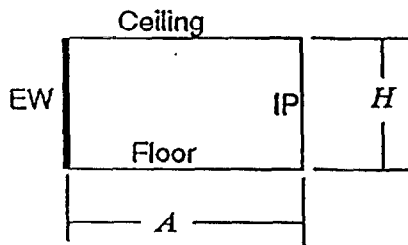
(b) Elevation of Enclosed room

OB

EW

OB

- - - CP - -

Area of
Detailed
Simulation

B

EW

D

A

OB

C
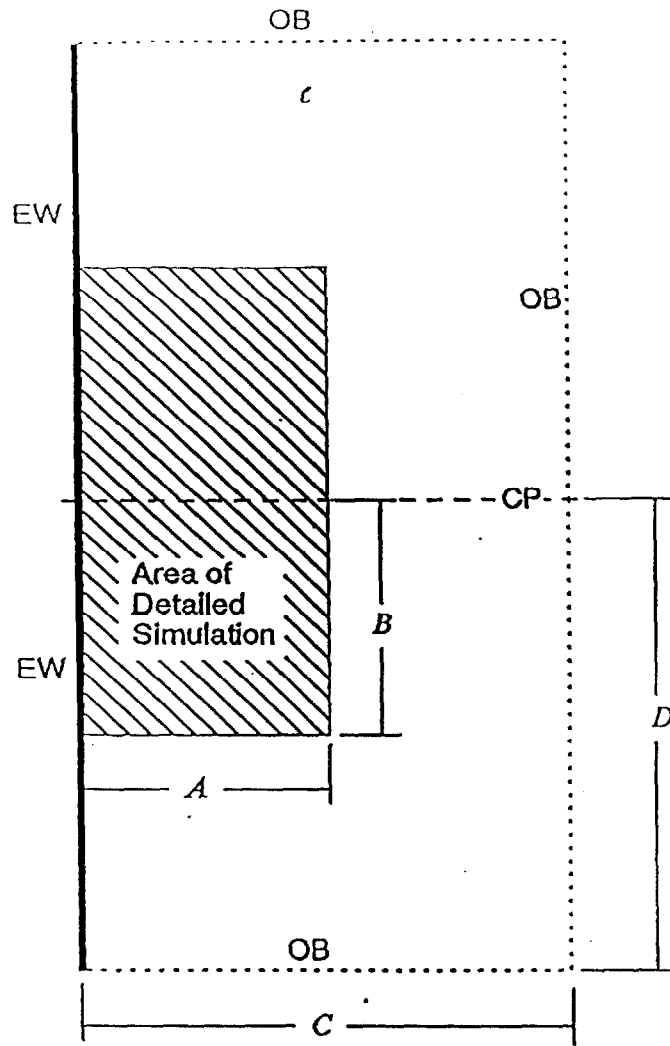
(c) Open plan room

Symboles:
CP   Plane of Symmetry
EW   Exterior Wall (or Interior Partition)
IP   Interior Partition
OB.   Open Boundary

Ceiling

Area of
Detailed
Simulation

OB

EW

H

Floor

A

C

(d) Elevation of open plan room

Note: Values of A, B, C, D and H
       are listed in talbe 1.

Figure 1: Layouts of enclosed rooms and open plan rooms

26

Plenum

Return

Room

x = 1.71   m0612496
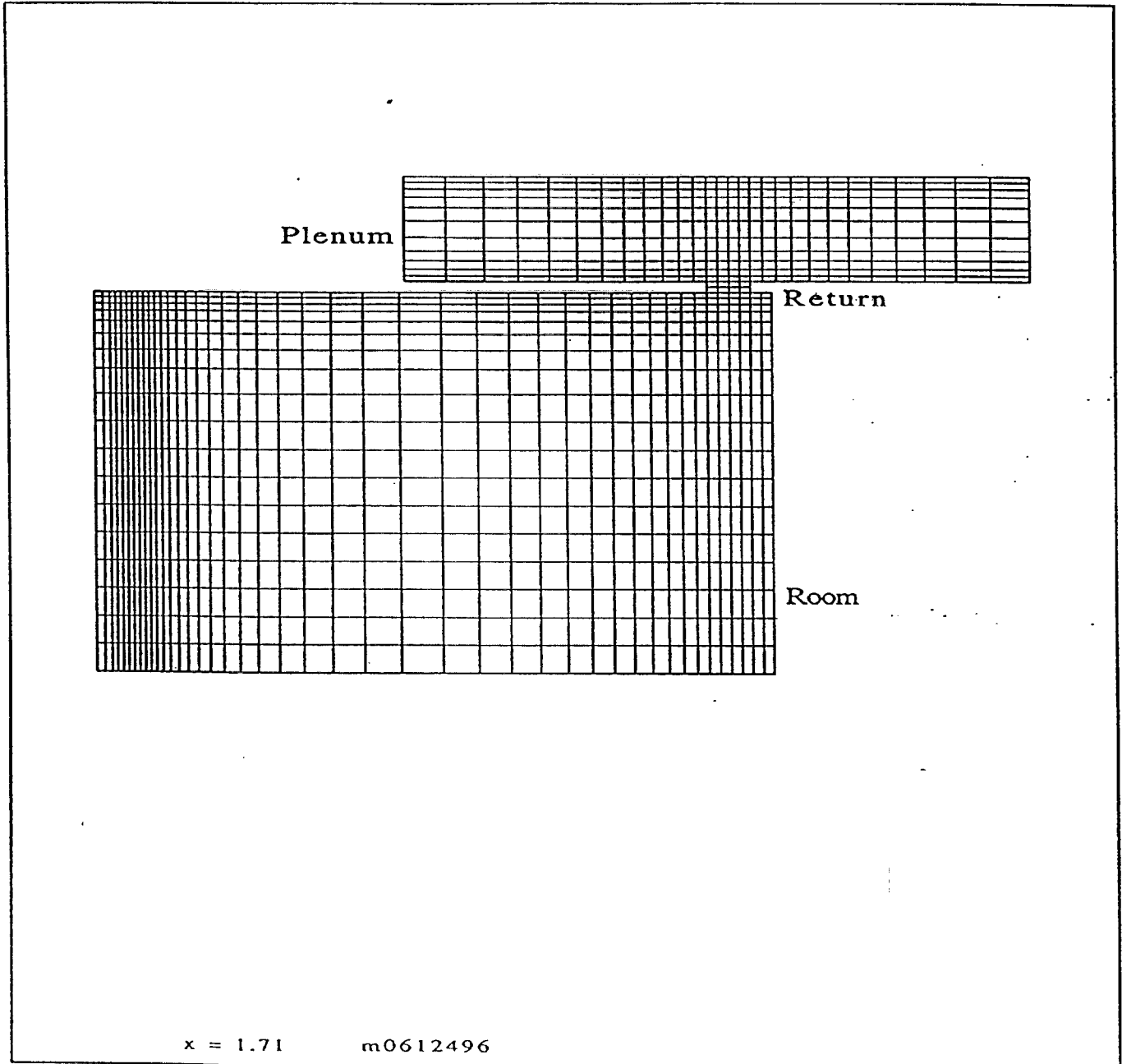
Figure 2: Grid typical of those used for simulations

27

Symbols:
CD   Centerline of Diffuser [or 1 m (3.3 ft) from CP]
CP   Plane of Symmetry
IP   Interior Partition (or Open Boundary)
S   Ceiling Slot Supply

Fire
Locations: 1   — CP —   2

S

- - - -CD- - - - - - - -

IP

IP   IP

IP

(a) HVAC arrangement 1

Fire
Locations: 1   — CP· —   2

- - - -CD· - - - - - -

IP   S

IP

IP

(b) HVAC arrangement 2
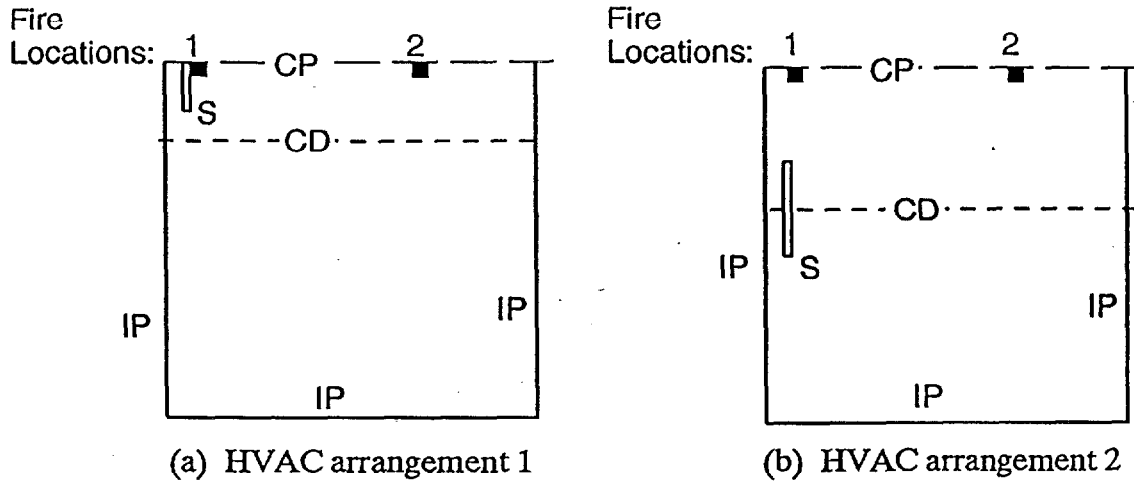
Figure 3: Fire locations and HVAC arrangements for room types O1 and E1

Symbols:
CD   Centerline of Diffuser [or 1 m (3.3 ft) from CP]
CP·   Plane of Symmetry
EW   Exterior Wall
IP   Interior Partition
S   Ceiling Slot Supply

Fire
Locations: 1   — CP —   2

S   IP

- - -CD· - - - - - -

EW

IP

(a) HVAC arrangement 1

Fire
Locations: 1   — CP· —   2

EW   IP

- - - ·CD· - - - - - -

S   IP

(b) HVAC arrangement 2
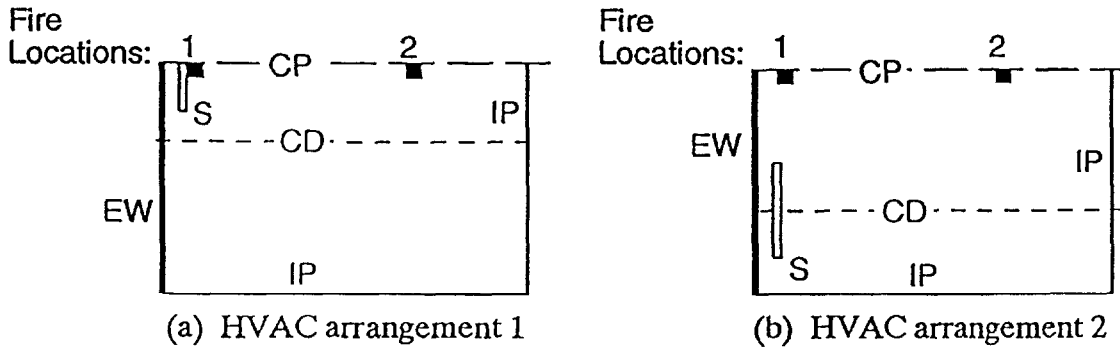
Figure 4: Fire locations and HVAC arrangements for room type E2

28

ℓ

Symbols:
CD   Centerline of Diffuser   IP   Interior Partition
CP   Plane of Symmetry   R   Heating & Cooling Return
EW   Exterior Wall   S   Ceiling Slot Supply
IP   Interior Partition   WS   Wall Slot Supply

Fire
Locations: 1   2   3 — CP — — —   4

EW   CD
R S   IP

(a) HVAC arrangement 1

Fire
Locations: 1   2   3 — CP — — —   4

EW   CD   IP
S   IP   R

(b) HVAC arrangement 2

Fire
Locations: 1   2   3 — CP — —   4

EW   CD   R
S   IP   IP

(c) HVAC arrangement 3

Fire
Locations: 1   2   3 — CP — —   4
EW   R
WS   CD   IP
                           IP

(d) HVAC arrangement 4

Figure 5: Fire locations and HVAC arrangements for room type E3

Fire
Locations: 1 2 — — CP — — ⊓ — — — — —   3
                           R

              S   T
EW   OB

              S   T
              CD
              S   OB

HVAC arrangement 2

Symbols:
CD   Centerline of Diffuser
CP   Plane of Symmetry   •
EW   Exterior Wall
IP   Interior Partition
OB   Open Boundary
R   Heating & Cooling Return
S   Ceiling Slot Supply
T   Ceiling Troffer Supply

Note: HVAC arrangement number
chosen for consistency with
arrangements of year 3.
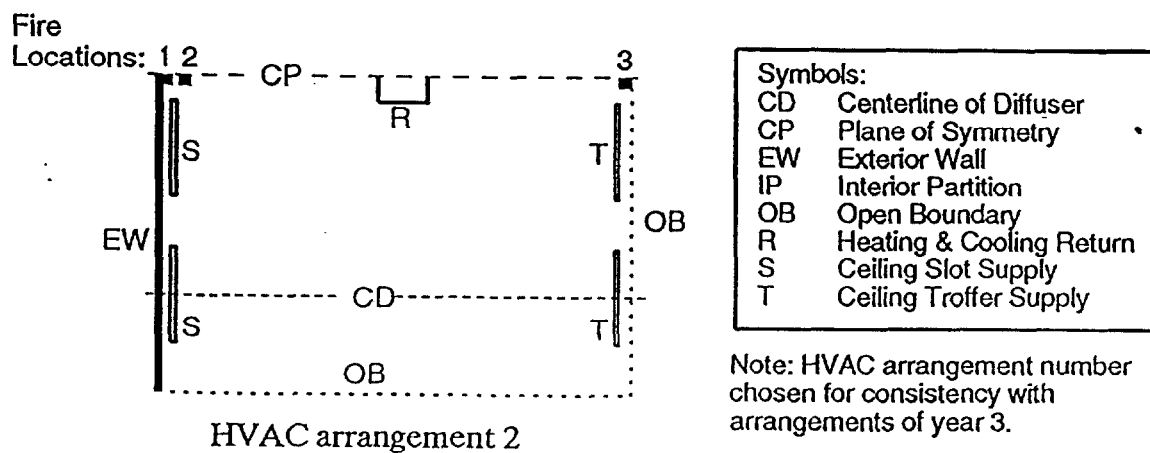
Figure 6: Fire locations and HVAC arrangements for room type O2

29

Fire
Locations: 1   2
    HSW ┌─────────── CP ─ ─ ┐
        │╲   R
        │ ╲
        │ ╲ ─ ─ ─ ─ CD ─ ─
        │   ╲
        │   ↘
    EW │   IP
        │
        └────── IP ───────┘

(a) HVAC arrangement 1

Fire   ε
Locations: 1   2
    HSW ┌──────────→── CP ─ ─ ┐
        ■   R
        │
        │ ─ ─ ─ ─ ─ ─ ─ CD · ─ ─
        │
    EW │   IP
        │
        └────── IP ───────┘

(b) HVAC arrangement 2

Fire
Locations: 1   2
    HSW ┌── ─ ─ ─── CP ─ ─ ─┐
        ■─────────→   ■
        │
        │─ ─ ─ ─ ─ ─ ─ CD ─ ─ ┤
        │
    EW │   IP
        │
        └────── IP ───────┘
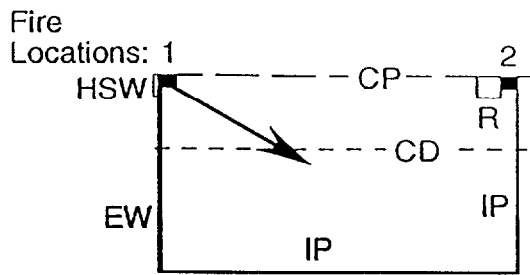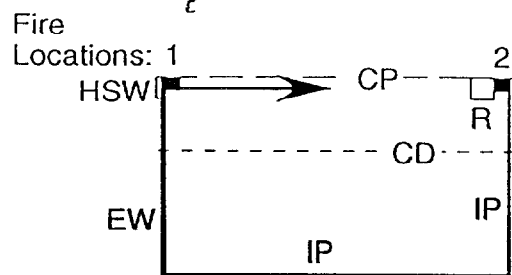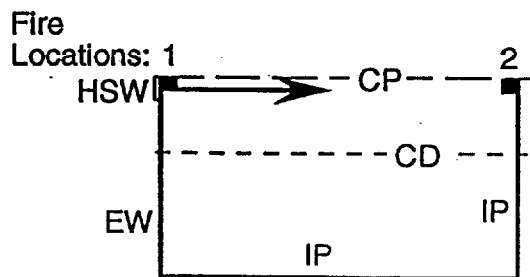
(c) HVAC arrangement 3

┌──────────────────────────────────┐
│ Symbols: │
│ CD   Plane 1 m (3.3 ft) from CP │
│ CP   Plane of Symmetry   │
│ EW   Exterior Wall   │
│ HSW   High Sidewall Supply   │
│ IP   Interior Partition   │
│ R   Heating & Cooling Return   │
└──────────────────────────────────┘

Notes: 1. Arrows indicate the direction of supply air leaving diffuser.
       2. Return of arrangement 3 located at floor under HSW.

Figure 7: Fire locations and HVAC arrangements for room type E4

Fire   See Note 1
Locations: 1   2   3
     ┌─ ─ ─ CP ─ ─ ─ ─ ─ ─ ─ ─ ─ ─ ─ ─ ─ ─ ─ ─ ─ ┐
     │ ┌Computer┐ ┌ES   ┌Computer┐ ┌ES
     │ │   │ │   │   │ │
     ─ ─┤ ─ ─ ─ ─┤─ · CD ─┐ ─ ─ ─ ─ ┤ ─ ─ ─ ─ ─
     │ └ ─ ─ ─ ─┘   └ ─ ─ ─ ─ ┘
  IP │   IP
     │   ▭ES   IP   ▭ES
     └───┘
See Note 2
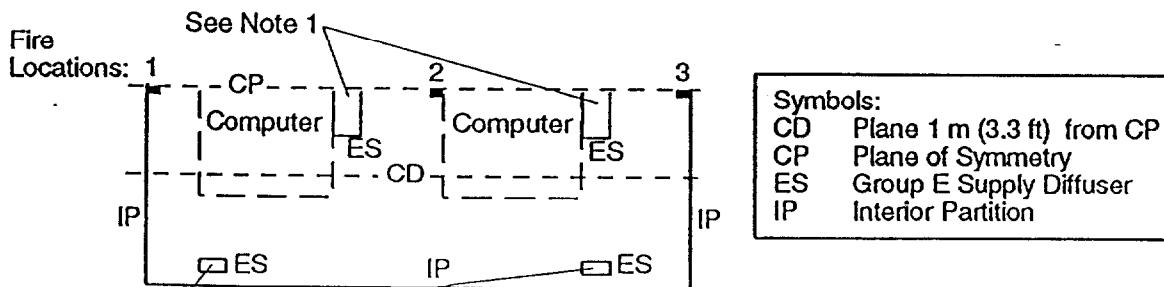
┌──┐
│ Symbols: │
│ CD   Plane 1 m (3.3 ft) from CP   │
│ CP   Plane of Symmetry   │
│ ES   Group E Supply Diffuser   │
│ IP   Interior Partition   │
└──┘

Notes: 1. Returns located in side of computer at floor under
          the group E supply.
       2. Returns located in floor under the group E supply.

Figure 8: Fire locations and HVAC arrangements for room type E5
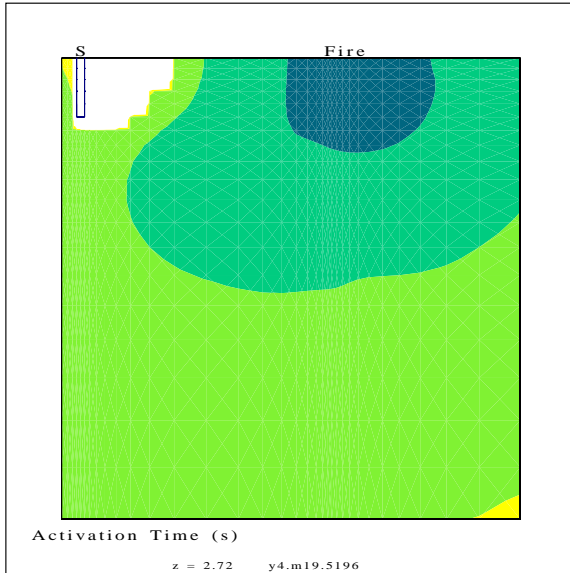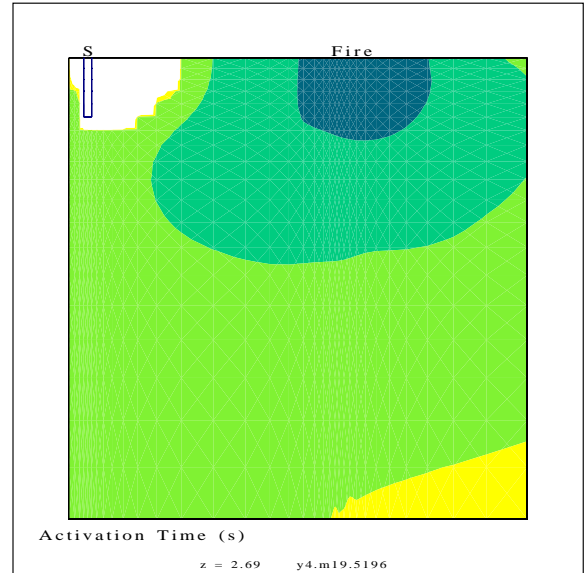
30

(a) At 0.02 m (0.79 in) below the ceiling


(b) At 0.05 m (2.0 in) below the ceiling
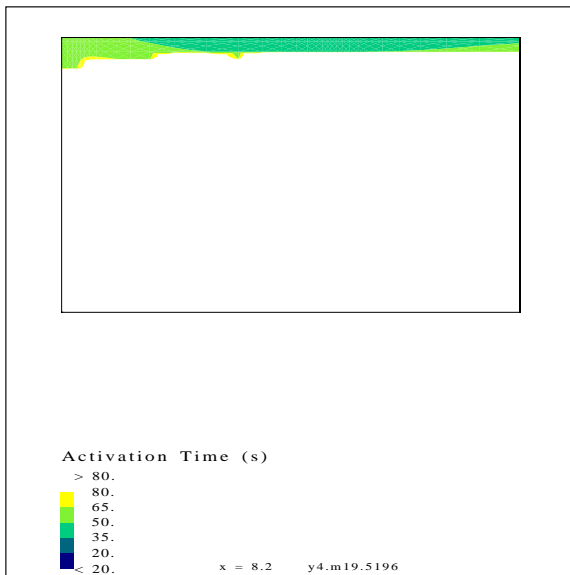

(c) Plane 1 m (3.3 ft) from plane of symmetry
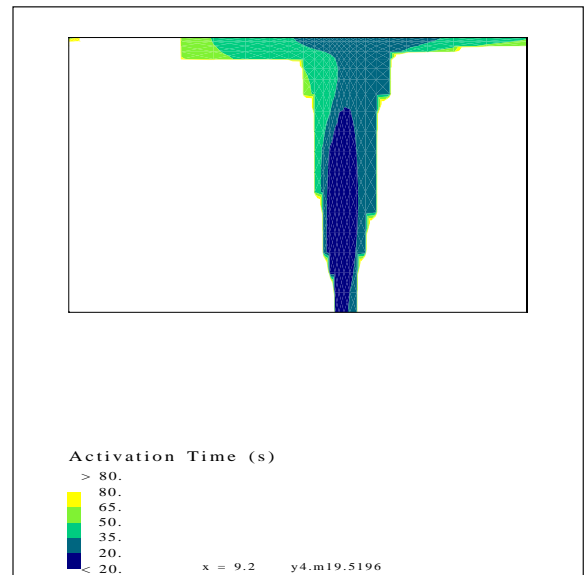

(d) Plane of symmetry

Figure 9: Simulated activation time in room type O1 from run 32.
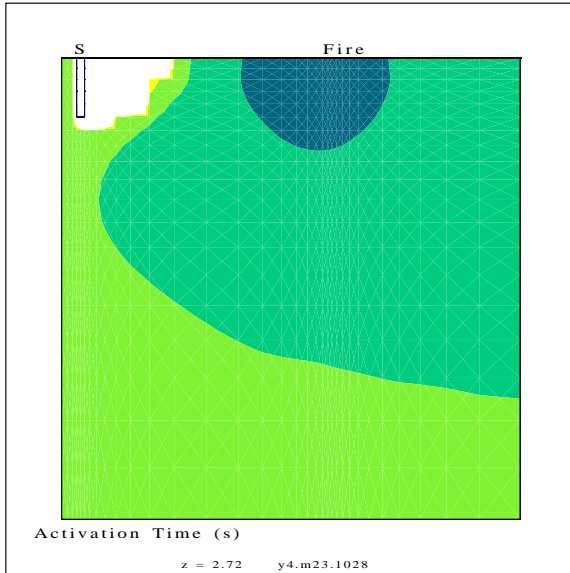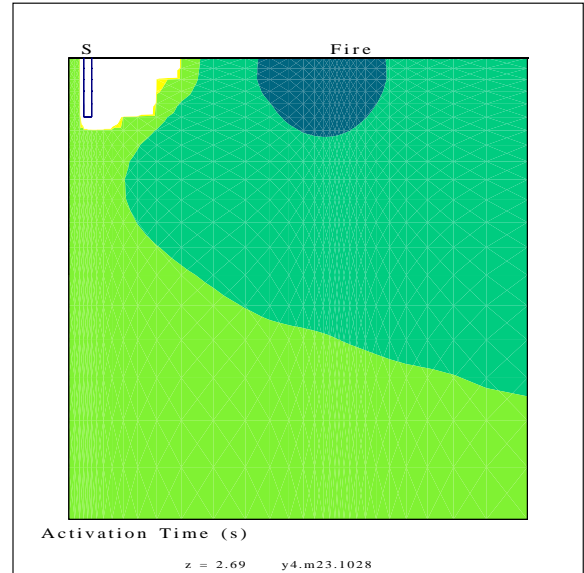
31

(a) At 0.02 m (0.79 in) below the ceiling

(b) At 0.05 m (2.0 in) below the ceiling
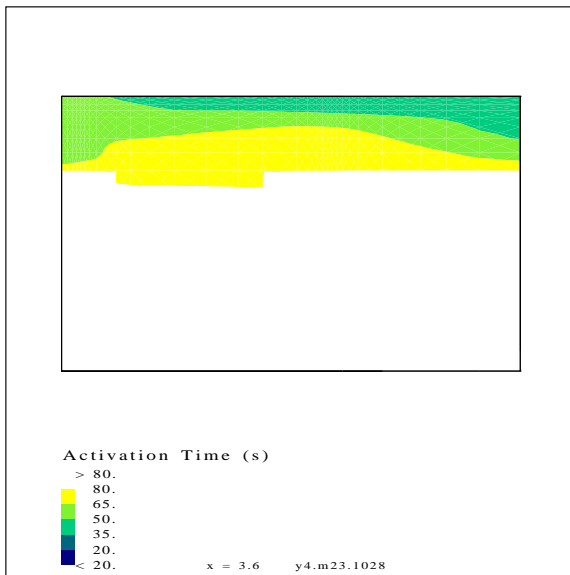
(c) Plane 1 m (3.3 ft) from plane of symmetry
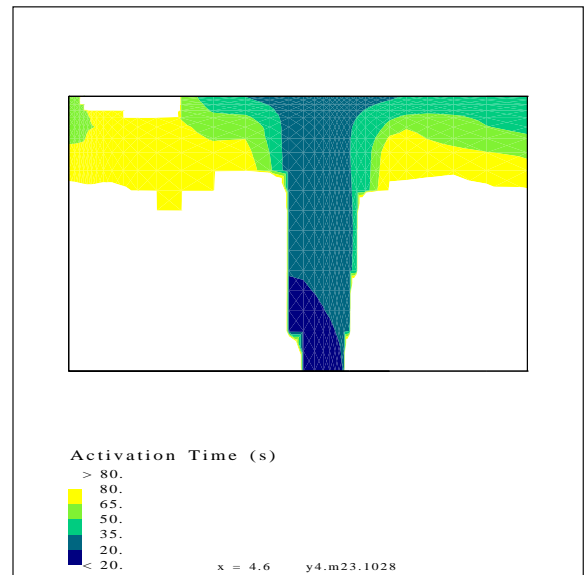
(d) Plane of symmetry

Figure 10: Simulated activation time in room type E1 from run 33.
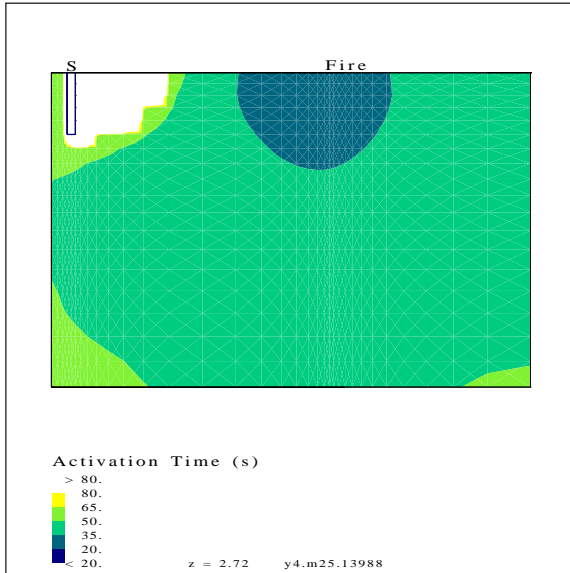
(a) At 0.02 m (0.79 in) below the ceiling
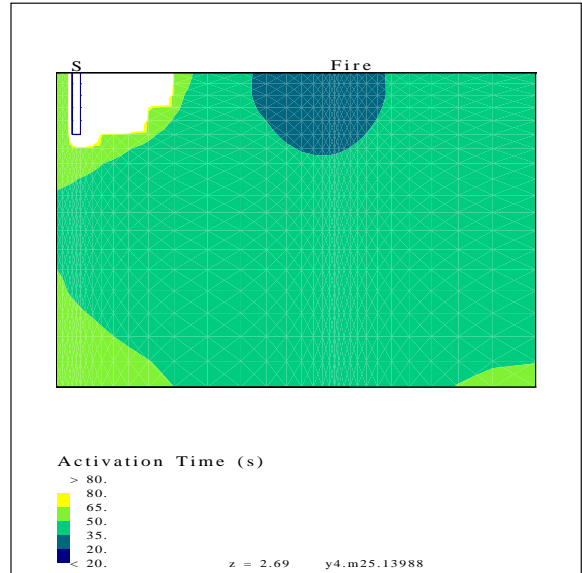
(b) At 0.05 m (2.0 in) below the ceiling
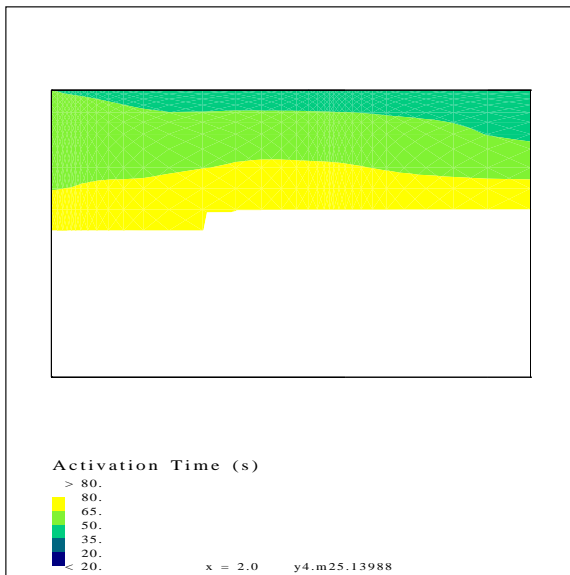
(c) Plane 1 m (3.3 ft) from plane of symmetry
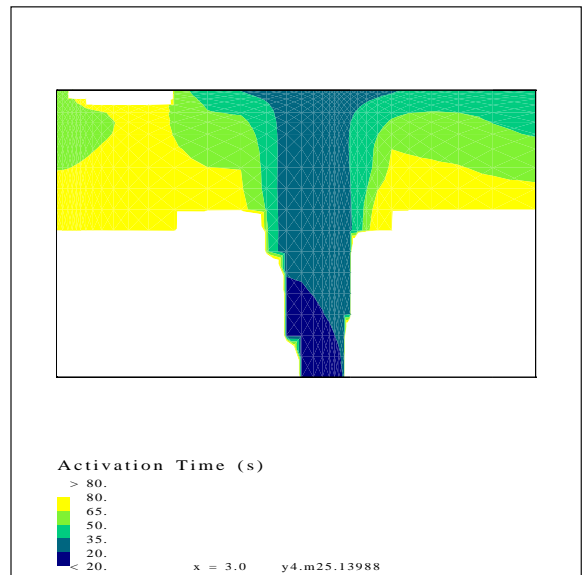

(d) Plane of symmetry

Figure 11: Simulated activation time in room type E2 from run 34.
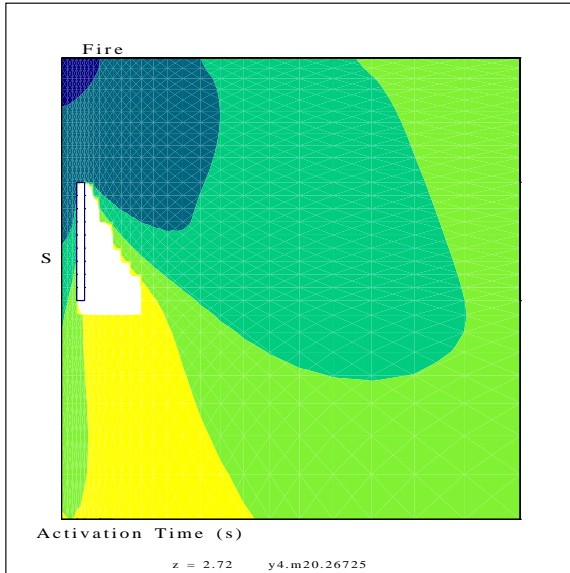
(a) At 0.02 m (0.79 in) below the ceiling
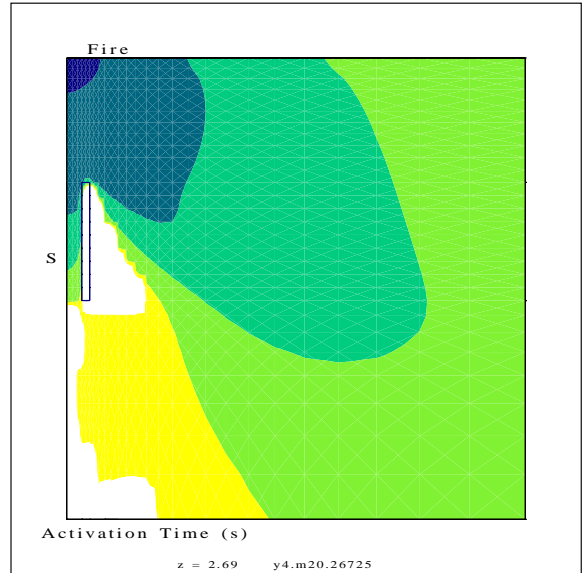
(b) At 0.05 m (2.0 in) below the ceiling
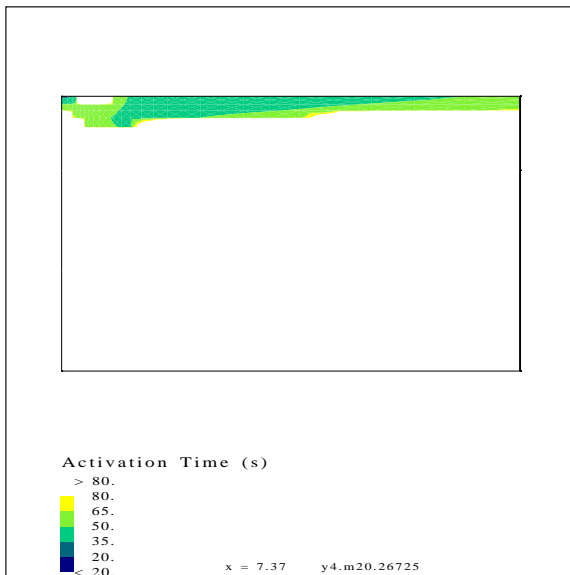
(c) Plane 1 m (3.3 ft) from plane of symmetry
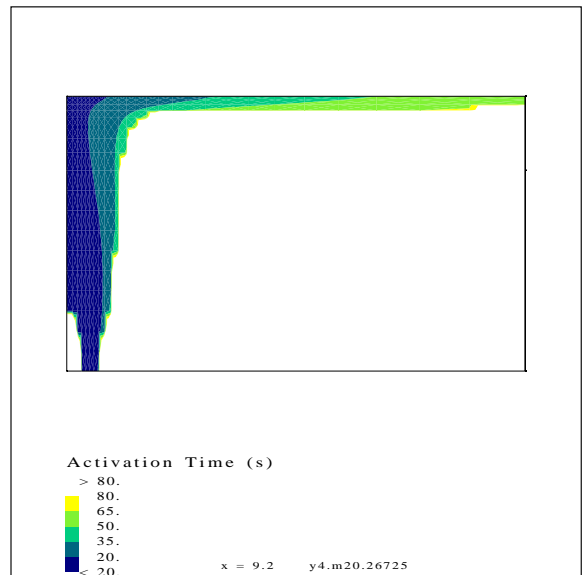
(d) Plane of symmetry

Figure 12: Simulated activation time in room type O1 from run 35.
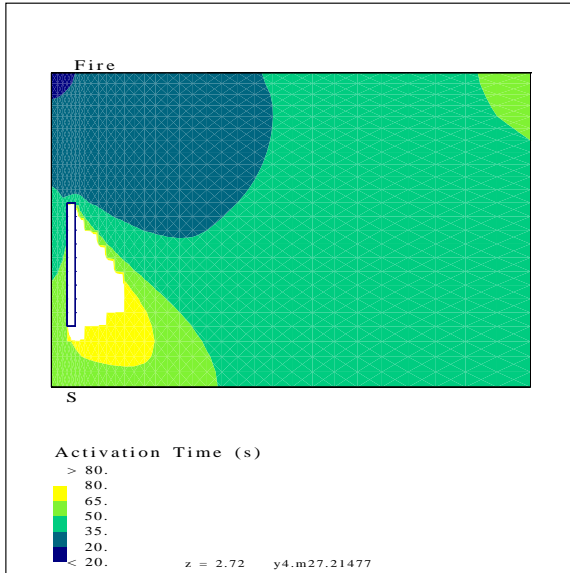
(a) At 0.02 m (0.79 in) below the ceiling
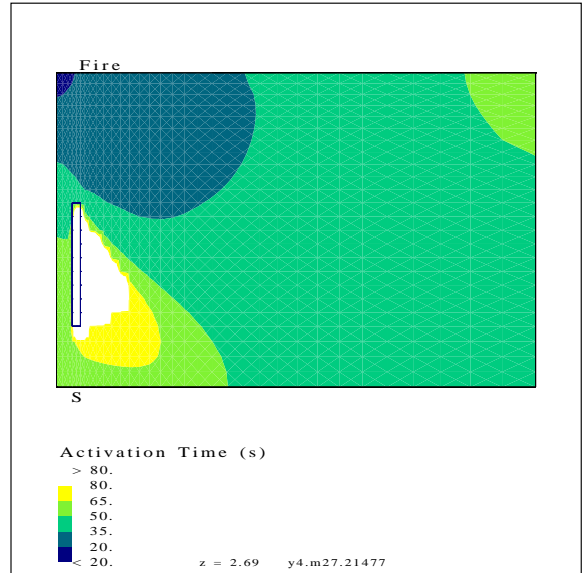
(b) At 0.05 m (2.0 in) below the ceiling
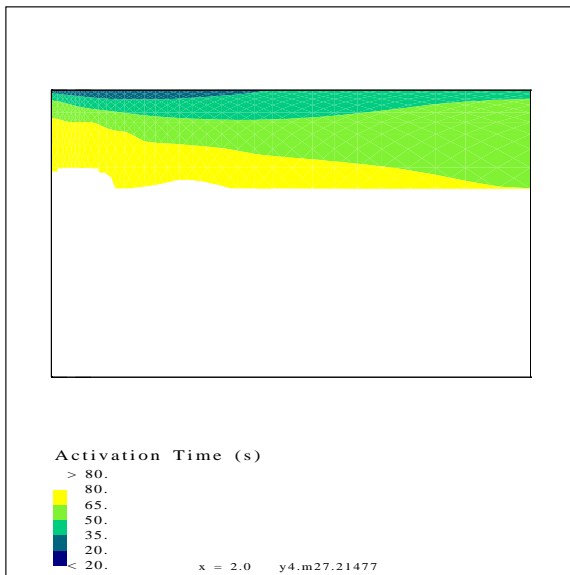

(c) Plane 1 m (3.3 ft) from plane of symmetry
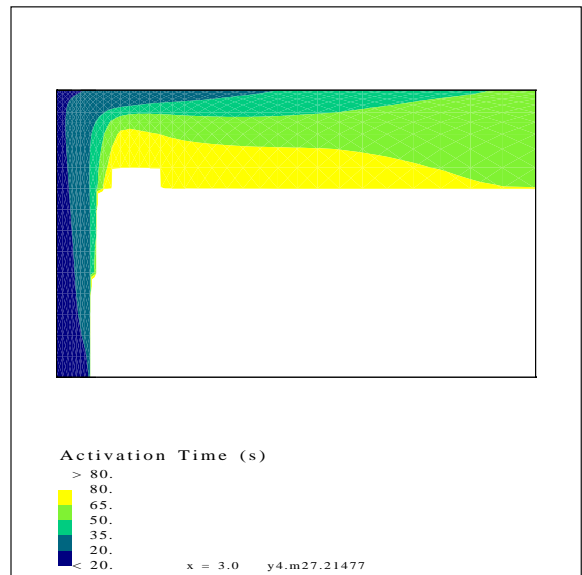
(d) Plane of symmetry

Figure 13: Simulated activation time in room type E2 from run 36.
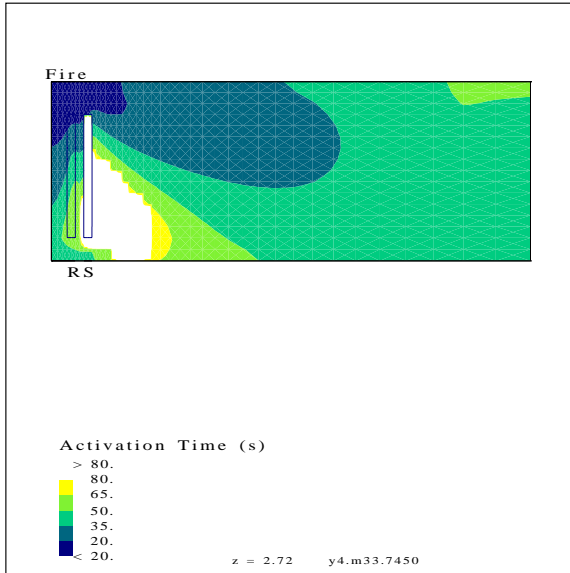
(a) At 0.02 m (0.79 in) below the ceiling
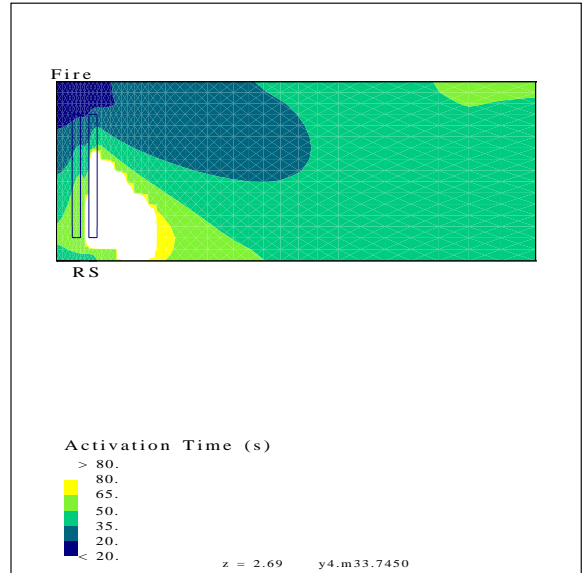
(b) At 0.05 m (2.0 in) below the ceiling
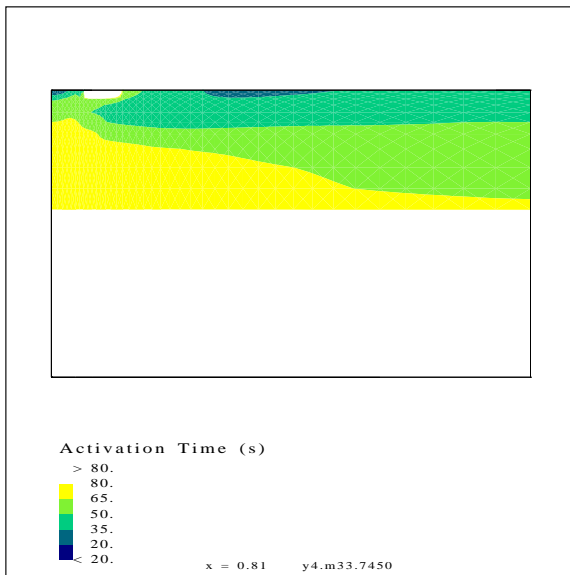
(c) Plane 1 m (3.3 ft) from plane of symmetry
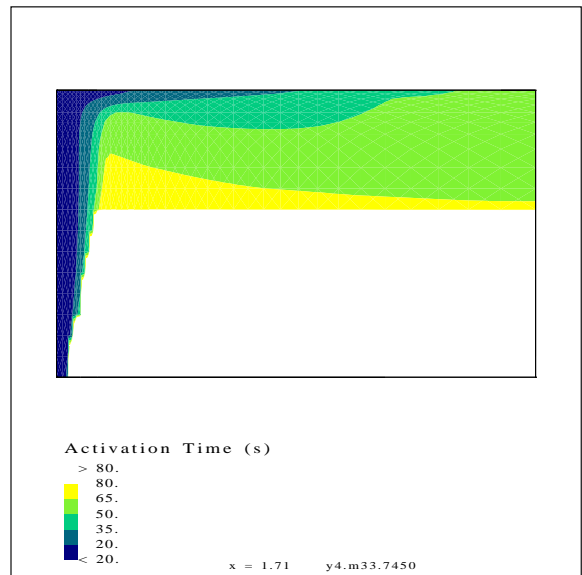

(d) Plane of symmetry

Figure 14: Simulated activation time in room type E3 from run 37.
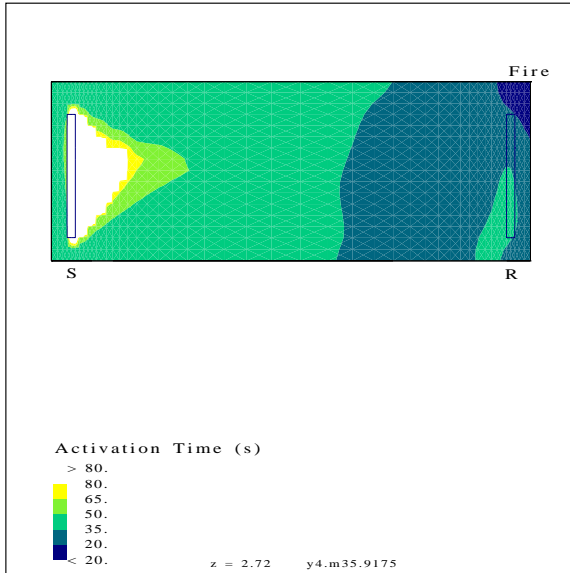
(a) At 0.02 m (0.79 in) below the ceiling
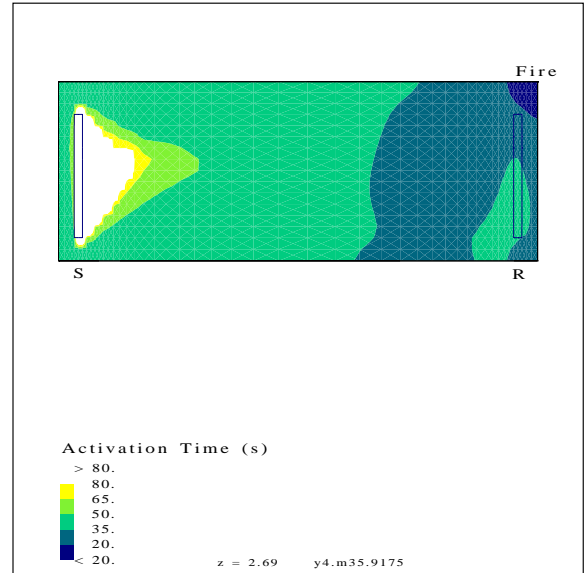
(b) At 0.05 m (2.0 in) below the ceiling
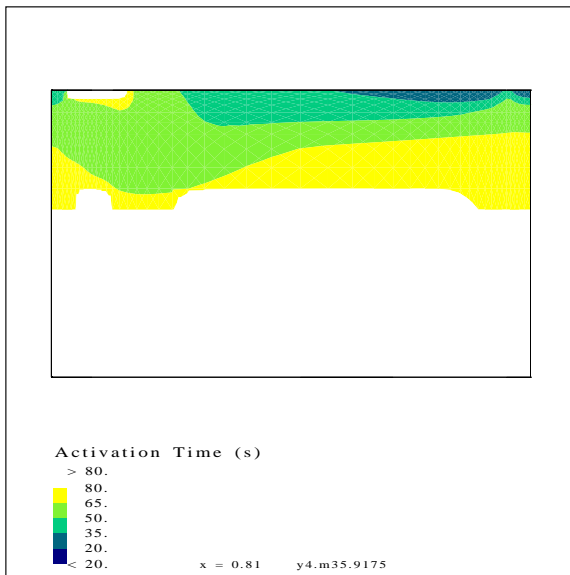
(c) Plane 1 m (3.3 ft) from plane of symmetry
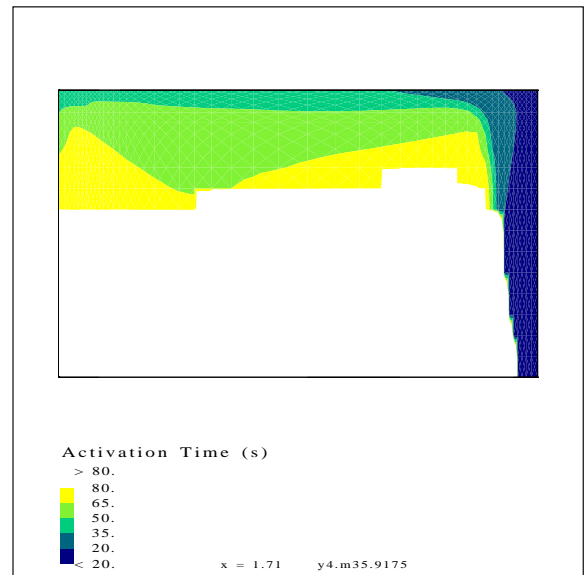
(d) Plane of symmetry

Figure 15: Simulated activation time in room type E3 from run 38.
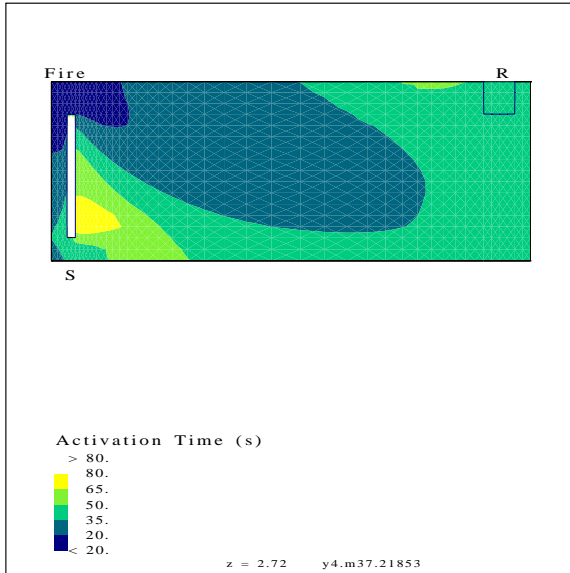
(a) At 0.02 m (0.79 in) below the ceiling
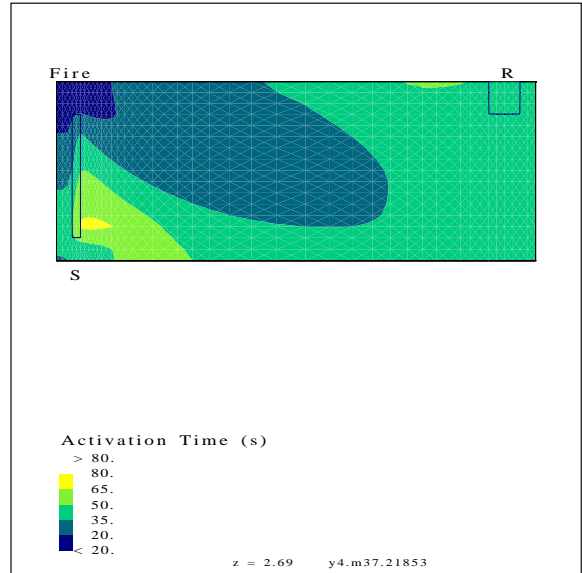

(b) At 0.05 m (2.0 in) below the ceiling
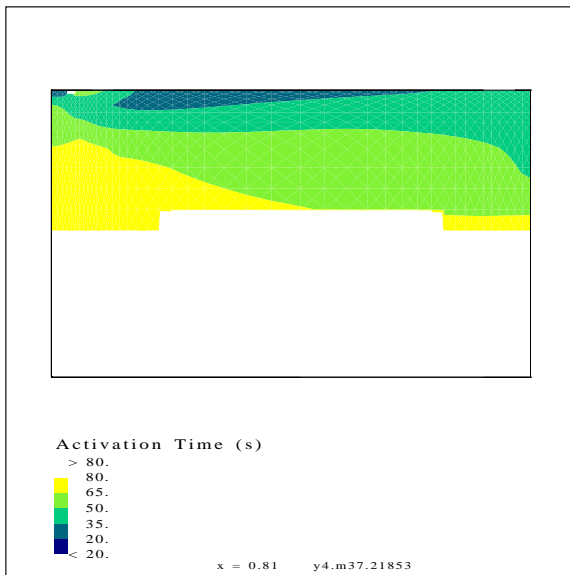
(c) Plane 1 m (3.3 ft) from plane of symmetry
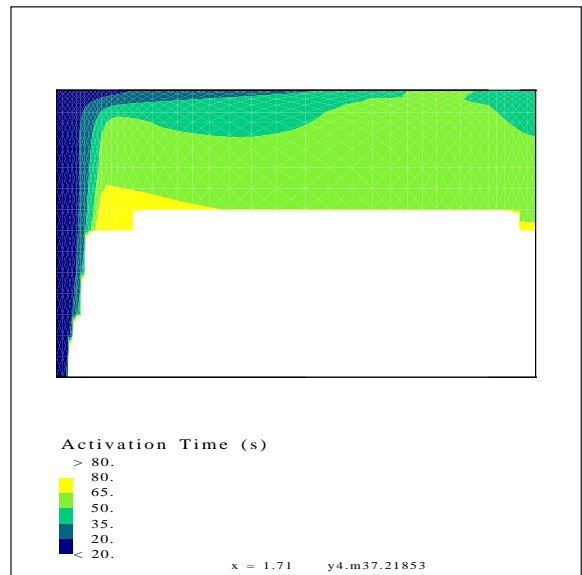
(d) Plane of symmetry

Figure 16: Simulated activation time in room type E3 from run 39.
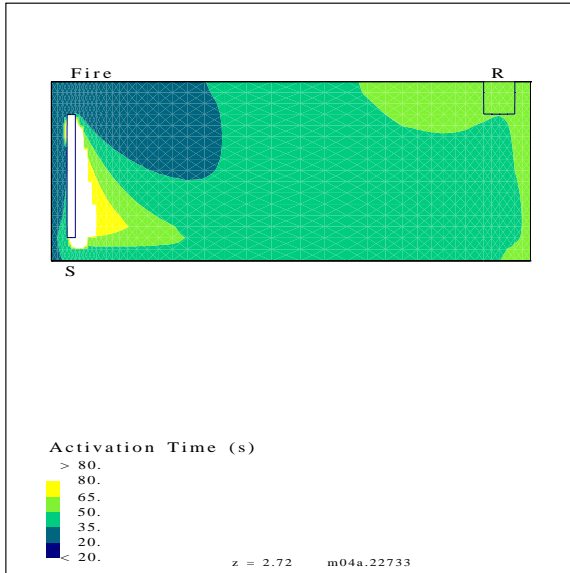
(a) At 0.02 m (0.79 in) below the ceiling
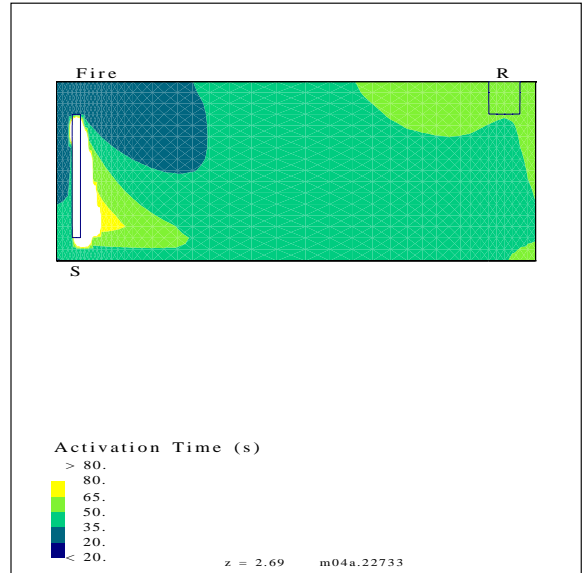
(b) At 0.05 m (2.0 in) below the ceiling
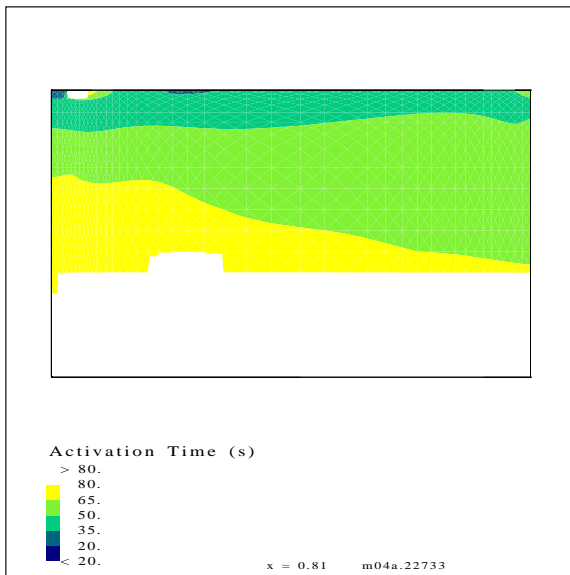
(c) Plane 1 m (3.3 ft) from plane of symmetry
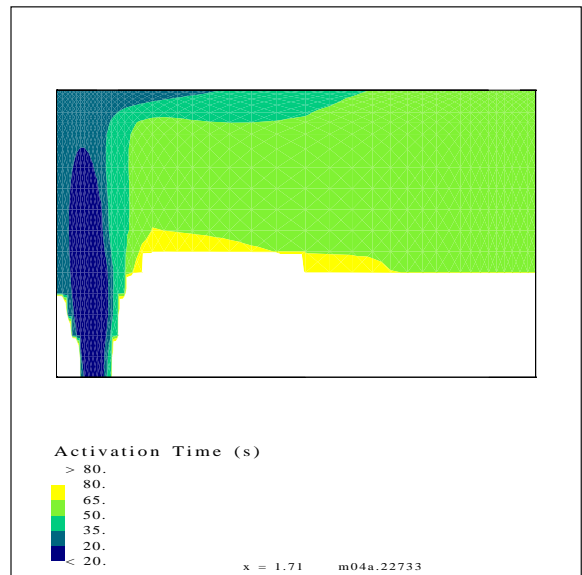
(d) Plane of symmetry

Figure 17: Simulated activation time in room type E3 from run 40.
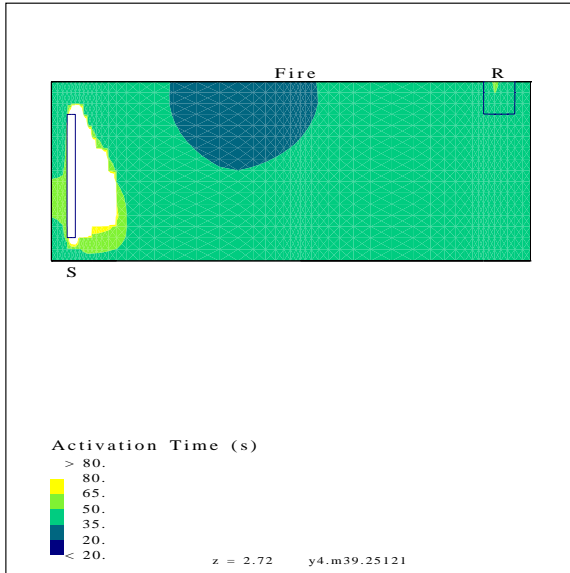
(a) At 0.02 m (0.79 in) below the ceiling
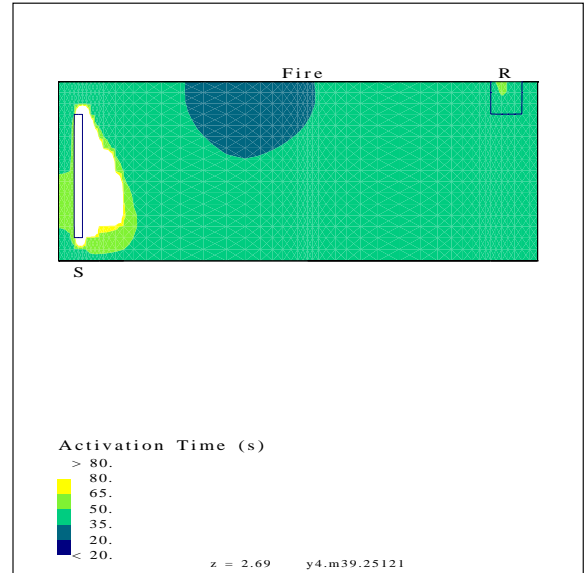
(b) At 0.05 m (2.0 in) below the ceiling
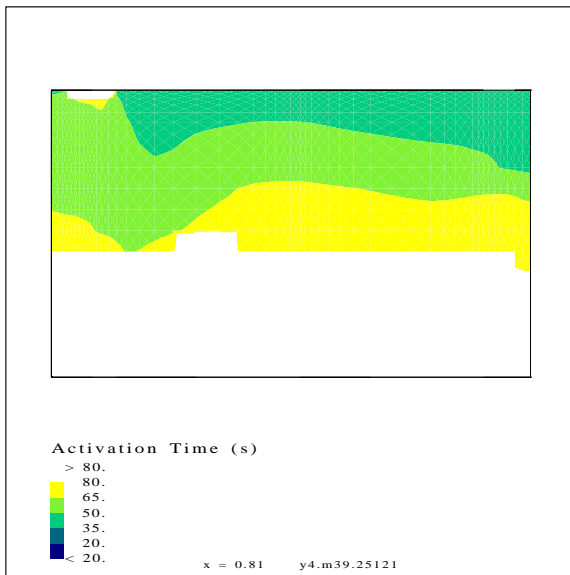
(c) Plane 1 m (3.3 ft) from plane of symmetry
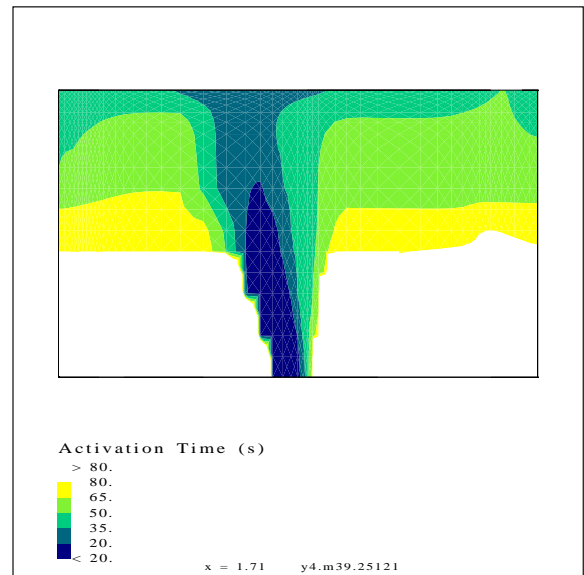
(d) Plane of symmetry

Figure 18: Simulated activation time in room type E3 from run 41.
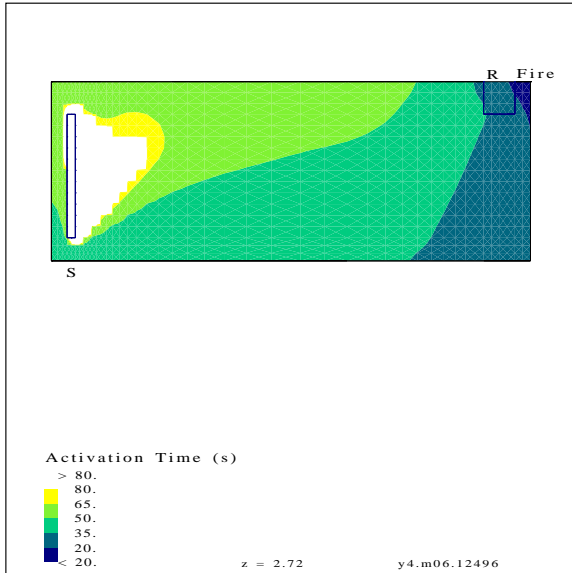
(a) At 0.02 m (0.79 in) below the ceiling
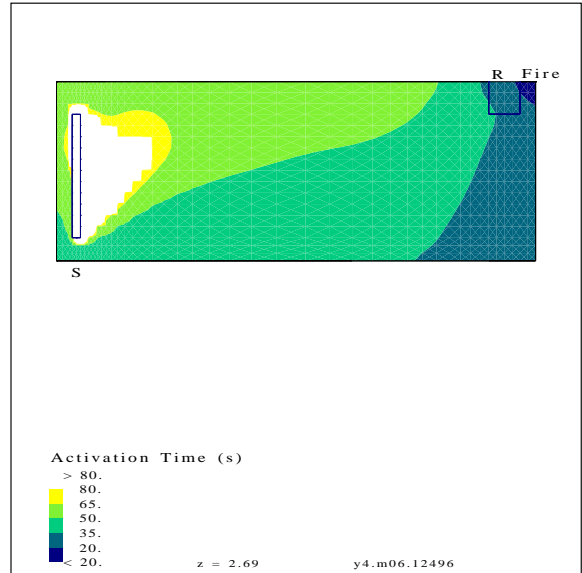
(b) At 0.05 m (2.0 in) below the ceiling
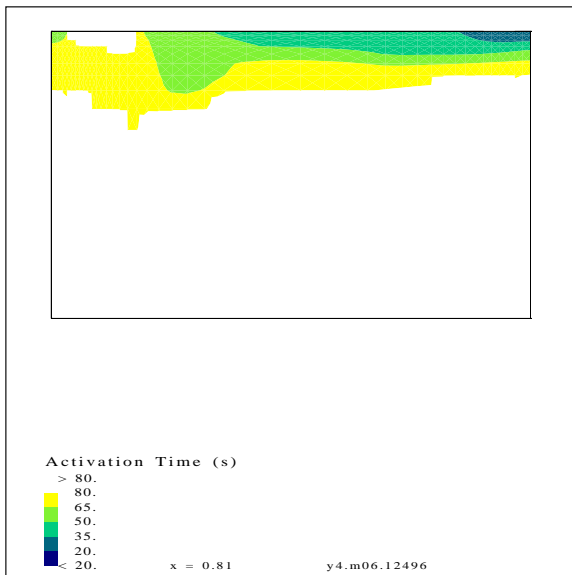
(c) Plane 1 m (3.3 ft) from plane of symmetry
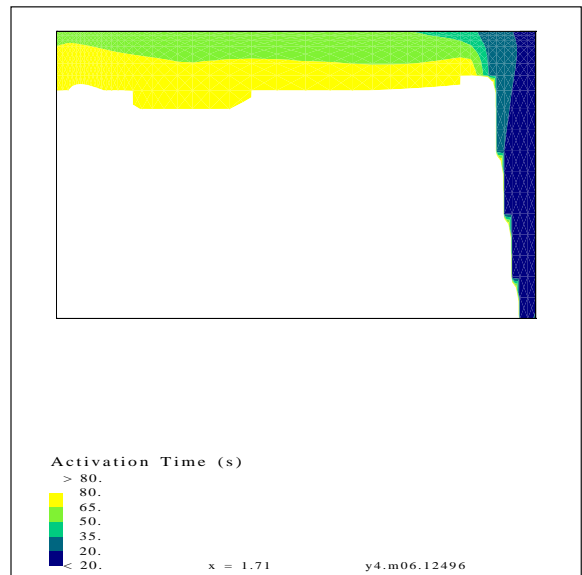
(d) Plane of symmetry

Figure 19: Simulated activation time in room type E3 from run 42.
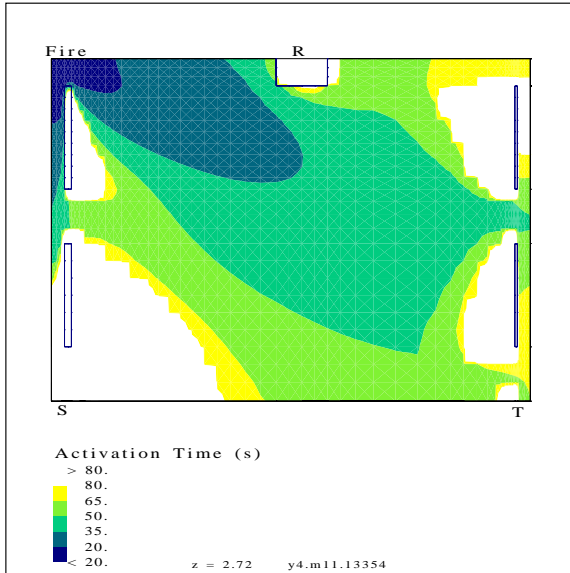
(a) At 0.02 m (0.79 in) below the ceiling
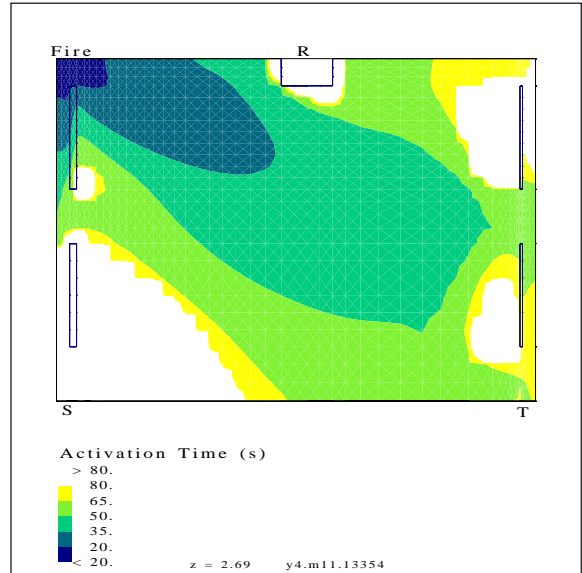

(b) At 0.05 m (2.0 in) below the ceiling
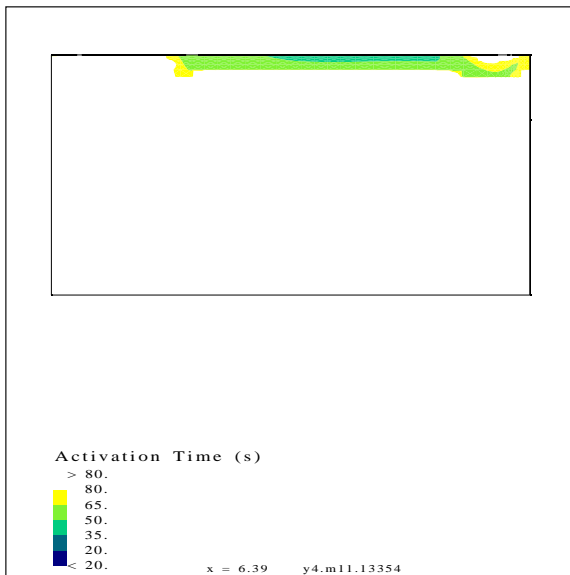
(c) Plane 1 m (3.3 ft) from plane of symmetry
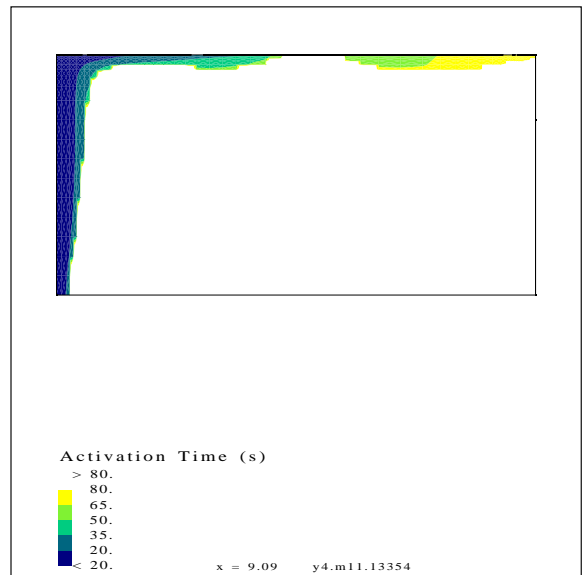
(d) Plane of symmetry

Figure 20: Simulated activation time in room type O2 from run 43.
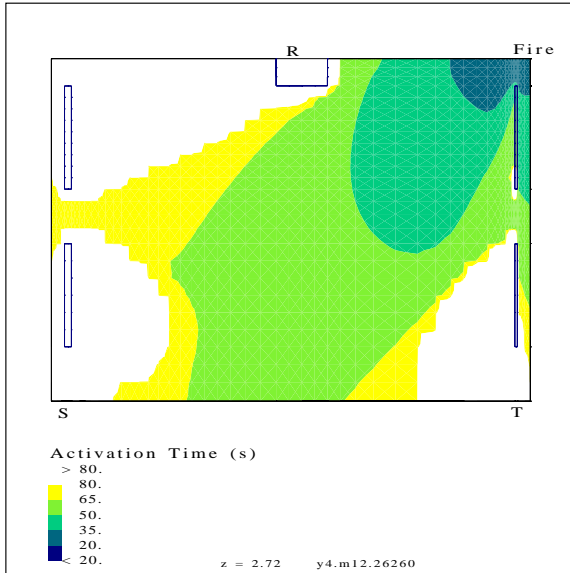
(a) At 0.02 m (0.79 in) below the ceiling
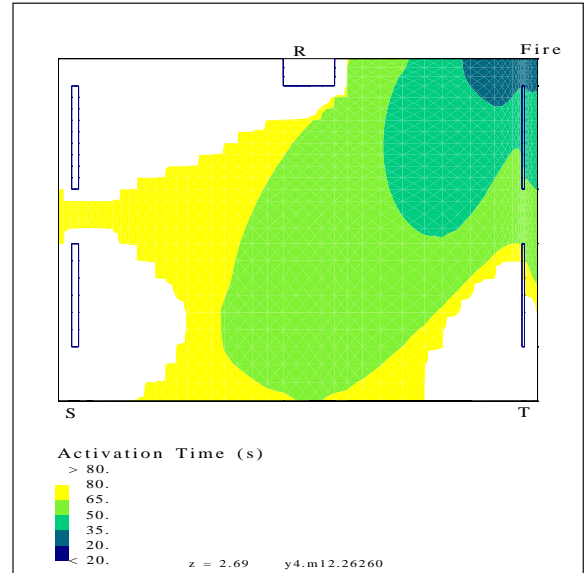
(b) At 0.05 m (2.0 in) below the ceiling
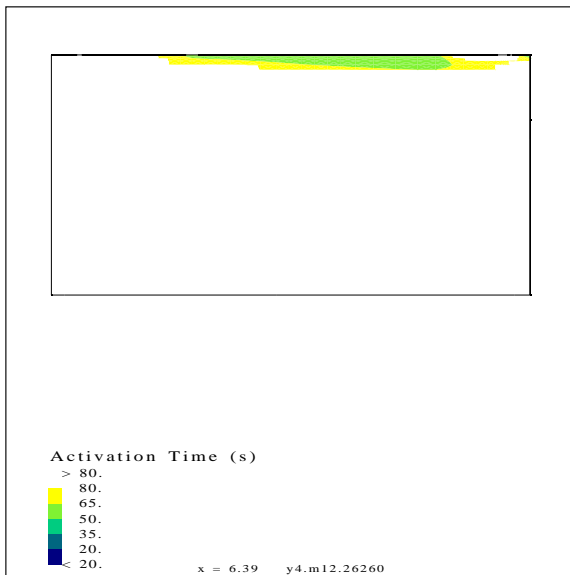
(c) Plane 1 m (3.3 ft) from plane of symmetry
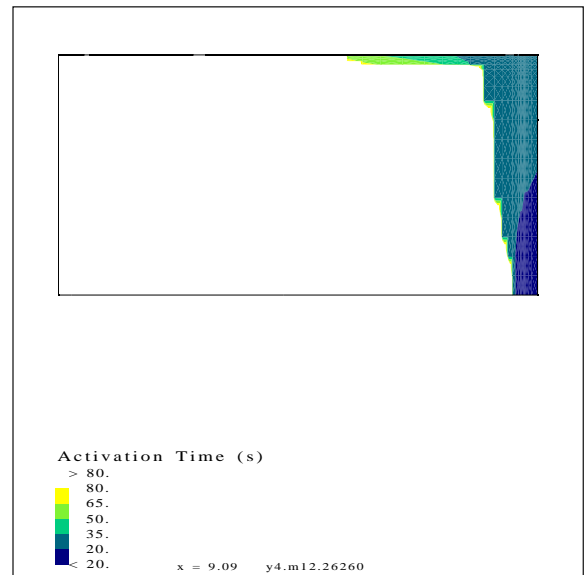

(d) Plane of symmetry

Figure 21: Simulated activation time in room type O2 from run 44.
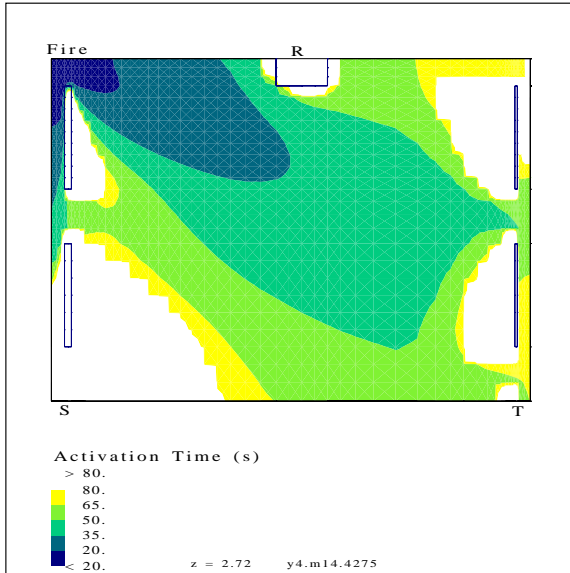
(a) At 0.02 m (0.79 in) below the ceiling
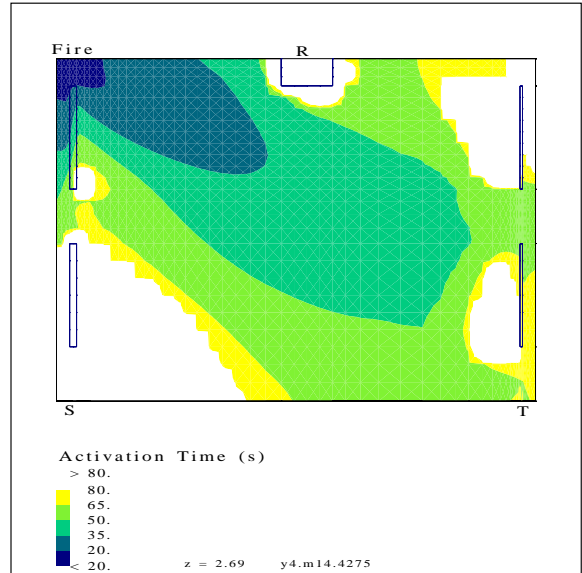
(b) At 0.05 m (2.0 in) below the ceiling
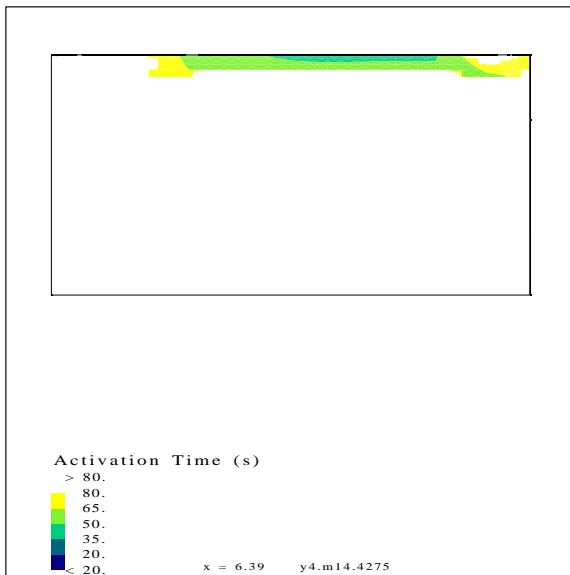
(c) Plane 1 m (3.3 ft) from plane of symmetry
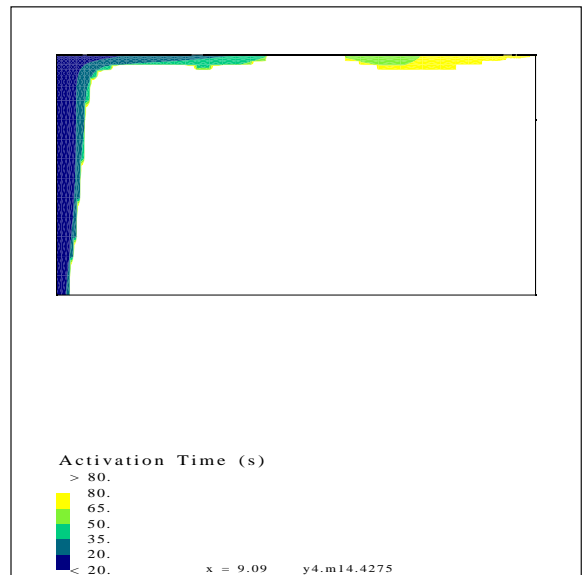
(d) Plane of symmetry

Figure 22: Simulated activation time in room type O2 from run 45.
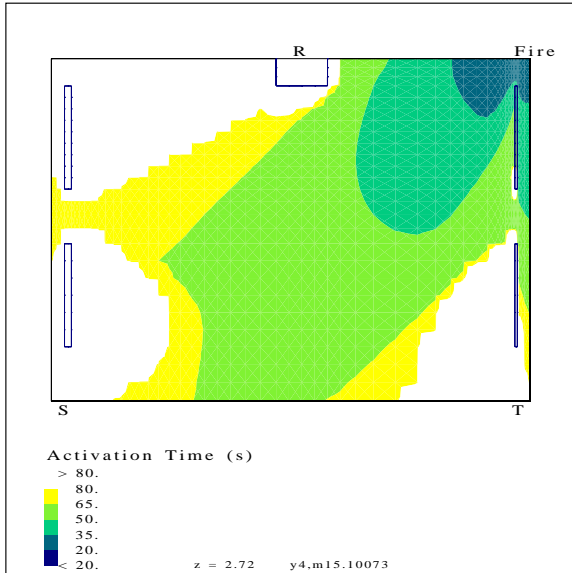
(a) At 0.02 m (0.79 in) below the ceiling
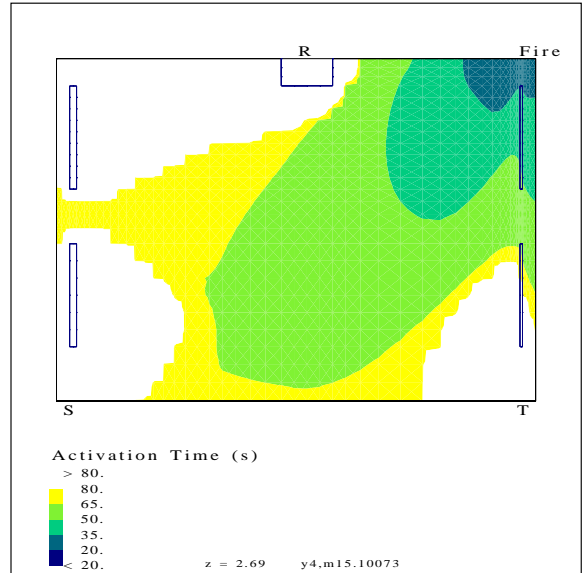

(b) At 0.05 m (2.0 in) below the ceiling
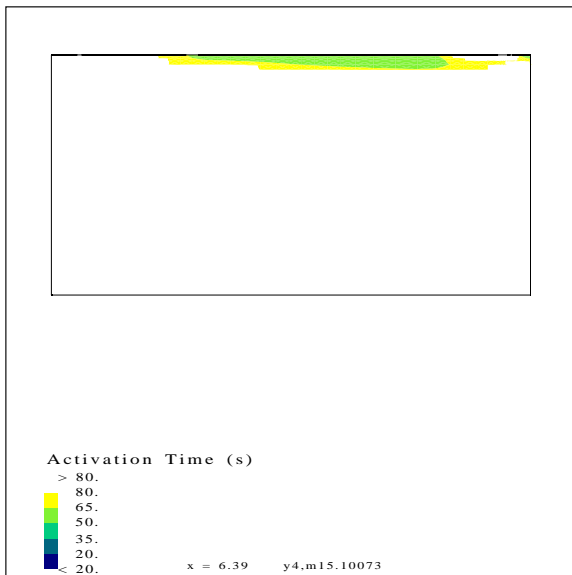
(c) Plane 1 m (3.3 ft) from plane of symmetry
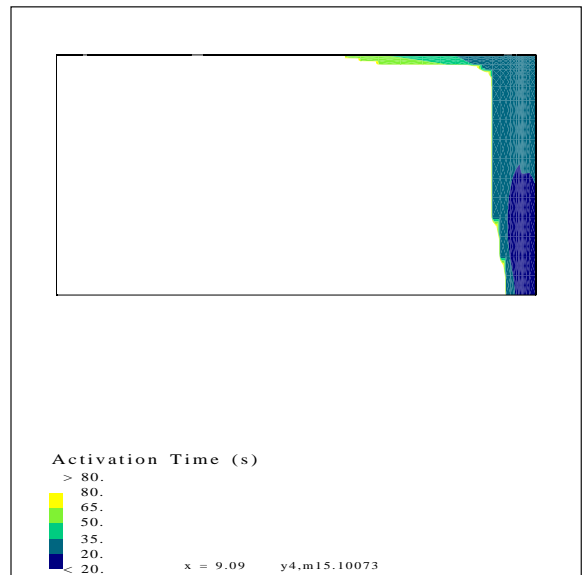
(d) Plane of symmetry

Figure 23: Simulated activation time in room type O2 from run 46.
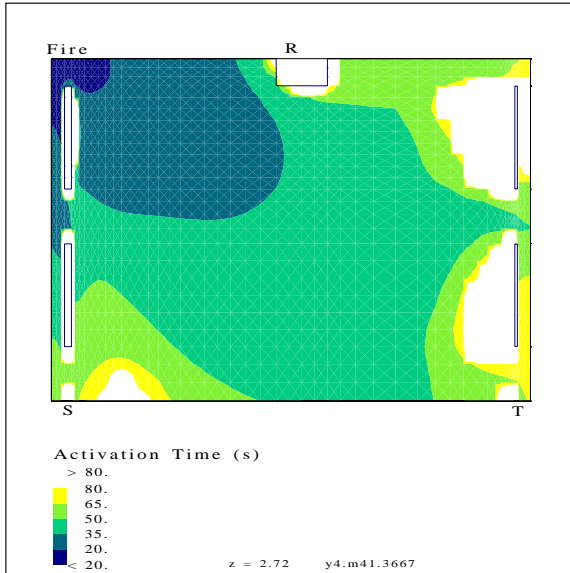
(a) At 0.02 m (0.79 in) below the ceiling
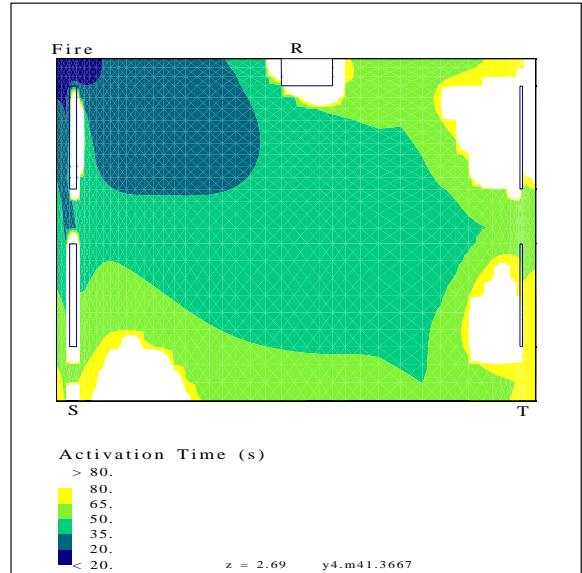
(b) At 0.05 m (2.0 in) below the ceiling
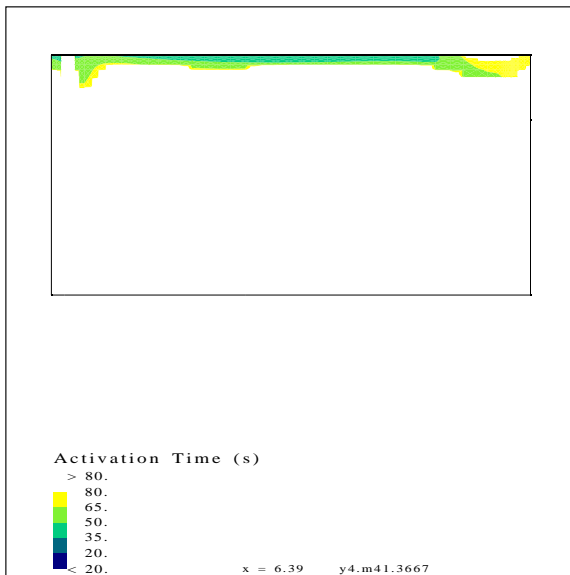
(c) Plane 1 m (3.3 ft) from plane of symmetry
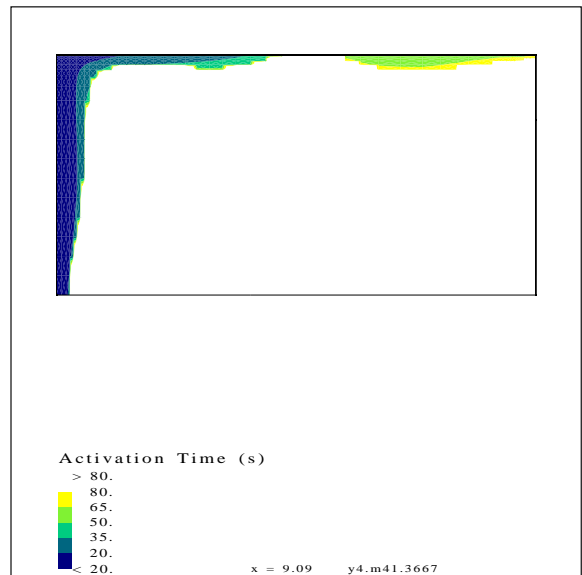

(d) Plane of symmetry

Figure 24: Simulated activation time in room type O2 from run 47.
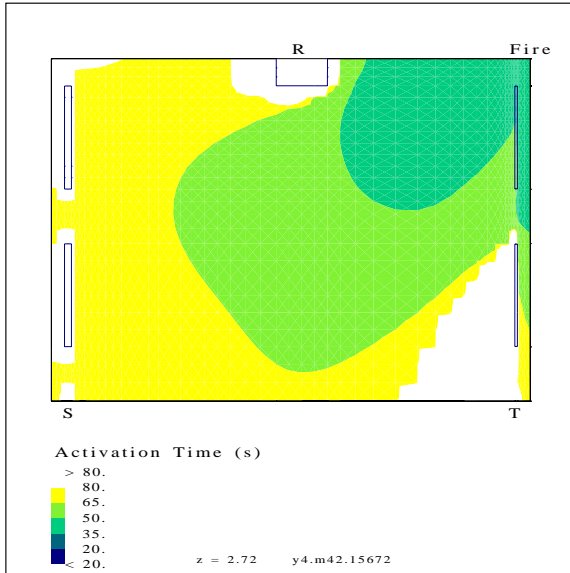
(a) At 0.02 m (0.79 in) below the ceiling
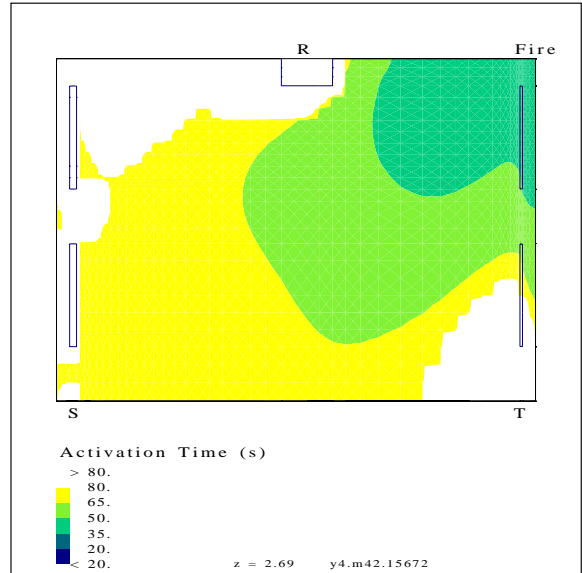
(b) At 0.05 m (2.0 in) below the ceiling
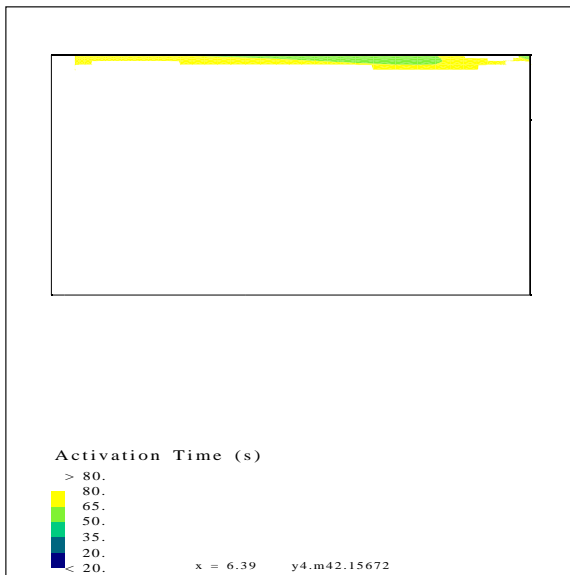
(c) Plane 1 m (3.3 ft) from plane of symmetry
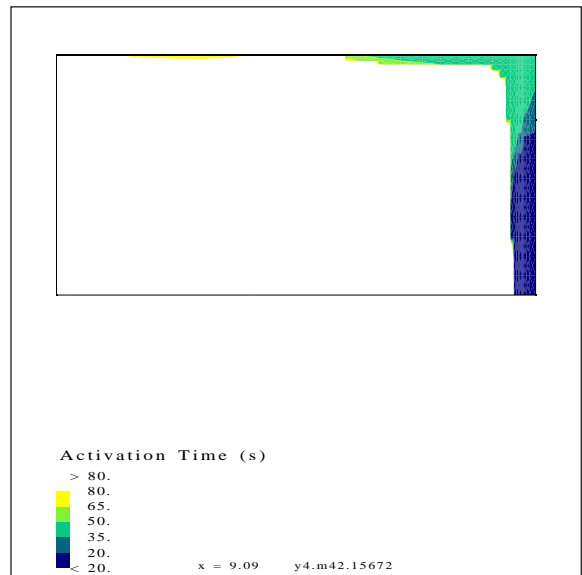
(d) Plane of symmetry

Figure 25: Simulated activation time in room type O2 from run 48.
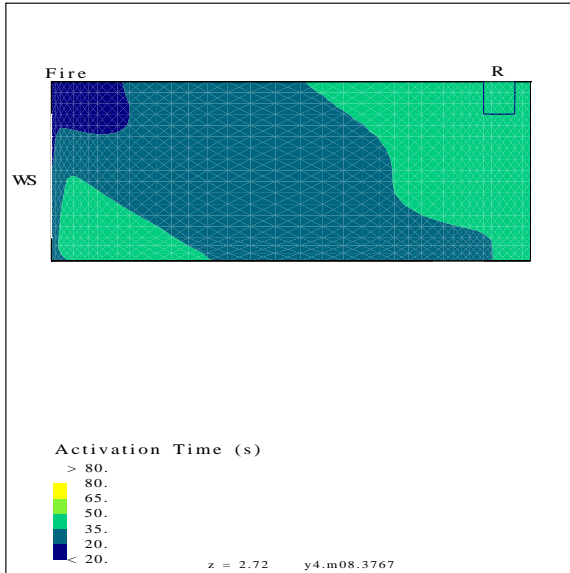
(a) At 0.02 m (0.79 in) below the ceiling
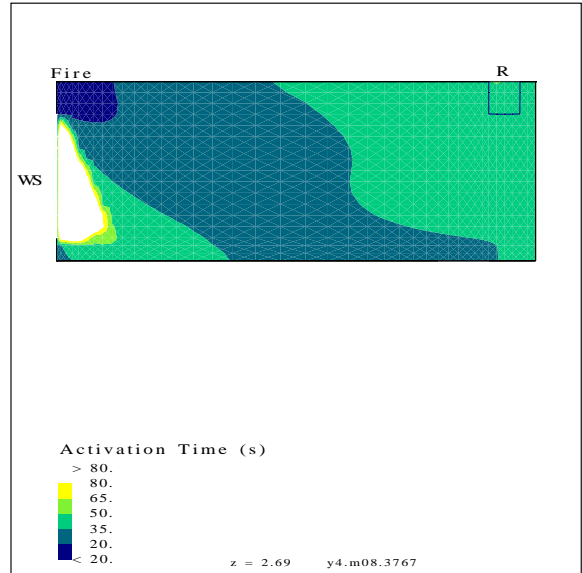
(b) At 0.05 m (2.0 in) below the ceiling
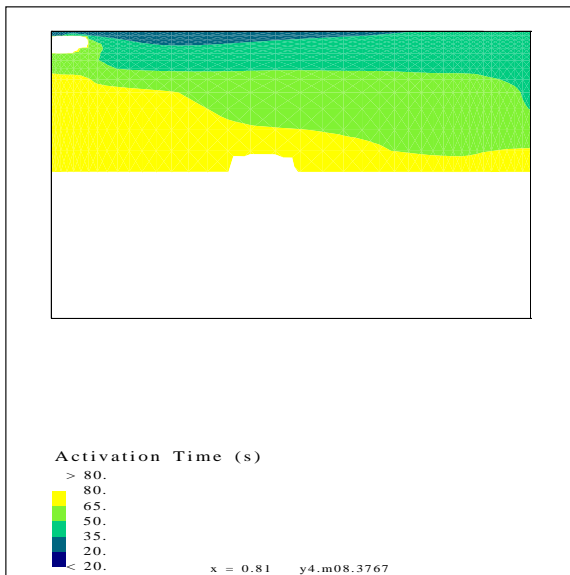
(c) Plane 1 m (3.3 ft) from plane of symmetry
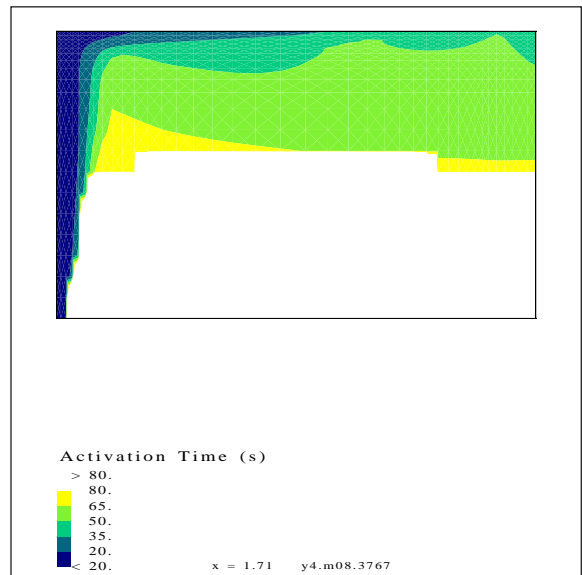
(d) Plane of symmetry

Figure 26: Simulated activation time in room type E3 from run 49.
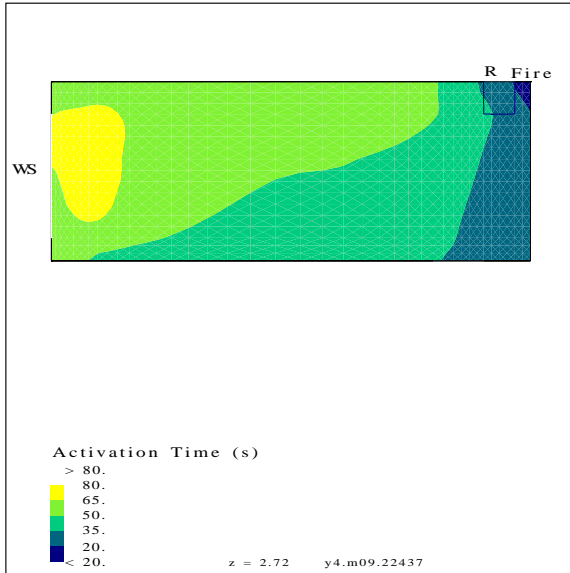
(a) At 0.02 m (0.79 in) below the ceiling
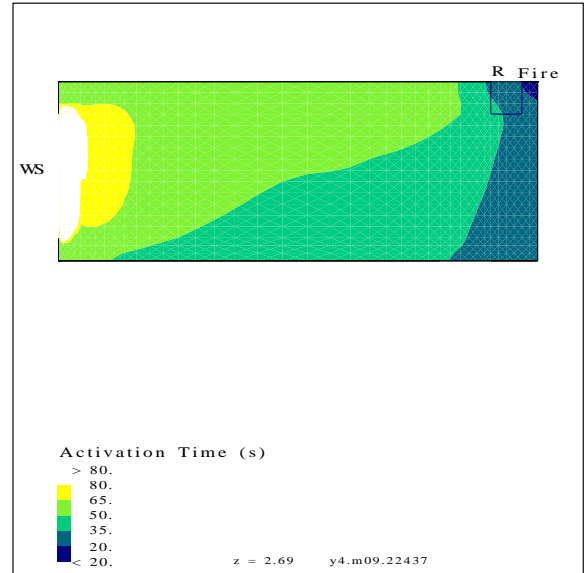
(b) At 0.05 m (2.0 in) below the ceiling
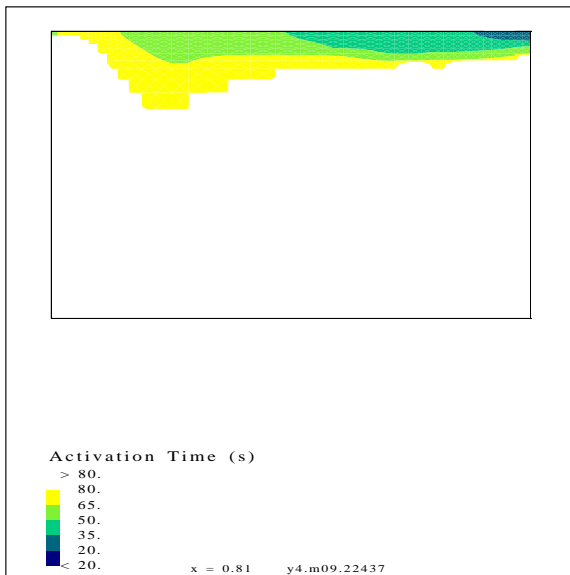
(c) Plane 1 m (3.3 ft) from plane of symmetry
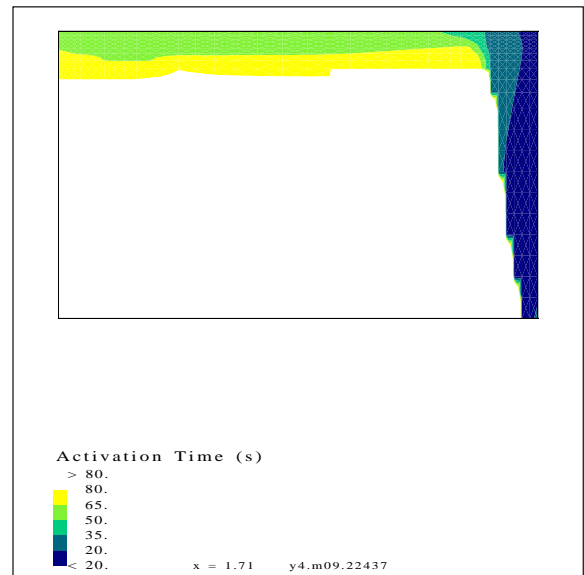

(d) Plane of symmetry

Figure 27: Simulated activation time in room type E3 from run 50.
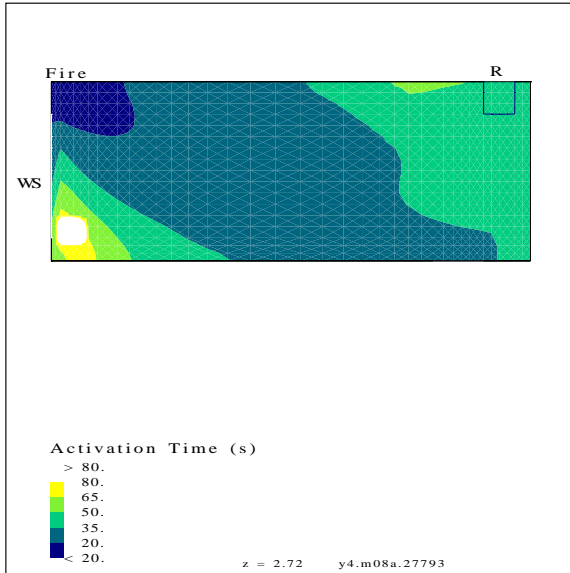
(a) At 0.02 m (0.79 in) below the ceiling
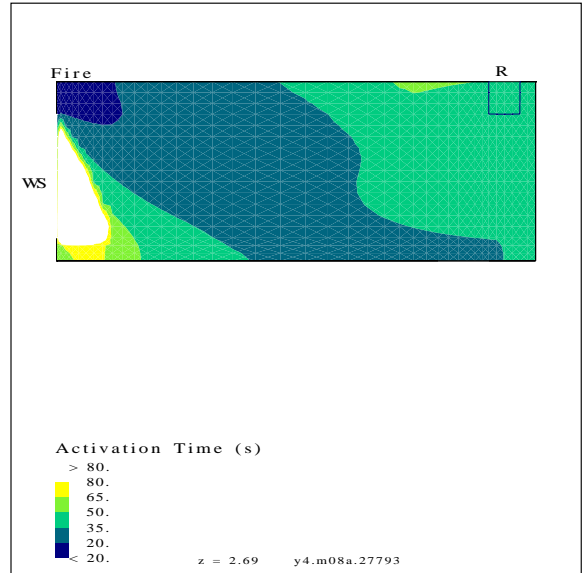
(b) At 0.05 m (2.0 in) below the ceiling
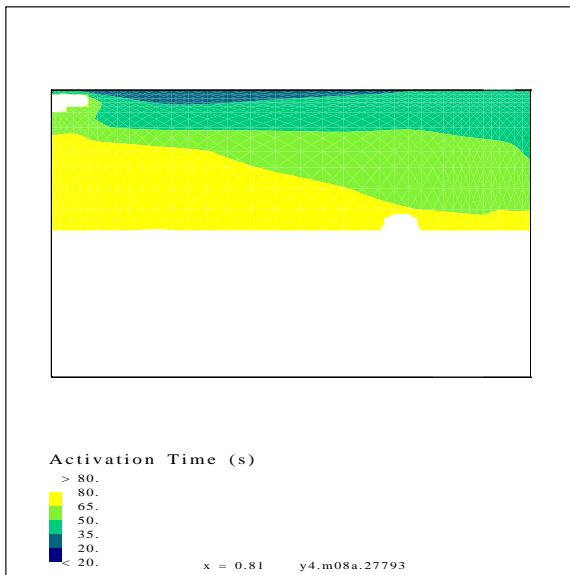
(c) Plane 1 m (3.3 ft) from plane of symmetry
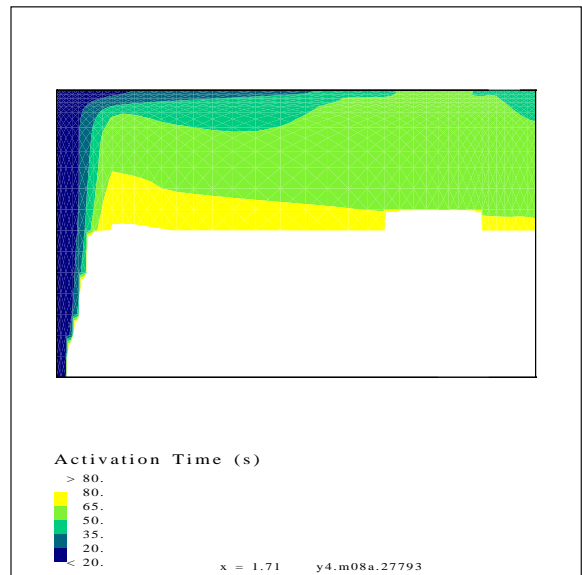
(d) Plane of symmetry

Figure 28: Simulated activation time in room type E3 from run 51.
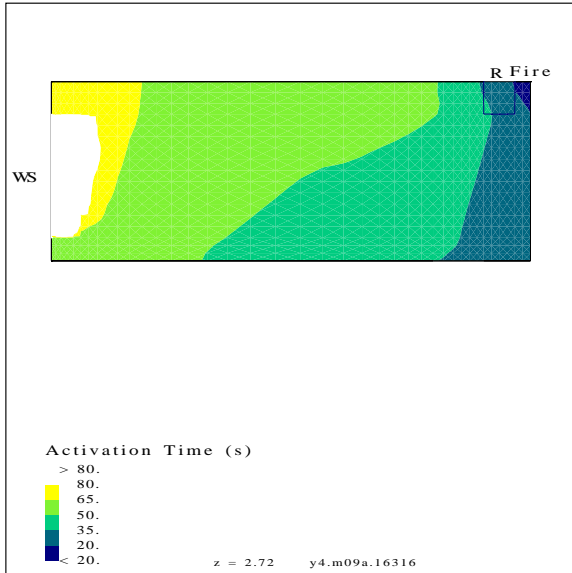
(a) At 0.02 m (0.79 in) below the ceiling
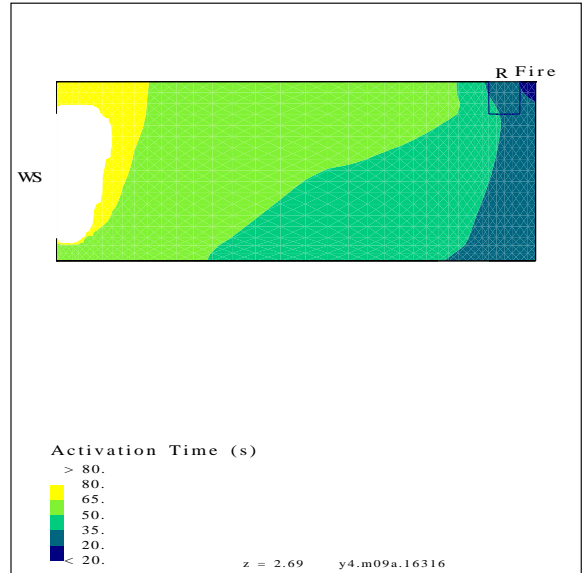
(b) At 0.05 m (2.0 in) below the ceiling
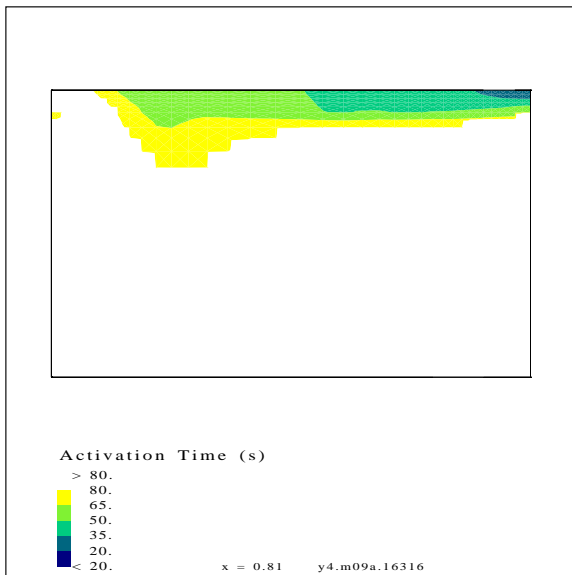
(c) Plane 1 m (3.3 ft) from plane of symmetry
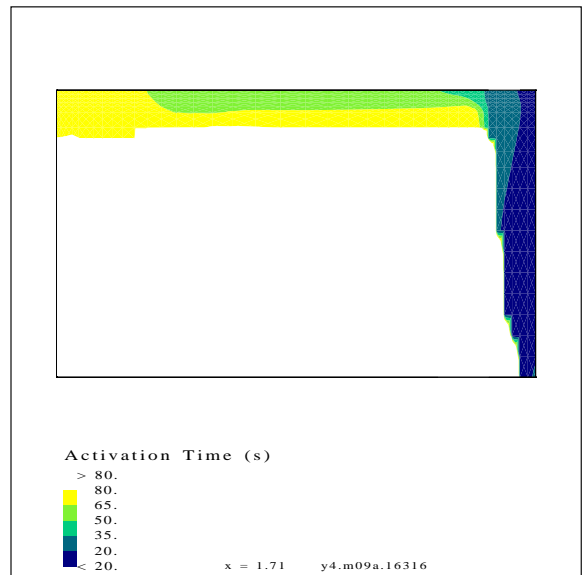
(d) Plane of symmetry

Figure 29: Simulated activation time in room type E3 from run 52.
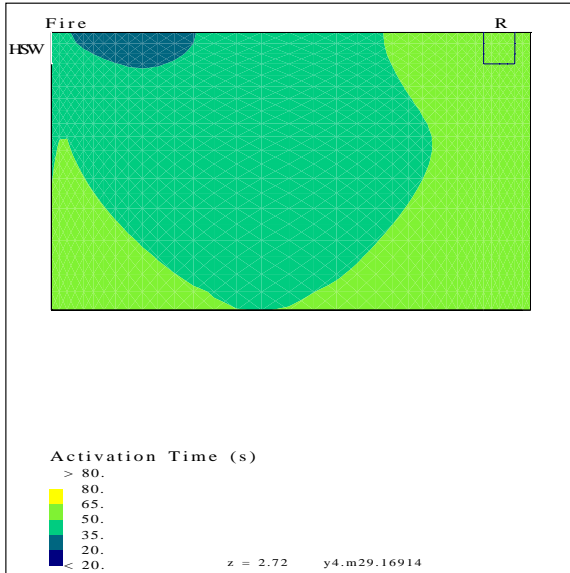
(a) At 0.02 m (0.79 in) below the ceiling
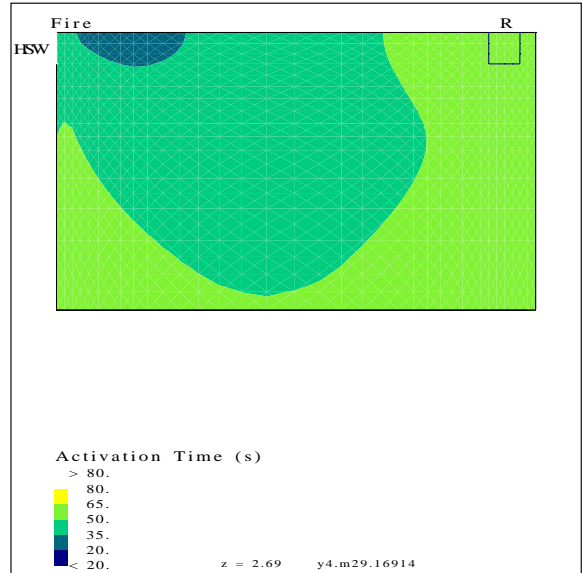
(b) At 0.05 m (2.0 in) below the ceiling
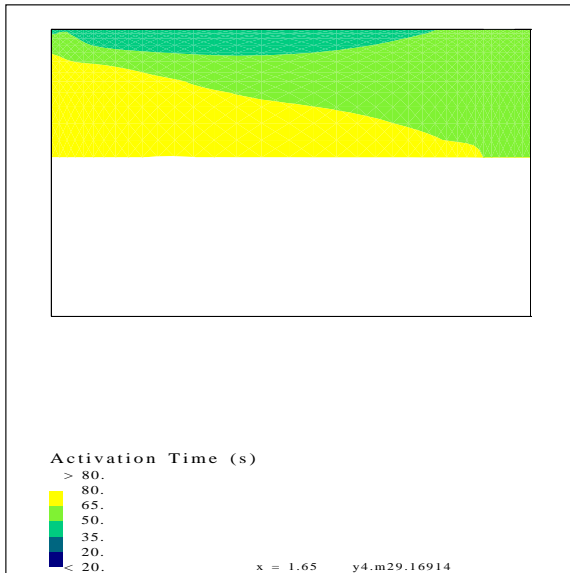

(c) Plane 1 m (3.3 ft) from plane of symmetry
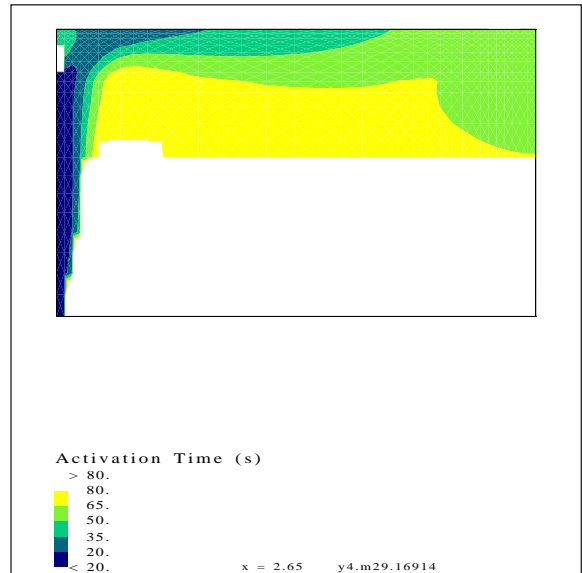
(d) Plane of symmetry

Figure 30: Simulated activation time in room type E4 from run 53.
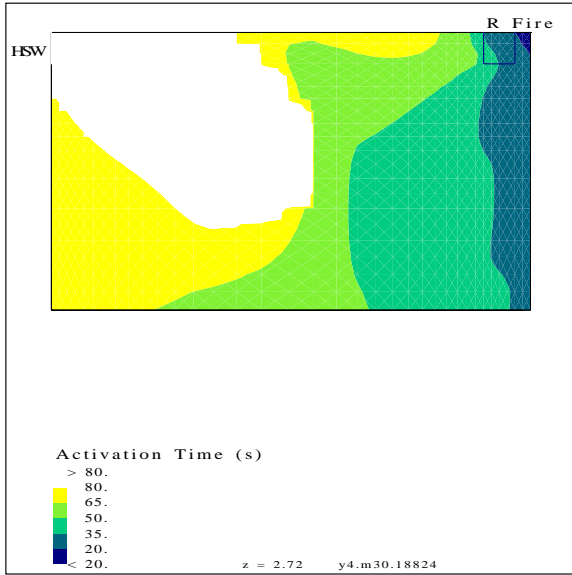
(a) At 0.02 m (0.79 in) below the ceiling
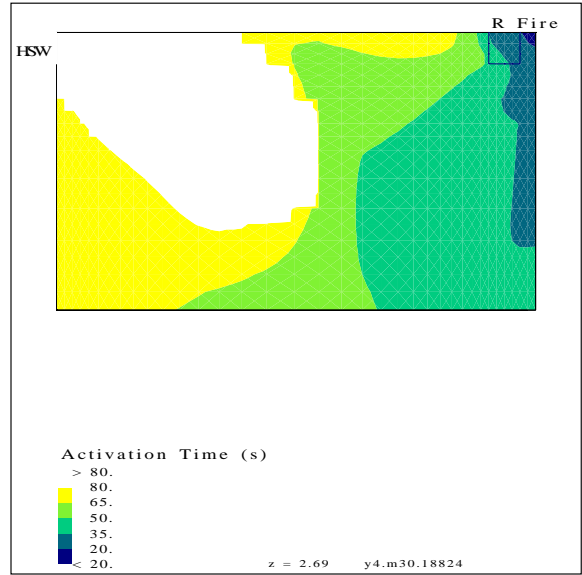
(b) At 0.05 m (2.0 in) below the ceiling
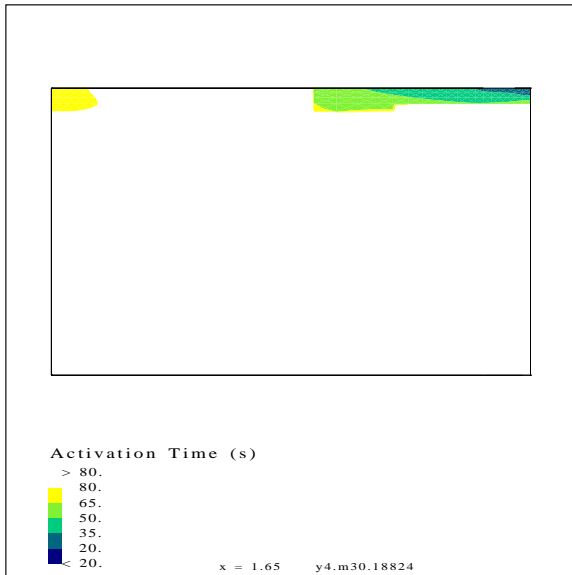
(c) Plane 1 m (3.3 ft) from plane of symmetry
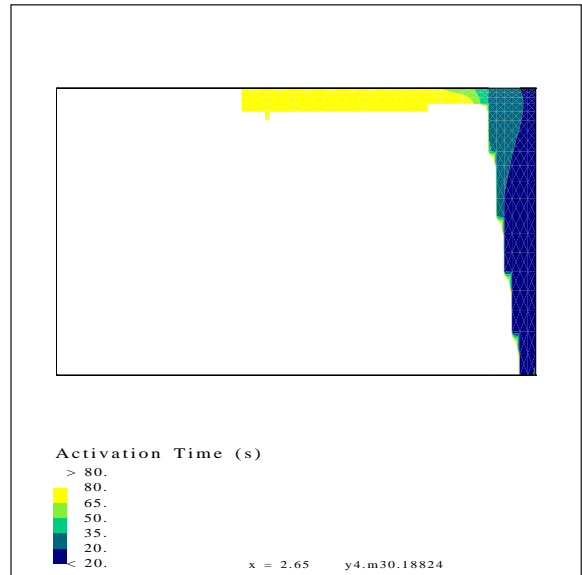

(d) Plane of symmetry

Figure 31: Simulated activation time in room type E4 from run 54.
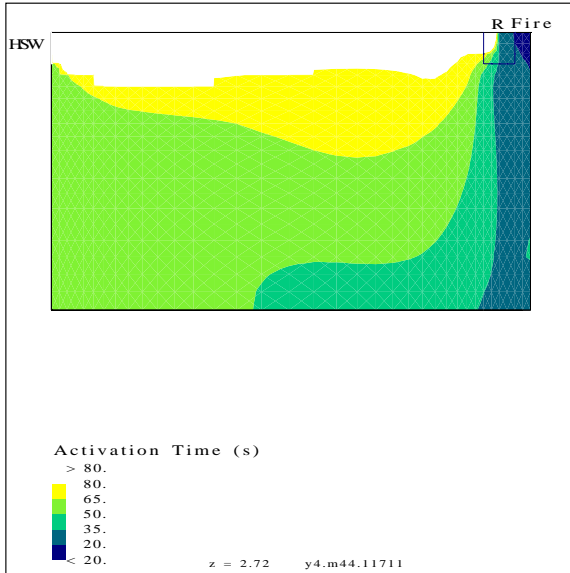
(a) At 0.02 m (0.79 in) below the ceiling
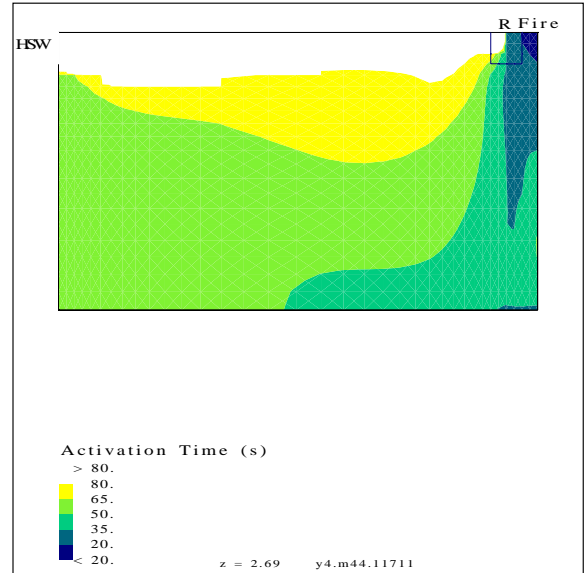
(b) At 0.05 m (2.0 in) below the ceiling
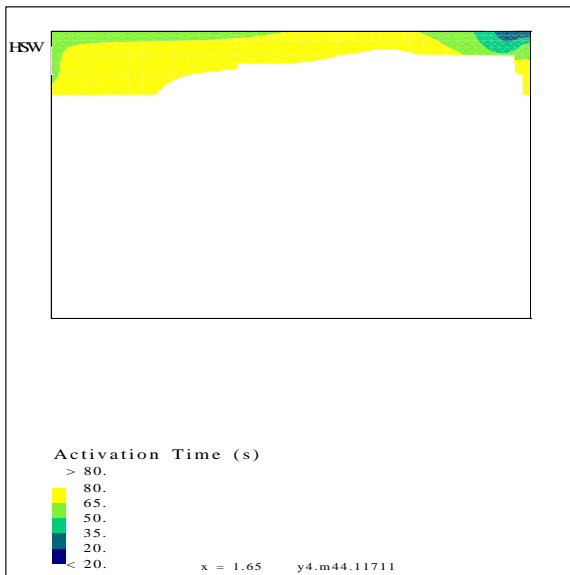
(c) Plane 1 m (3.3 ft) from plane of symmetry
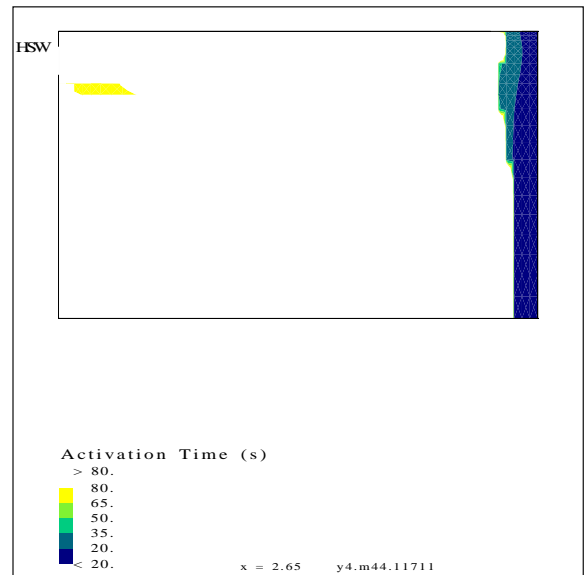
(d) Plane of symmetry

Figure 32: Simulated activation time in room type E4 from run 55.
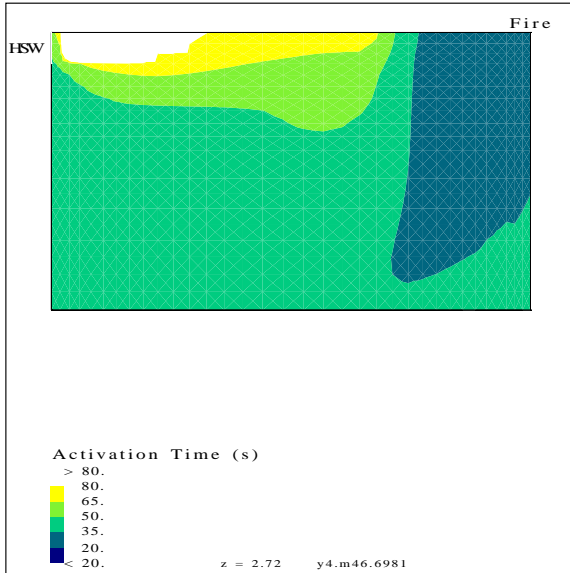
(a) At 0.02 m (0.79 in) below the ceiling
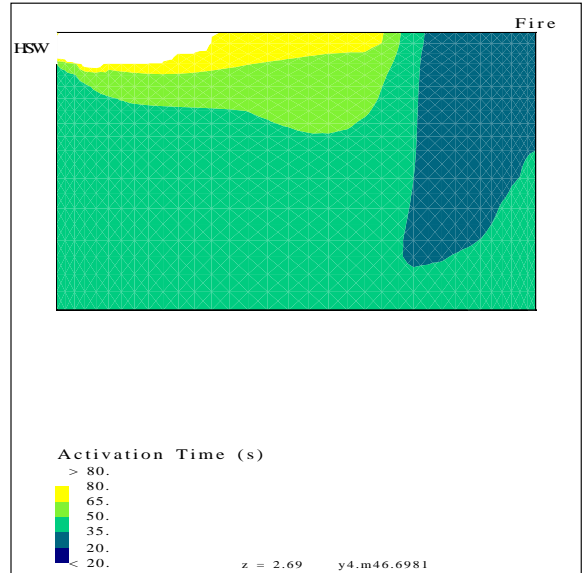

(b) At 0.05 m (2.0 in) below the ceiling
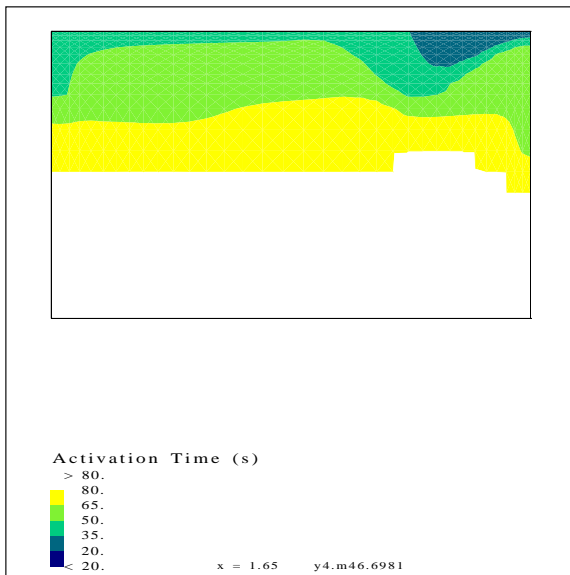
(c) Plane 1 m (3.3 ft) from plane of symmetry
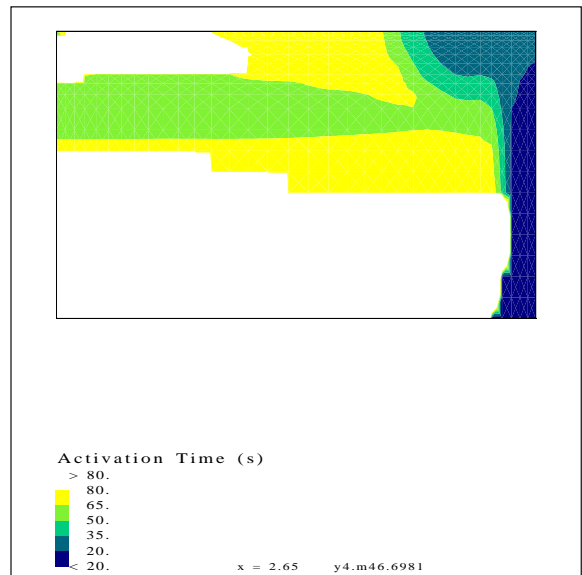
(d) Plane of symmetry

Figure 33: Simulated activation time in room type E4 from run 56.
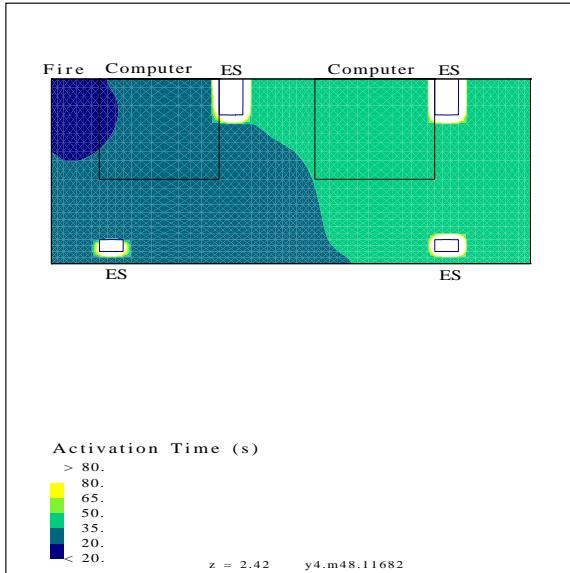
(a) At 0.02 m (0.79 in) below the ceiling
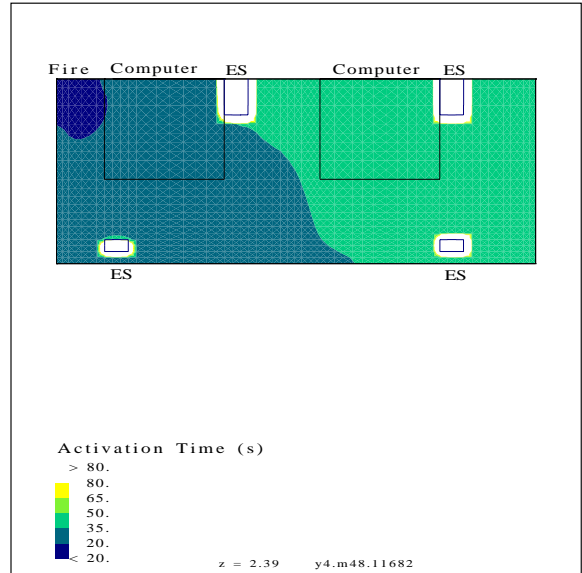
(b) At 0.05 m (2.0 in) below the ceiling
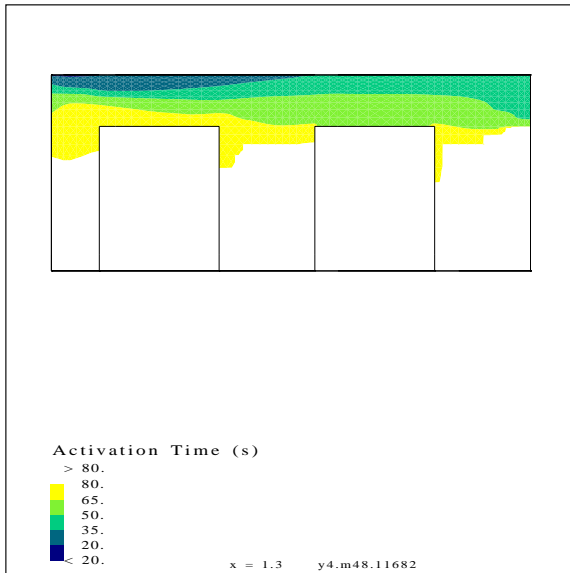
(c) Plane 1 m (3.3 ft) from plane of symmetry
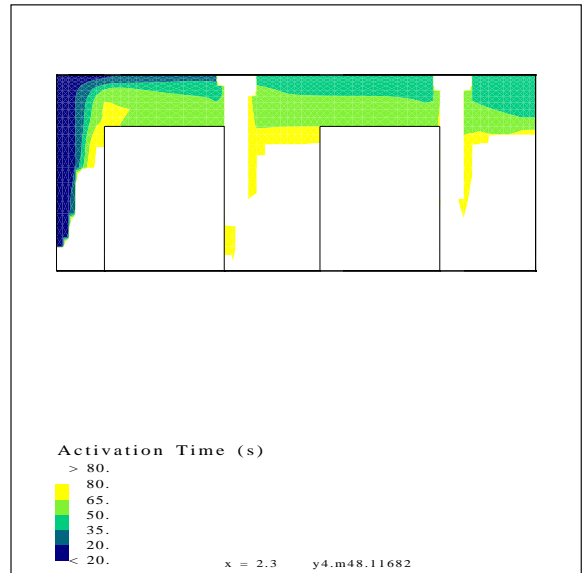

(d) Plane of symmetry

Figure 34: Simulated activation time in room type E5 from run 57.
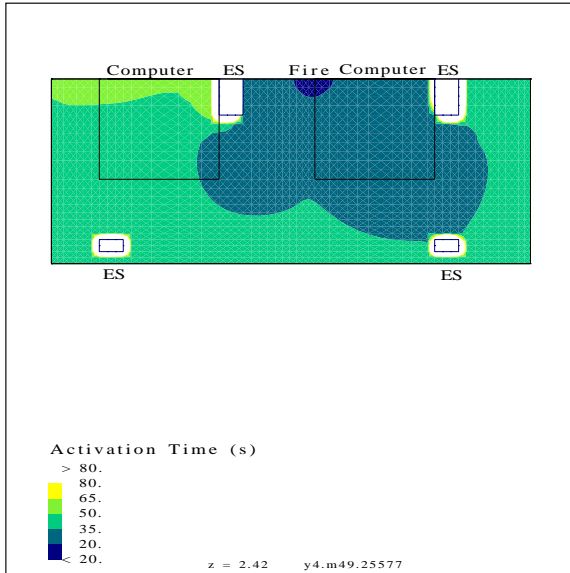
(a) At 0.02 m (0.79 in) below the ceiling
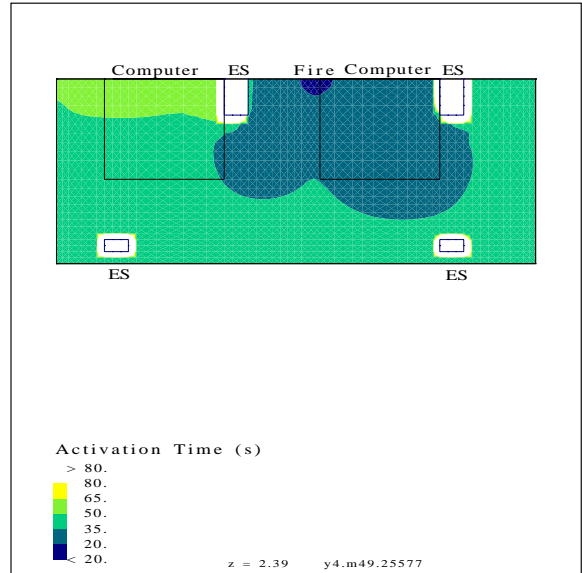
(b) At 0.05 m (2.0 in) below the ceiling
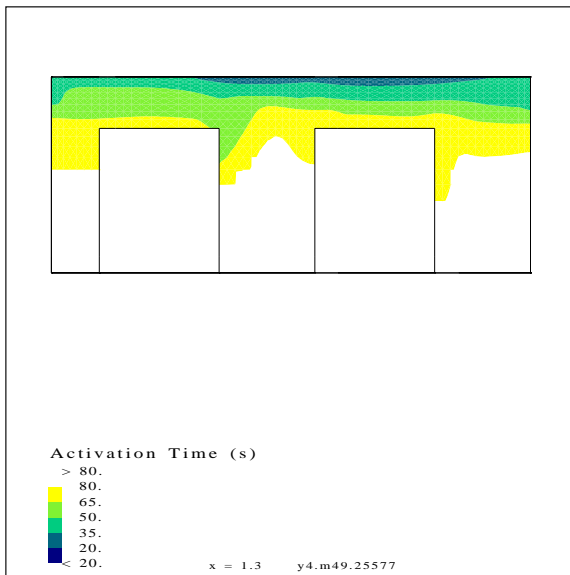
(c) Plane 1 m (3.3 ft) from plane of symmetry
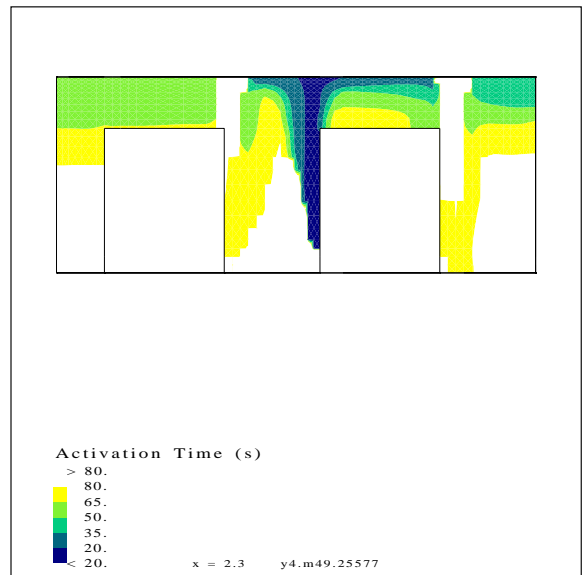
(d) Plane of symmetry

Figure 35: Simulated activation time in room type E5 from run 58.
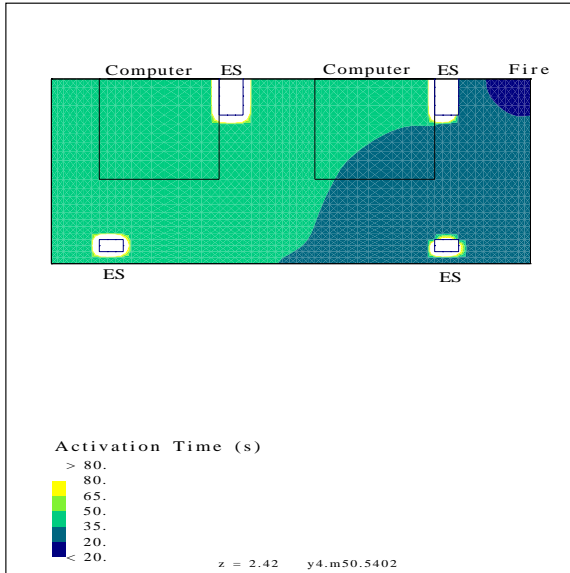
(a) At 0.02 m (0.79 in) below the ceiling
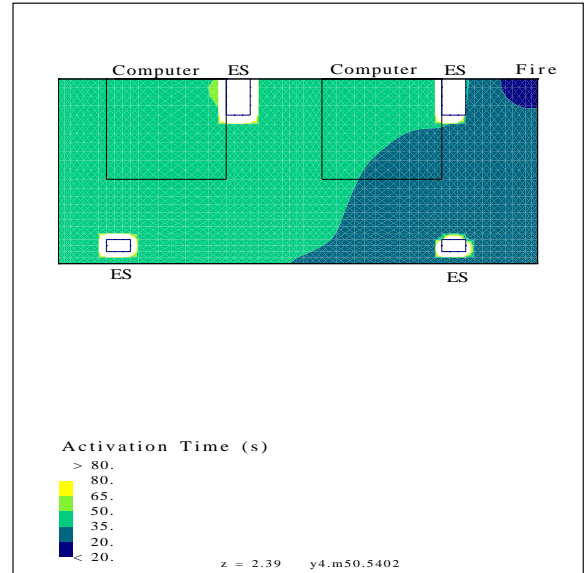
(b) At 0.05 m (2.0 in) below the ceiling
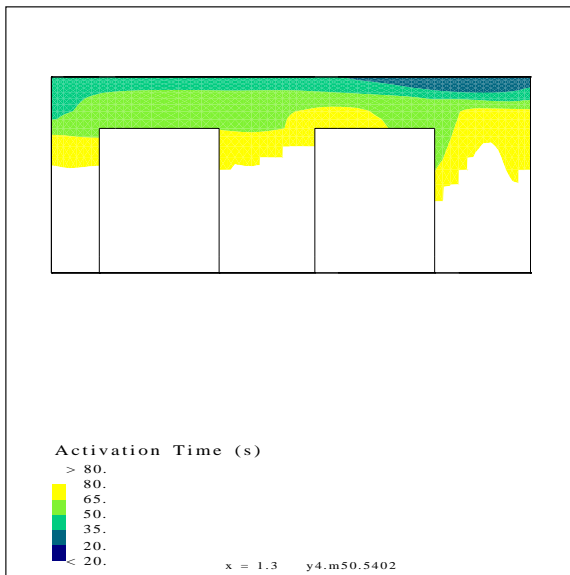

(c) Plane 1 m (3.3 ft) from plane of symmetry
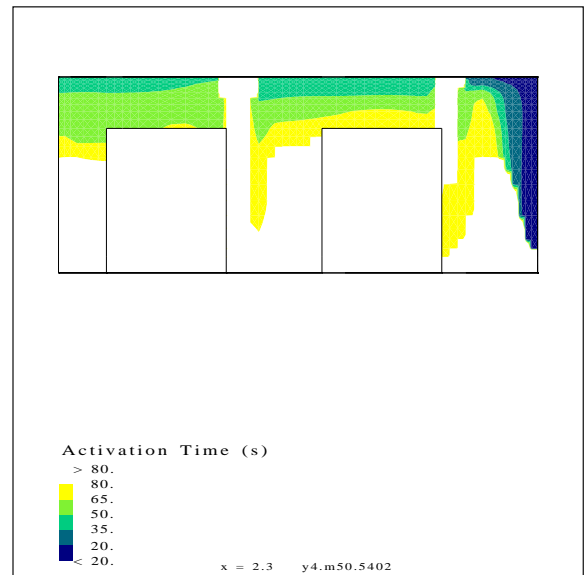

(d) Plane of symmetry

Figure 36: Simulated activation time in room type E5 from run 59.
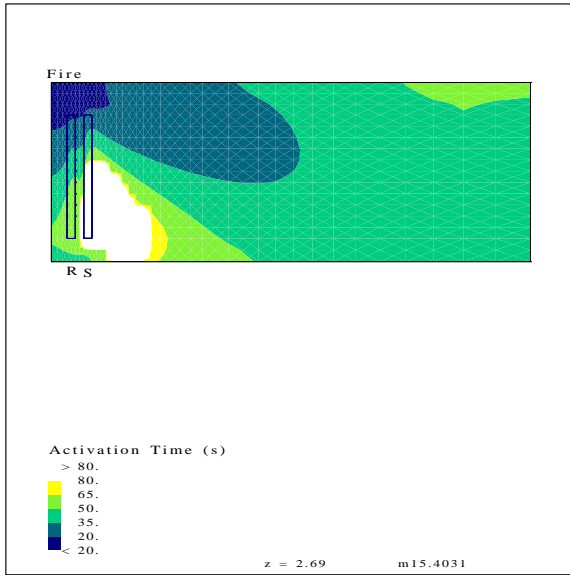
(a) Run 3
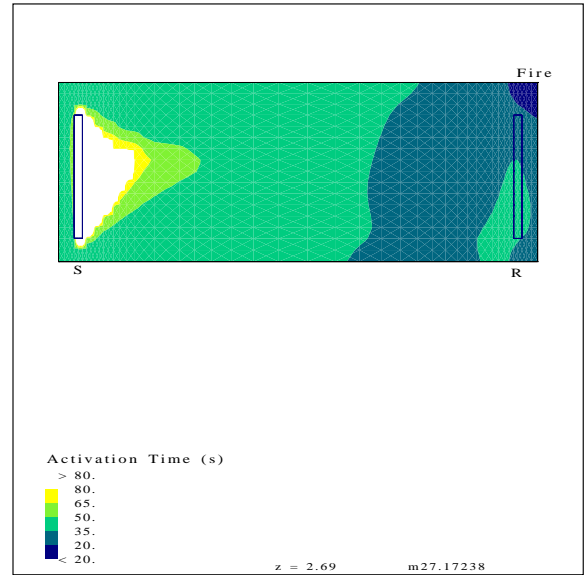
(b) Run 10
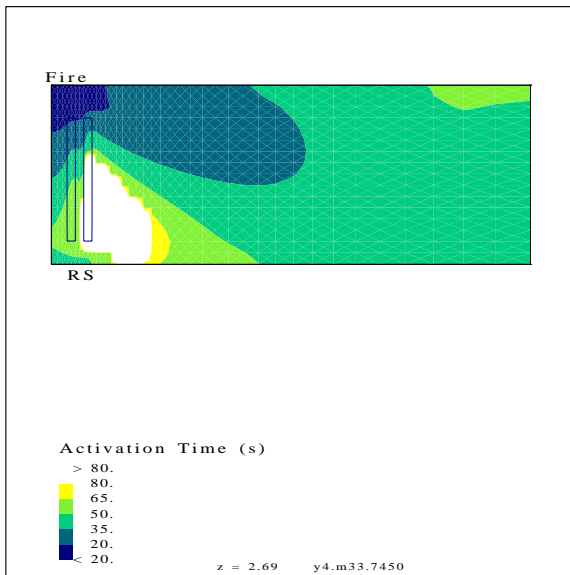
(c) Run 37
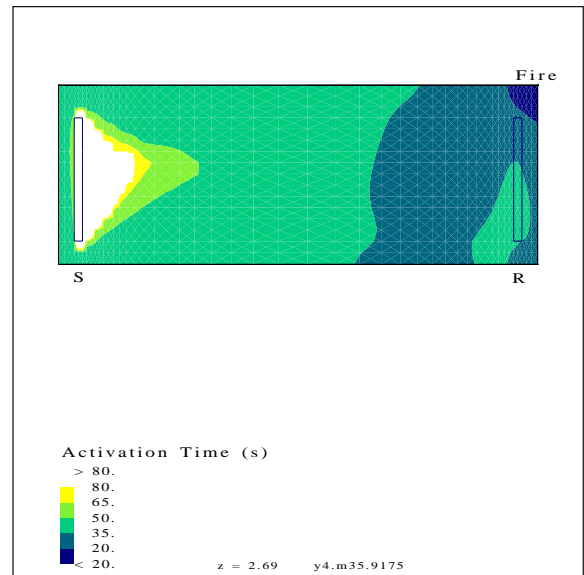
(d) Run 38

Figure 37: Comparison of simulated activation times with and without plenum return at 0.05 m (2.0 in) below the ceiling (runs 3, 10, 37, 38)
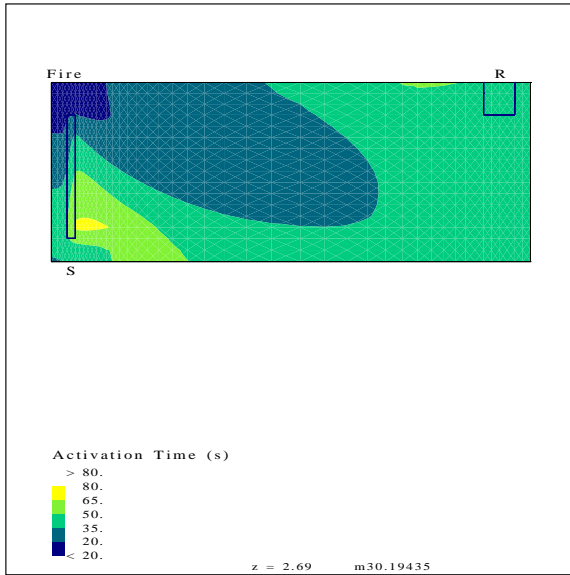
(a) Run 11
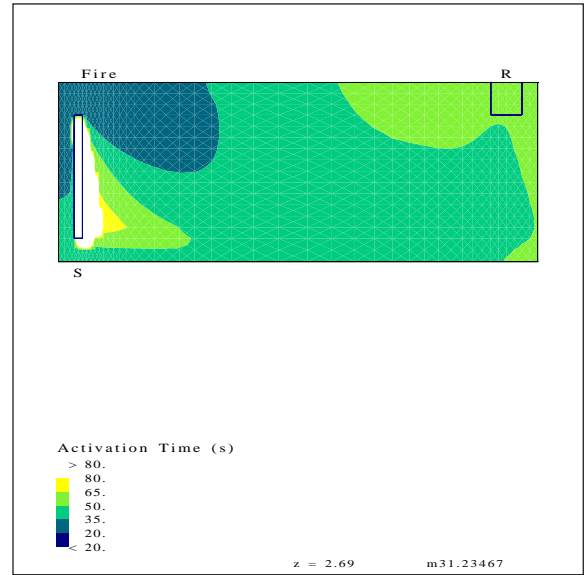
(b) Run 12
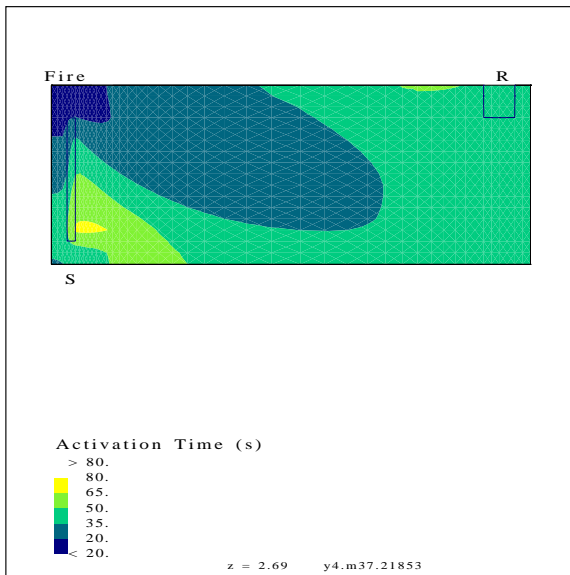
(c) Run 39
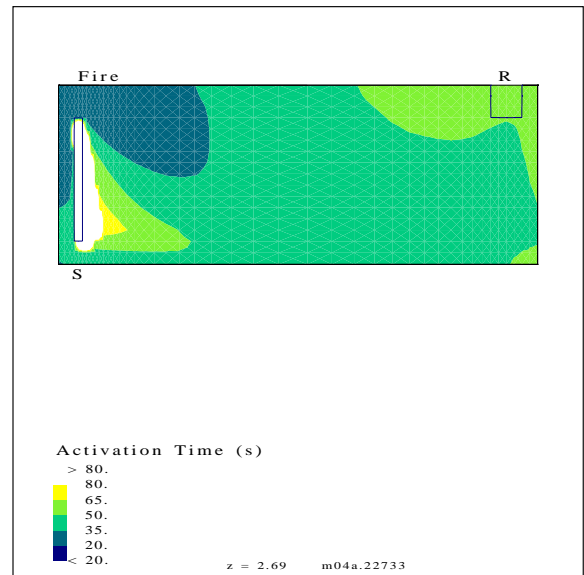
(d) Run 40

Figure 38: Comparison of simulated activation times with and without plenum return at 0.05 m (2.0 in) below the ceiling (runs 11, 12, 39, 40)
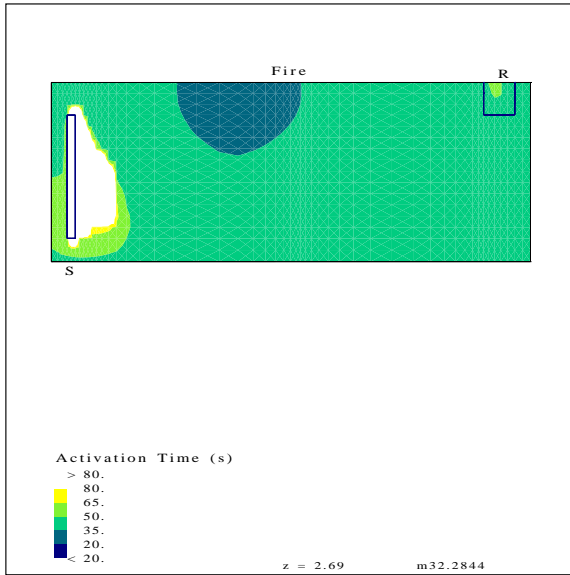
(a) Run 13
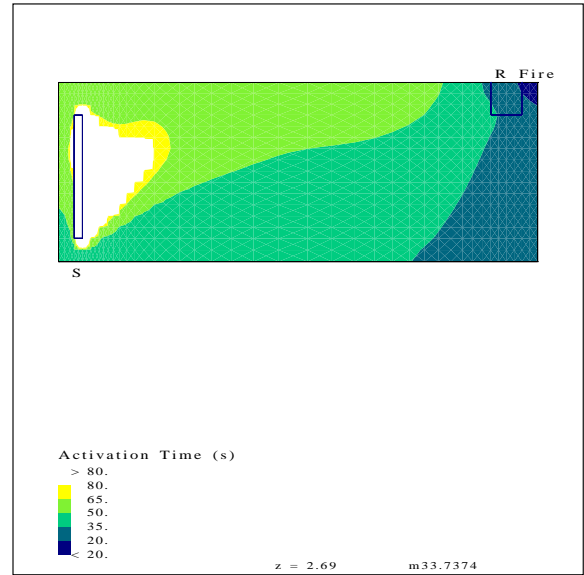
(b) Run 14
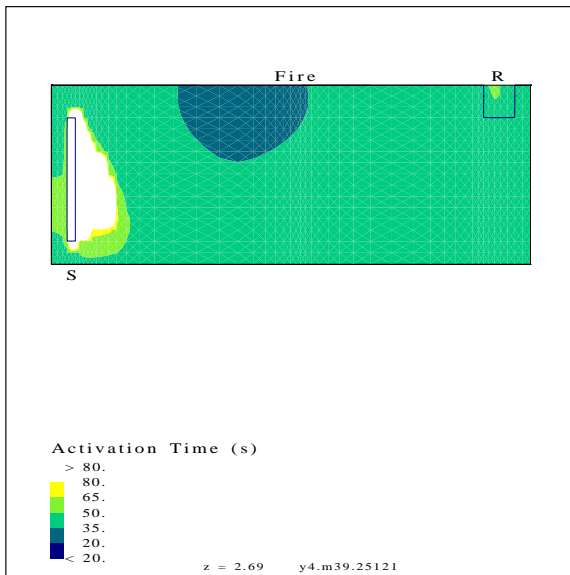
(c) Run 41
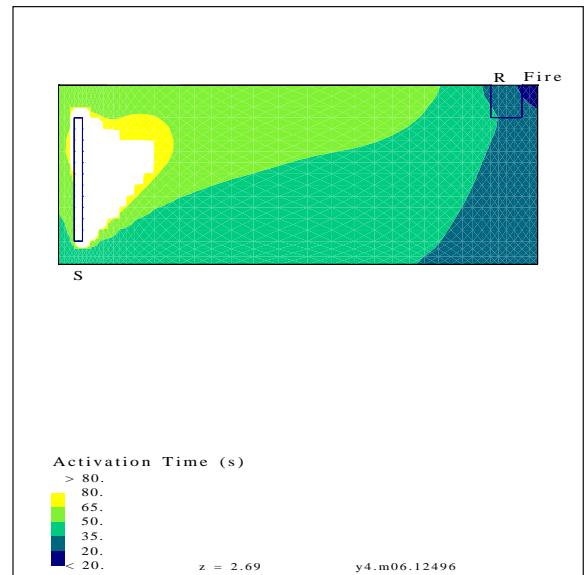
(d) Run 42

Figure 39: Comparison of simulated activation times with and without plenum return at 0.05 m (2.0 in) below the ceiling (runs 13, 14, 41, 42)
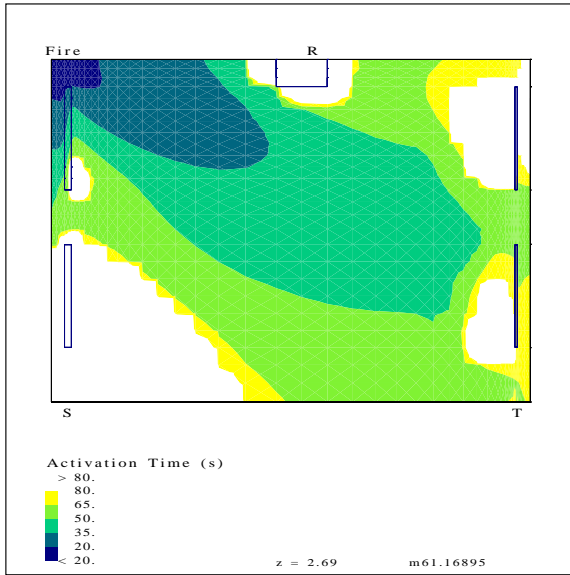
(a) Run 26
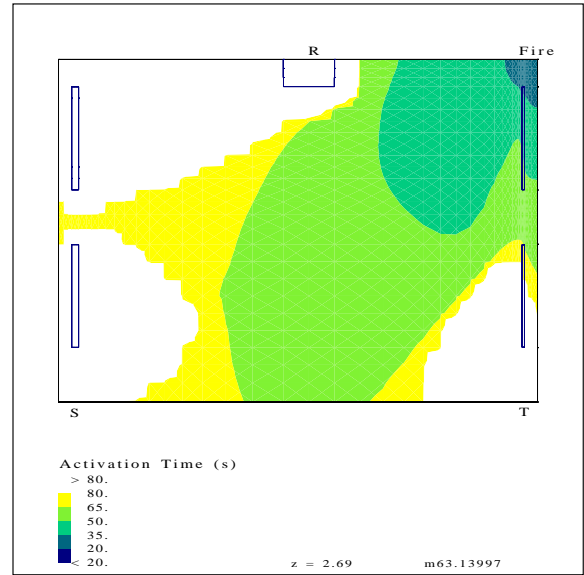
(b) Run 28
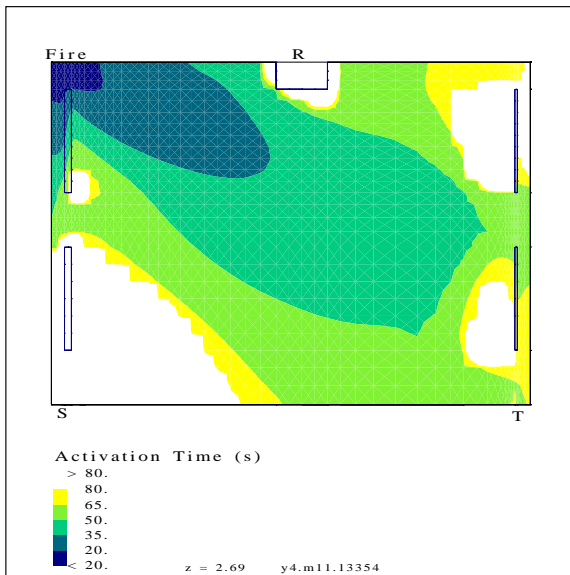
(c) Run 43
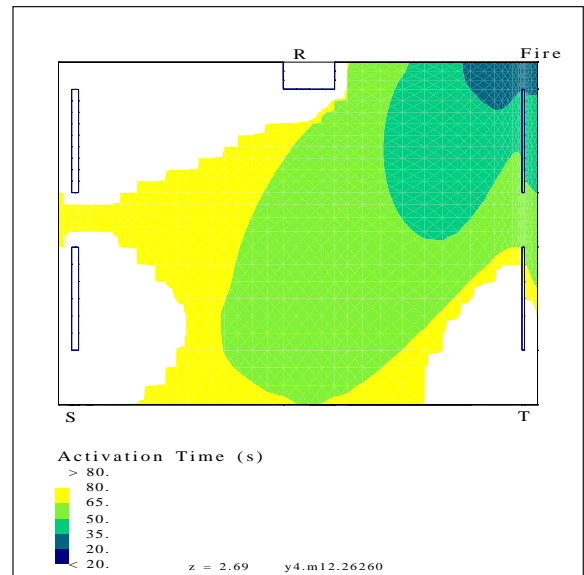
(d) Run 44

Figure 40: Comparison of simulated activation times with and without plenum return at 0.05 m (2.0 in) below the ceiling (runs 26, 28, 43, 44)
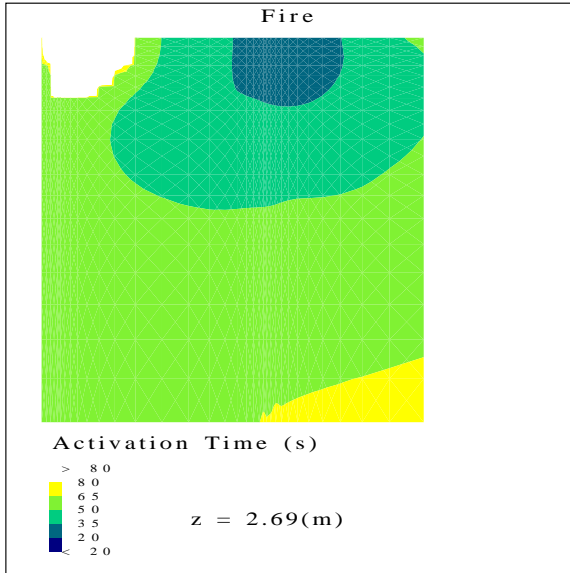
(a) Run 32 Grid - 0.05 m below the ceiling
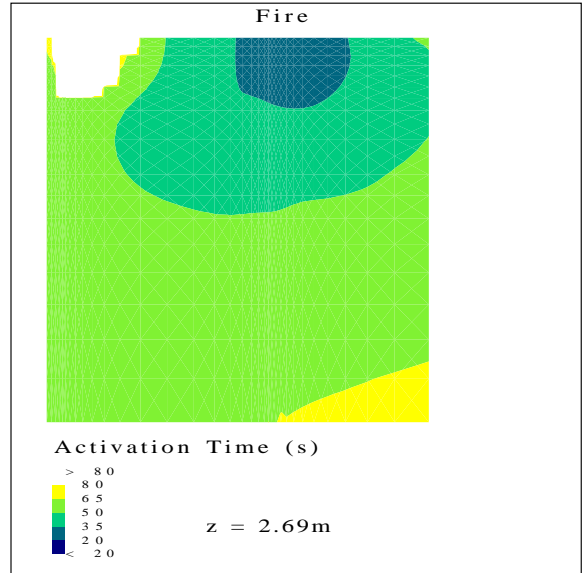
(b) Refined Grid - 0.05 m below the ceiling
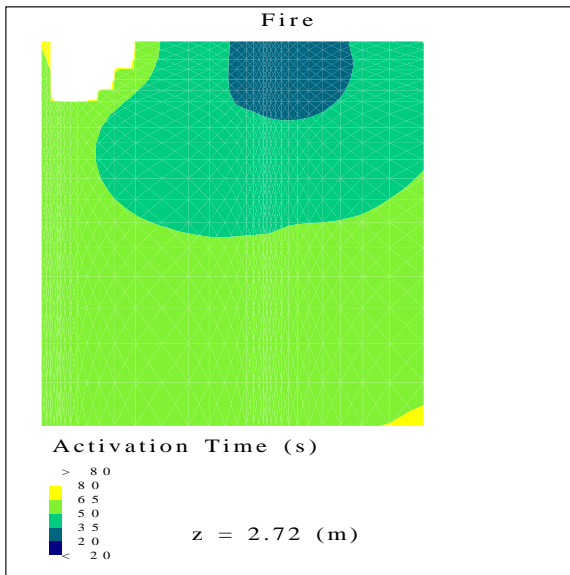
(c) Run 32 Grid - 0.02 m below the ceiling
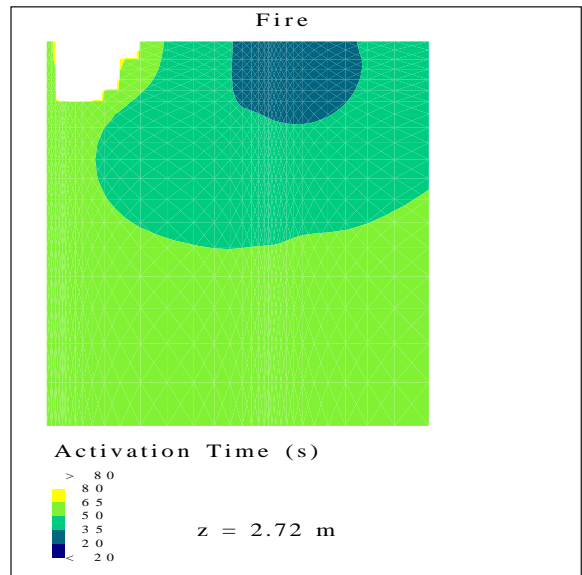
(d) Refined Grid - 0.02 m below the ceiling

Figure 41: Activation time comparisons for run 32 and refined grids.

Appendix A: *k*-ε Turbulence Model

In computational fluid dynamic (CFD) modeling, the space where flow is to be simulated is divided into a number of cells (or finite volumes), and the governing equations of fluid flow are solved numerically for each cell and for each time step of the simulation. The governing equations alone can be used to simulate the effects of turbulence on a scale larger than that of the cells. However, use of these flow equations alone cannot account for turbulence on a scale smaller than the cells. Turbulence modeling was developed to account for turbulence effects inside the cells. In such models a number of empirically developed partial differential equations are added to the flow equations which are solved for each cell and for each time step. Because turbulence models account for turbulent effects inside the cells, the number of cells needed for a particular application can be reduced.

The turbulence model used for this work is the *k*-ε model developed by Launder and Spalding [1] in the early seventies. This is probably the most extensively used turbulence model. The *k*-ε model is referred to as a two equation model, because it amounts to increasing the number of partial differential equations for the simulation by two. The purpose of this appendix is to provide introductory information about the *k*-ε model and provide the constants used in the simulations for this report.

The reader should be aware that a thorough knowledge of the *k*-ε model requires extensive understanding of graduate level fluid dynamics. For more information about CFD modeling and the *k*-ε model, readers are referred to Launder and Spalding and [2][3][4][5][6].

The effective viscosity, μ_{eff}, used in the governing equations is the sum of the kinematic viscosity, μ, and the turbulent viscosity, μ_T.

$$\mu_{eff} = \mu + \mu_T$$

It is assumed that

$$\mu_T = C_\mu \, \rho \, \frac{k^2}{\epsilon} \quad .$$

The transport equations for the turbulent kinetic energy, k, and the turbulent dissipation rate, ϵ, are

$$\frac{\partial \rho k}{\partial t} + \nabla \cdot (\rho U k) - \nabla \cdot \left(\left(\mu + \frac{\mu_T}{\sigma_k} \right) \nabla k \right) = P + G + \rho \epsilon$$

and

$$\frac{\partial \rho \epsilon}{\partial t} + \nabla \cdot (\rho U \epsilon) - \nabla \cdot \left(\left(\mu + \frac{\mu_T}{\sigma_\epsilon} \right) \nabla \epsilon \right) = C_1 \frac{\epsilon}{k} (P + C_3 \max(G,0)) - C_2 \rho \frac{\epsilon^2}{k} \quad .$$

In addition to defining k and ϵ, the above equations are the two added partial differential equations of the *k*-ε model.

The symbol ∇ is called the gradient, and it is written as

$$\nabla = i \frac{\partial}{\partial x} + j \frac{\partial}{\partial y} + k \frac{\partial}{\partial z} \quad ,$$

and the velocity vector is

$$U = u i + v j + w k$$

64

where $\boldsymbol{i}$, $\boldsymbol{j}$ and $\boldsymbol{k}$ are unit vectors in the x, y and z direction, and where u, v and w are the velocity components in the x, y and z direction. The operation $max(a,b)$ has the greater value of a or b.

The shear production, P, is defined as

$$P = \mu_{eff} \nabla \boldsymbol{U} \cdot (\nabla \boldsymbol{U} + (\nabla \boldsymbol{U})^T) - \frac{2}{3} \nabla \cdot \boldsymbol{U} (\mu_{eff} \nabla \cdot \boldsymbol{U} + \rho k) ,$$

where $(\nabla \boldsymbol{U})^T$ is the transpose of the tensor $\nabla \boldsymbol{U}$. For information about tensors readers are referred to [7][8][9][10].

The production, G, due to body force is defined as

$$G = - \frac{\mu_{eff}}{\rho \sigma_T} \boldsymbol{g} \nabla \rho .$$

The turbulent Prandtl number, σ_ϵ, is

$$\sigma_\epsilon = \frac{\kappa^2}{(C_2 - C_1)\sqrt{C_\mu}} .$$

Table A1 lists default values of the empirical coefficients and the values used in this study. The values used in this study are the same as the default values except for C_μ and C_3, which were shown by Nam and Bill [11] to result in somewhat improved plume simulation in comparison to simulations using the default coefficients.

Table A1.Values of constants used in turbulence equations

	Software Default	Used In This Paper
C_μ	0.09	0.18
C_1	1.44	1.44
C_2	1.92	1.92
C_3	0.0	1.0
K	0.4187	0.4187
σ_k	1.0	1.0

Nomenclature

C_μ	= constant
C_1	= constant
C_2	= constant
C_3	= constant
G	= production due to body force
k	= turbulent kinetic energy
P	= shear production
t	= time
U	= velocity vector
ϵ	= turbulent dissipation rate
K	= Von Karman constant
μ	= kinematic viscosity
μ_{eff}	= effective viscosity
μ_T	= turbulent viscosity
ρ	= density
σ_ϵ	= turbulent Prandtl number for ϵ
σ_k	= turbulent Prandtl number for k

References

[1]   Launder, B.E. and Spalding, D.B. The numerical computation of turbulent flows, Computer Methods in Applied Mechanics and Engineering, 3:269-289, 1974.

[2]   Abbott, M.B. and Basco, D.R. Computational Fluid Dynamics: An Introduction for Engineers, Wiley, New York, NY, 1989.

[3]   Anderson, D.A., Tannehill J.C. and Pletcher, R.H. Computational Fluid Mechanics and Heat Transfer, Hemisphere, New York, NY, 1984.

[4]   Hirsch, C. Numerical Computation of Internal and External Flows, Vol 2: Computational Methods for Inviscid and Viscous Flows, Wiley, New York, NY, 1990.

[5]   Hoffmann, K.A. Computational Fluid Dynamics for Engineers, Engineering Education System, Austin, TX, 1989.

[6]   Kumar, S. Mathematical Modelling of Natural Convection in Fire - A State of the Art Review of the Field Modelling of Variable Density Turbulent Flow, *Fire and Materials*, Vol 7, No 1, pp 1-24, 1983.

[7]   Aris, R. Vectors, Tensors, and the Basic Equations of Fluid Mechanics, Dover, NY, 1962.

[8]   Kay, D.C. Theory and Problems of Tensor Calculus, McGraw, New York, 1988.

[9]   Borisenko, A.I. and Tarapov, I.E. Vector and Tensor Analysis with Applications, Translated by R.A. Silverman, Dover, New York, 1968.

[10]   Hay, G.E. Vector and Tensor Analysis, Dover, New York, 1953.

[11]   Nam, S. and Bill, R.G. Jr. Numerical simulation of thermal plumes, *Life Safety Journal*, 21:231-256, 1993.

Appendix B: Smoke Generation and Mass Density of Smoke

Fundamental Equations

Two of the fundamental equations are examined below with the intent of providing insight into the relationship between smoke generation and mass density of smoke. For the simulations of this study, the energy equation was that for weakly compressible flow

$$\frac{\partial \rho H}{\partial t} + \nabla \cdot (\rho U H) - \nabla \cdot (\lambda \nabla T) = E \quad , \tag{1}$$

and the scalar equation was used for simulation of the mass density of smoke

$$\frac{\partial \rho \phi}{\partial t} + \nabla \cdot (\rho U \phi) - \nabla \cdot (\rho D_\phi \nabla \phi) = S \quad , \tag{2}$$

where

ρ = fluid density, kg/m^3,
H = total enthalpy of fluid, J/kg,
U = fluid velocity vector, m/s,
λ = fluid thermal conductivity, W/(m K),
T = fluid temperature, K,
t = time, s,
E = energy source term, W, which is approximated as a t-squared convective heat release rate.
ϕ = species mass fraction, dimensionless,
D_ϕ = mass diffusivity of species, m^2/s, and
S = species source term, $kg/(s\ m^3)$, which is approximated as a constant times the convective heat release rate.

The total enthalpy is

$$H = C_p T + \frac{1}{2} U^2 \tag{3}$$

where C_p is the specific heat of fluid, J/(kg K).

Equations (1) and (2) are similar. The third term on the left of equation (1) is the thermal diffusion term, and the third term on the left of equation (2) is the species diffusion term. The Lewis number is the ratio of thermal diffusion to species diffusion. If the Lewis number is one, equations (1) and (2) would be the same. In view of the similarity between the energy equation and the mass density equation, it should not be surprising that activation times calculated based of temperature rise were almost identical to those calculated by mass density for years 3 and 4 of this study.

Mass concentration calculations using equation (2) can be explained by analogy to water flow visualization by dye injection. To prevent the dye from affecting the water flow, the flow rate of the dye is small in comparison to the water flow. The dye flows downstream and mixes with the water. Downstream of the injection point, the dye can be observed, and dye concentration can be measured. The dye injection rate can be constant or it can vary with time. If the injection rate is multiplied by a constant, the dye concentration at every point in the flow field will by multiplied by that same constant (provided that the injection flow rate is still relatively small).

Physical Explanation of Species Calculation

In the CFD model, the species generation rate corresponds to the dye injection rate, and the mass density of species corresponds to the dye concentration. The species calculation is a perfect idealization of the dye injection experiment in the respect that the species generation rate adds no mass to the flow field. Thus a species calculation has absolutely no impact on the simulated flow field. As with the dye experiment, multiplication of the species generation rate by a constant results in multiplying the mass density at every point in the flow field by that same constant. Because this species calculation adds no mass to the flow field, this relationship between species generation and mass density is exact.

The species mass fraction approach is appropriate to simulate the flow of any species provided that the mass generation of the species and the differences in properties (specific heat, thermal conductivity and gas constant) due to the addition of species have an insignificant effect on the fluid flow. Two assumptions that are fundamental to most fire modeling are (1) that the mass released into the flow field due to the combustion process is so small in comparison to the total fire plume flow that this mass release (or mass generation) can be neglected, and (2) that the differences in properties of air and those of the mixture of air and combustion products do not have a significant effect on the flow. By these same assumptions, the species mass fraction approach is appropriate for simulation of the gases and particulates produced by the fire.

The smoke particles are assumed to move with the fluid flow and the effects of particle deposition on the walls and agglomeration resulting from particles colliding and sticking are not included.

Another way of expressing the relationship between species generation and mass density is to state that they are normalized. The characteristics of this normalization can be summarized as:

1. Multiplication of the species generation rate by a constant results in multiplying the mass density at every point in the flow field by that same constant.

2. The species generation and mass density are independent of units. The species generation and the mass density can be considered dimensionless, or they can be considered as being in any convenient units.

Species generation and the mass density can be considered dimensionless, with one unit of mass being "generated" or marked per kilowatt of convective heat released by the fire. In year 3 [1], a normalized mass density activation criteria was calibrated to be equivalent to activation based on a 13 °C (23 °F) temperature rise. Smoke was generated at a rate of one non-dimensional unit of mass per second per kW of convective heat released.

Dimensional Variables

Because some engineering practitioners might prefer an alternate approach using dimensional variables, the conditions of detector activation and smoke generation for the simulations of years 3 and 4 of this study can be stated as:

1. mass density of smoke at activation is $m_{a1} = 0.021$ g/m^3, and
2. smoke generation rate per unit of heat release is $m_{g1} = 0.0024$ g/(s kW).

These values were calculated in appendix B of the year 3 report and are based on the normalized smoke concentration found to be equivalent to the 13 °C (23 °F) activation criteria used in the year 1 and 2 reports. The value of the mass density of smoke at activation, 0.021 g/m^3, corresponds to an optical density of 0.07 m^{-1}. The smoke generation rate per unit heat release, 0.0024 g/(s kW), is the rate at which smoke must be generated by the fire in order to produce a 0.07 m^{-1} optical density in a computational volume when the gas temperature in that volume reaches 13 °C (23 °F).

For a simulation with specific geometry, HVAC supply, HVAC return and heat release due to fire; these conditions determine activation time throughout the flow field. Further, there are alternative conditions that result in the same activation times, and these conditions can be related as

$$\frac{m_{a1}}{m_{g1}} = \frac{m_{a2}}{m_{g2}} \tag{4}$$

where

m_{a1} = mass density at activation for condition 1, g/m^3;
m_{a2} = mass density at activation for condition 2, g/m^3;
m_{g1} = mass generation for condition 1, $g/(s\ kW)$; and
m_{g2} = mass generation for condition 2, $g/(s\ kW)$.

For the year 3 and 4 simulations, the mass density of smoke at activation of $0.021\ g/m^3$ is approximately equivalent to a detector that goes into alarm when the smoke reaches an optical density of $D_1 = 0.07\ m^{-1}$ (example 1, appendix B reference 1). For alternate conditions of detector activation and smoke generation, the corresponding optical density is

$$\frac{D_1}{m_{a1}} = \frac{D_2}{m_{a2}} \tag{5}$$

where

D_1 = optical density at activation for condition 1, m^{-1}; and
D_2 = optical density at activation for condition 2, m^{-1}.

Optical density per unit distance is

$$D = -\frac{\log_{10}(I_x/I_o)}{x} \tag{6}$$

where

D = optical density per unit distance, m^{-1},
I_o = intensity of light at the beginning of the path length,
I_x = intensity of light remaining after it has passed through the path length,
x = path length the light travels, m.

The units of light intensity are arbitrary, and such units are unnecessary for the discussion that follows. The extinction coefficient per unit length is

$$K = -\frac{\log_e(I_x/I_o)}{x} \tag{7}$$

where K is the extinction coefficient with units of m^{-1}. The two coefficients are related as

$$D = \frac{K}{2.3} \tag{8}$$

The extinction coefficient can also be expressed as

$$K = K_m m \tag{9}$$

where
K_m = specific extinction coefficient, m^2/g,
m = mass concentration of smoke, g/m^3.

Small scale experiments on wood, cellulose and plastics by Seader and Einhorn [2] resulted in average values of K_m of 7.6 m^2/g for smoke produced by flaming combustion and of 4.4 m^2/g for smoke produced by non-flaming combustion. However, only the value for flaming combustion is relevant to this project. The relationship of Seader and Einhorn was used in year 3 to estimate the previously stated equivalency between mass density and optical density of smoke at activation.

Various Fire Sizes

For a t-squared fire, the convective heat released by the fire was

$$Q_c = C_s\, C_c\, 1055 \left(\frac{t}{t_g} \right)^2 \tag{10}$$

where
Q_c = convective heat release rate, kW,
C_s = symmetry factor,
C_c = convective fraction of heat release,
t = time from ignition, s,
t_g = growth time, s.

Because all the fires were on the plane of symmetry, a symmetry factor of ½ was used. A convective factor of 0.65 was used, and a growth time of 275 s was used. The fire was modeled by releasing energy over several grid cells. The number of cells occupied by the fire was varied during the simulation such that the heat release rate per unit volume would not exceed 2.6 kW/m^3.

The simulations of years 3 and 4 can be extended for different t-squared fires provided that detector activation is dominated by the ceiling jet and that the developing hot layer has an insignificant impact on activation. Consider a second fire described as

$$Q_{c2} = C_{s2}\, C_{c2}\, 1055 \left(\frac{t_2}{t_{g2}} \right)^2 \tag{11}$$

where
Q_{c2} = convective heat release rate of the second fire, kW,
C_{s2} = symmetry factor of the second fire,
C_{c2} = convective fraction of heat release of the second fire,
t_2 = time from ignition of the second fire, s,
t_{g2} = growth time of the second fire, s.

In adjusting simulation time, the simulation geometry remains unchanged as does the symmetry factors ($C_{s2}=C_s$). Corresponding time is when the convective heat release rates are the same for both fires ($Q_c=Q_{c2}$). Equating equations (1) and (8) and canceling like terms results in

$$t_2 = t \frac{t_{g2}}{t_g} \sqrt{\frac{C_c}{C_{c2}}} \qquad\qquad (12)$$

When the convective fraction of the first fire is the same as that of the second fire, the above equation becomes

$$t_2 = t \frac{t_{g2}}{t_g} \qquad\qquad (13)$$

In the absence of well defined application criteria for this equation, it is suggested use of it be restricted to (t_{g2}/t_g) from 0.5 to 2.

Example 1:

For a detector that goes into alarm at an optical density of 0.1 m⁻¹, what conditions of detector activation and smoke generation would result in the same activation times as the simulations of years 3 and 4 of this study?

Rearranging equation (5): the mass density at activation is

$$m_{a2} = m_{a1} \frac{D_2}{D_1} = 0.021 \frac{0.1}{0.07} = 0.03 \text{ g/m}^3$$

Rearranging equation (4): the mass generation is

$$m_{g2} = m_{g1} \frac{m_{a2}}{m_{a1}} = 0.0024 \frac{0.03}{0.021} = 0.0034 \text{g/m}^3$$

Example 2:

Assuming the convective fraction is unchanged, how does a faster fire growth time of $t_g = 190$ s affect the simulated activation time?

From equation (13), the times are related as

$$t_2 = t \frac{t_{g2}}{t_g} = t \frac{190}{275} = 0.69 \, t$$

Where 80 seconds is shown on one of the activation time figures in the paper, the adjusted time would be $(80)(.69) = 55$ seconds.

This is used to adjust the time scale on the activation time figures as follows:

Existing Scale	Adjusted Scale
> 80	> 55
80	55

72

65	45
50	35
35	24
20	14
< 20	< 14

The adjusted scale above can be used with any of the activation time figures in the report to see the pattern of activation resulting from a fire with a growth time of 190 seconds.

References

[1]   Klote, J.H., Forney, G.P., Davis, W.D., Bukowski, R.W. Simulating the effect of HVAC induced air flow from slot diffusers on detector response, 1996. Available from the National Fire Protection Association, Batterymarch Park, Quincy, MA.

[2]   Seader, J. and Einhorn, I., Some physical, chemical, toxicological, and physiological aspects of fire smoke, National Science Foundation Report PB83-2502, July 1976.

Appendix C: HVAC Diffusers and Returns

Supply Air Outlets

Air velocities leaving diffusers are normally much greater than those acceptable for human comfort. Depending on the current status of heating or cooling, the temperature of supplied air may be above or below that of the occupied space. Diffuser jets mix with room air by entrainment, which reduces air velocity and equalizes air temperature. The approach normally taken to promote human comfort is to restrict the high velocity portion of a diffuser jet to spaces that are not normally occupied, and to rely on mixing to produce relatively uniform air velocity and temperature in spaces that are normally occupied.

The following classification of outlets and principles of air diffusion are adapted from the ASHRAE Fundamental Handbook [1] and Straub *et al.* [2]. Straub classified outlets into the following groups:
Group A: Outlets mounted in or near the ceiling that discharge air horizontally.
Group B: Outlets mounted in or near the floor that discharge air vertically in a nonspreading jet.
Group C: Outlets mounted in or near the floor that discharge air in a vertical spreading jet.
Group D: Outlets mounted in or near the floor that discharge air horizontally.
Group E: Outlets mounted in or near the ceiling that project primary air vertically.

Figures C1 through C5 show the room air motion characteristics of the five outlet groups; exterior walls are depicted by heavy lines. The principles of air diffusion emphasized by Straub's tests are:

1.   The primary air (shown by clear envelopes in figures C1-C5) from the outlet down to a velocity of about 0.75 m/s (150 fpm) can be treated analytically. The heating or cooling load has a strong effect on the characteristics of the primary air.

2.   The total air, shown by diagonally lined envelopes in the figures is influenced by the primary air and is of relatively high velocity [but less than 0.75 m/s (150 fpm)], with air temperatures generally within 0.5 °C (1 °F) of room temperature. The total air is also influenced by the environment and drops during cooling and rises during heating; it is not subject to precise analytical treatment.

3.   Natural convection currents form a stagnant zone from the ceiling down during cooling, and from the floor up during heating. This zone forms below the terminal point of the total air during heating and above the terminal point during cooling. Since this zone results from natural convection currents, the air velocities within it are usually low [approximately 0.1 m/s (20 fpm)], and the air stratifies in layers of increasing temperature. The concept of a stagnant zone is important in properly applying and selecting outlets, since it considers the natural convection currents from warm and cold surfaces and internal heating and cooling loads.

4.   A return inlet affects the room air motion only within its immediate vicinity. The intake should be located in the stagnant zone to return the warmest room air during cooling or the coolest room air during heating. The importance of the location depends on the relative size of the stagnant zone that results from various types of outlets.

5.   The general room motion (shown by clear areas in the figures) is a gentle drift toward the total air. Room conditions are maintained by the entrainment of the room air into the total airstream. The room air motion between the stagnant zone and the total air is relatively slow and uniform. The highest air motion occurs in and near the total airstream.

Group A outlets blow air under the ceiling, and their potential for impacting the performance ceiling detectors is of concern. Accordingly, most of the outlets studied in this project were group A. This group includes high sidewall grills, ceiling diffusers, linear ceiling diffusers, and linear wall diffusers. The high sidewall grills and the ceiling diffusers are shown in figure C1. Slot diffusers and light troffers are the common in commercial properties when used in variable air volume HVAC systems. Variable air volume systems are popular for their energy efficiency and comfort features. Light troffers are a common form of slot diffuser located on the sides of ceiling lights.

Because there is a concern that airflow from group E outlets could block smoke flow at the ceiling, some group E outlets were included in the study. It should be noted that the outlet group refers to resulting airflow pattern in the rooms not the kind of grill or diffuser used on the outlet. While manufacturers make hundreds of different designs of diffusers and grills, a few of the more common types are illustrated in figure C6. Additional information about diffusers and grills is provided by Straub [3]. A particular diffuser or grill could be applied to many of the outlet groups. Further, it is possible to field adjust many group A outlets into group E outlets. Some slot diffusers can automatically adjust themselves so that the perform as group A outlets for cooling and group E outlets for heating. Eggcrate grills are used for some group E outlets in computer rooms which makes them appear similar to ceiling returns.

HVAC System Noise

This section provides introductory information about HVAC system noise and noise considerations relating to HVAC diffusers and returns. Equipment such as fans, chillers, rooftop air conditioning units are sources of noise. Other common sources of HVAC system noise are airflow in ducts, dampers, duct bends, supply diffusers and returns. Because of the complexity of this topic, the information in this section very limited. Readers desiring further information about HVAC noise are referred to the ASHRAE Applications Handbook [4] and the ASHRAE Fundamentals Handbook [5].

The primary method used to determine the acceptability of background HVAC-related noise is the room criterion (RC) rating. This method takes into account the noise energy at various frequencies, and details of calculation of the RC rating are described in the ASHRAE Application Handbook. Noise that has an excess of high-frequency sound energy will have a "hissy" quality, and noise that has an excess of low-frequency sound energy will have a "rumble" quality. Noise that has no particular identity with frequency is classified as neutral, and such noise is usually bland and unobtrusive. When background noise is neutral, (N) is placed after the RC rating.

Sound associated with HVAC systems is usually considered part of the background sound in a building. Acceptable background sounds must neither noticeably mask sounds people want to hear nor be otherwise intrusive or annoying in character. In an office environment, the acceptable levels of background noise are determined by speech requirements. However, in a concert hall, background noise is governed by the need to avoid masking the faintest sounds likely to occur in a performance. Table C1 lists normally acceptable HVAC background sound levels for a variety of space uses.

Room air terminal devices such as grilles, registers, diffusers and light troffers are usually rated by the manufacturer for noise generation. Ideally, the air terminal device is selected to meet the RC rating for the specific application keeping in mind that the manufacturer's RC rating is measured with a uniform velocity over the face of the terminal device. If a balancing damper is installed immediately before a diffuser, this will result in non-uniform face velocity and increased noise generation at the diffuser. Table C2 gives typical velocities at supply outlets and return air openings needed to achieve specified RC ratings, but specific terminal devices may be significantly different especially if they are in close proximity to dampers.

Returns

All of the ceiling returns of year 4 included simulation of a section of plenum. For the open plan rooms, the return was simulated by an opening sized for an average velocity of 2 m/s (400 fpm) except for runs 45 and 46 which were at 3 m/s (600 fpm). From table C1, the range ASHRAE guideline for HVAC system noise for most rooms of office building is in the range of 25 to 35 RC, and from table C2 it can be observed that the approximate noise produced by the above return flows is in the same range of room criterion. The return area was taken to represent an eggcrate return [figure C6 (a) and (b)] which is almost all open space. Because this return is almost all open space, the velocity in an eggrate return is nearly the same as that in the open return space that was simulated. Also, these simulations are applicable for holes in the ceiling such as missing ceiling tiles.

As discussed in the report, there were non-activation areas around ceiling returns in the open plan rooms. This paragraph discusses the flows in the vicinity of the return of run 45 with the intent of providing some insight into these non-activation areas. The average velocity at this return is 3 m/s (600 fpm). Figure C7 shows the velocity vectors at the start of the simulation in the plane of symmetry near the return. It can be seen from this figure that the air is flowing toward the return in all directions below the ceiling. Figure C8 shows the velocity vectors at the end of this simulation in the plane of symmetry near the return. The same velocity trends occur at the beginning and at the end of the simulation. Figure C8 also shows that activation at 80 s does to reach the return. A possible explanation of the mechanism responsible for non-activation near these returns is that, in the vicinity of the return, the ceiling jet is diluted by flow from below the jet going toward the return. This dilution tends to delay activation near the return.

Slot Diffusers and an Idealized Model

Simulations of this project included the following diffusers: slots, light troffers, high sidewall, and rectangular group E outlets. This section addresses the slots and light troffers, and the other diffusers are discussed later.

If computer memory and running time were not concerns, the best way to simulate a slot diffuser would be model the flow inside the diffuser along with the rest of the room simulation. Because this approach would approximately double the number of cells in the simulation, another method was needed. Most computer simulations of room airflow have used constant velocity at the supply outlet to model HVAC supply (for example [6][7][8][9][10][11]). While these references have some information about CFD simulation of the effects of wall diffusers, there is no corresponding information about ceiling mounted slot diffusers.

This section describes the idealized slot diffuser model that was used for years 3 and 4 of this project. Because troffer diffusers are similar to slot diffusers, this model was also used for the troffers.

The intent of ceiling mounted slot diffusers is to discharge the air in a direction such that the flow attaches itself to the ceiling. This attached flow is referred to as Coanda effect [12], and this effect is often desired in HVAC applications to prevent supply jets from blowing on occupants. The mass flow rate of supply air is

$$\dot{m} = \rho \, h \, L \, V_z \qquad (15)$$

where

$\dot{m}$ = mass flow rate,
ρ = supply air density,
h = slot width,
L = slot length,
V_z = downward component of outlet velocity.

The component of outlet velocity in the ceiling direction is

$$V_x = \frac{V_z}{\tan \theta} \qquad (16)$$

76

where
V_x = component of outlet velocity in the direction of the ceiling,
θ = discharge angle between inlet velocity and the ceiling.

This idealized model is intended to result in computer simulated flows near the ceiling that are representative of those produced by slot diffusers. However, this model does not simulate flow details within the diffuser. Accordingly, values h and θ should not be considered the values of an actual diffuser. The values of h and θ should be thought of as parameters of the idealized model that can be adjusted to yield HVAC jet flows that are desired for the simulations. The idealized model is illustrated in figure C9. CFD simulations showed that for discharge angles of about 45° or less, the jet was attached to the ceiling.

The throw of a jet is the distance that the jet travels for it to slow down to a particular speed. Manufacturers supply throw data for many diffusers, and common values are for velocities of 0.25, 0.5 and 0.75 m/s (50, 100 and 150 fpm). The throw is represented by L_v, where v is the value of the velocity. Accordingly, $L_{.25}$, L_5 and $L_{.75}$ are the throws to 0.25, 0.5 and 0.75 m/s (50, 100 and 150 fpm). For this application, $L_{.75}$ is of most interest because the velocity 0.75 m (150 fpm) is more likely to adversely affect detector performance than the lower velocities. Thus in selection of the idealized slot diffuser for this project, particular emphasis was places on $L_{.75}$.

In the diffuser industry, it is generally accepted that $L_{.75}$ is nearly the same for isothermal jets, cooling jets and heating jets [13]. Figure C10 demonstrates the this industry rule for a few CFD simulations. The level of agreement among the throws of this figure provides added confidence in the industry rule. The simulations of this study (runs 3-31) were made for isothermal jets. For the reasons above, it can be concluded that the results of these simulations can be applied to both cooling and heating jets.

Throw recommendations for various applications are provided by ASHRAE [14] and Straub [15]. Based on ASHRAE recommendations, an L_5 of 1.5 m (5 ft) would be used to achieve a high level of comfort in the enclosed rooms of this study. However, HVAC designers have indicated that the ASHRAE recommendations concerning throws for ceiling mounted slot diffusers have often been exceeded in practice. For the enclosed rooms of this study, Straub's suggestions amount to selecting a diffuser with an $L_{.25}$ of 7 to 15 m (23 to 50 ft). This can result in an L_5 much greater than the ASHRAE recommendations. For this study an $L_{.75}$ of 1.5 m (4.9 ft) was selected as a value which might be considered an upper limit for such an application.

It was desired to have a slot length, L, of 1.18 m (3.9 ft), for all the simulations because this length is common in the industry. For a perimeter office, supply air is usually in the range of 0.01 to 0.015 m³/s per m² of floor area (2 to 3 cfm per ft² of floor area). The value of 0.0125 m³/s per m² of floor area (2.5 cfm per ft² of floor area) was selected. For the slot diffuser in small room of this project this amounted to supply air 0.106 m³/s (225 cfm). This slot was also used for the medium and the open plan rooms at the same flow rate per unit of floor area.

In summary, the desired values for the slot diffuser were:

Throw to 0.75 m/s	$L_{.75}$	1.5 m (5 ft)
Slot Length	L	1.18 m (3.9 ft)
Volumetric Flow	G	0.106 m³/s (225 cfm)

The CFD model was used to find the other values of the supply slot as described below. It is the nature of a CFD model that geometry and boundary conditions are specified, and the model calculates the flows at each cell. For the small room of this project, simulations were made with values of L, h, V_x and V_z specified, and the output was examined to determine L_5 and $L_{.75}$ resulting from the specified values. Slot widths, h, were considered from 0.06 to 0.10 m (2.36 to 3.94 in). For each slot width, V_z was calculated as $V_z = G/(Lh)$, and simulations were made for values of V_x representing discharge angles, θ, from 30° to 45° using equation (2).

A number of CFD simulations were required to determine that values of $\theta = 39°$ and $h = 0.08$ m (3.1 in) resulted in the desired $L_{.75}$. These simulations were in the small room with return arrangement 1. Table C3 compares the throw from this idealized slot diffuser with two commercial diffusers all with the same values of L and G. The differences between the throws of the commercial and idealized diffusers is -7% and 6% for L_5 and -27% and -5% for $L_{.75}$. This level of agreement indicates that the throws of the idealized diffuser can be considered in the range of throws that could occur from commercial slot diffusers.

Lack of data for slot diffusers prevented detailed comparison of the CFD simulated jet with experimental data. However, the general trends of the CFD simulated jet from the above slot diffuser agrees with observed trends of jets from other types of diffusers based on experimental data. The experimental data shown in figure C11(a) and (b) shows that for HVAC jets adjacent to surfaces (walls or ceilings) [16]:

    (a)   the maximum velocity, V_{max}, decreases with distance, x, from the diffuser,
    (b)   at any distance, x, from the diffuser, the maximum velocity, V_{max}, is near the surface, and
    (c)   the thickness of the jet [dashed lines in figure C11(a) and (b)] increases with distance, x, from the diffuser.

The CFD simulated jet from the idealized slot diffuser of this project shows that same trends, as shown in figure C11(c).

The light troffers were modeled in the same way as the slot diffuser. The troffers were also 1.18 m (3.9 ft) long, and they had a flow rate of 0.0236 m^3/s (50 cfm). A value of 0.4 m (1.3 ft) was selected as a conservative value of the 0.75 m/s (150 fpm) throw for this troffer. In the same manner as the slot diffusers, a number of CFD simulations were made to find that values of $\theta = 21°$ and $h = 0.03$ m (1.1 in) resulted in the desired throw. Comparison with the throws of a commercial troffer shows much larger differences than those of the slot diffusers (table C3). The difficulty in getting better agreement could be a basic limitation of the idealized diffuser model presented in this appendix. However, the idealized troffer jet is a longer jet than that of the commercial troffer. Considering that flow of the troffers was 22% of that from the slot diffusers, it seems that the main detection challenge was due to the slots, and that the troffers were included in the simulations to account for the relatively small level detection interference they would produce. Further, it should be noted that the trends of jet flows attached to surfaces discussed above also occurred for the idealized troffer jet.

An additional goal not mentioned above was that the background noise produced by airflow through the slot diffusers and light troffers should not exceed the guidelines listed in table C1 for office building rooms (25-35 RC). The manufacturer's noise data for one of the commercial slot B was 25 NC and for the commercial troffer was 14 NC. As discussed in the ASHRAE Handbook of Fundamentals, NC is noise criterion that differs in some respects from the RC ratings. However, it should be possible that a system could be built with these diffusers and troffers that meets the above goal.

High Sidewall Diffusers

The high sidewall had a flow of 0.318 m^3/s (674 cfm) and diffuser area at 0.155 m^2 (1.67 ft^2), resulting in a normal velocity component of 2.05 m/s (410 fpm). From table C3, a the typical design room criterion for a supply air outlet with this velocity is about 28 RC. This is within the range of guideline values recommended by ASHRAE (table C1) for most office building rooms.

The normal velocity component of high sidewall diffusers was 2.05 m/s (410 fpm) and additional velocity components of 1.18 m/s (236 fpm) to the side and 0.746 m/s (149 fpm) upward for runs 53 and 54; 0.70 m/s (140 fpm) upward for runs 55 and 56. The slot diffusers are discussed later. The high sidewall outlet and the group E outlets over the computers are located at the plane of symmetry. Therefore, they have half of the volumetric flow rate listed above flowing into the simulated space.

The supply velocities for the high sidewall diffusers were selected based on noise considerations, realizing that this might result in conservatively high velocities from comfort considerations. The resulting throws were $L_{75} = 2.9$ m (9.5 ft) for the diagonal supply discharge and $L_{75} = 4.3$ m (14 ft) for the discharge straight across the room. These throws indicate that the supply velocities were high from a comfort stand point for many applications, and any further studies that include high sidewall diffusers should address comfort considerations for the specific application that the rooms are intended.

Rectangular Group E Outlets

The group E outlets in the computer room simulations (runs 57, 58 and 59) were at 1 m/s (200 fpm) flowing directly downward for flows of 0.27 m^3/s (572 cfm) above each computer and of 0.045 m^3/s (95 cfm) for each of the smaller outlets.

References

[1]   ASHRAE, Chapter 31: *Space Air Diffusion*, Fundamentals Handbook, American Society of Heating and Air-Conditioning Engineers, Atlanta, GA, 1993.

[2]   Straub, H.E., Gilman, S.F., Konzo, S. Distribution of air within a room for year-round air conditioning - Part I. University of Illinois Engineering Experiment Station Bulletin No. 435.

[3]   Straub, H. Engineering Data: Grills, Registers, Diffusers, Terminals, Catalog T49, TITUS, Richardson TX, 1994.

[4]   ASHRAE, Chapter 43: *Sound and Vibration Control*, Applications Handbook, American Society of Heating and Air-Conditioning Engineers, Atlanta, GA, 1995.

[5]   ASHRAE, Chapter 7: *Sound and Vibration*, Fundamentals Handbook, American Society of Heating and Air-Conditioning Engineers, Atlanta, GA, 1993.

[6]   Horace, H. and Nakamura, Y. Room Airflow Analysis by Means of Differential Stress Model, International Symposium on Room Air Convection and Ventilation Effectiveness, ASHRAE, Atlanta, GA, pp 153-162, 1992.

[7]   Chow, W.K. and Fung, W.Y., Indoor Aerodynamics and Ventilation Design in Large Enclosed Spaces, International Symposium on Room Air Convection and Ventilation Effectiveness, ASHRAE, Atlanta, GA, pp 87-97, 1992.

[8]   Kato, S., Murakami, S. and Kobayashi, H., New Scales for Evaluating Ventilation Efficiency as Affected by Supply and Exhaust Openings Based on Spatial Distribution of Contaminant, International Symposium on Room Air Convection and Ventilation Effectiveness, ASHRAE, Atlanta, GA, pp 177-186, 1992.

[9]   Matsumoto, M., Hokol, S. and Hanibuchi, H., A Study of the Differential Reynolds Stress Model for Application to Airflow in a Room, International Symposium on Room Air Convection and Ventilation Effectiveness, ASHRAE, Atlanta, GA, pp 163-170, 1992.

[10]   Nielsen, P.V., Stratified Flow in a Room With Displacement Ventilation and Wall-Mounted Air Terminal Devices, ASHRAE Transactions, Vol 100, Part 1, 1994.

[11]   Skovgaard, M. and Nielsen, P.V., Modelling Complex Inlet Geometries in CFD - Applied to Air Flow in Ventilated Rooms, IET Paper No. 21, Aalborg Univ., Aalborg Denmark, 1991.

[12]   Oakes, W.C., Experimental investigation of a Coanda jet, MS Thesis, Michigan State Univ, 1987.

[13]   Straub, H. Telephone Conversation with John Klote, TITUS, Richardson TX, 1995.

[14]   ASHRAE, Chapter 31: *Space Air Diffusion*, Fundamentals Handbook, American Society of Heating and Air-Conditioning Engineers, Atlanta, GA, 1993.

[15]   Straub, H. *Engineering Data: Grills, Registers, Diffusers, Terminals*, Catalog T49, TITUS, Richardson TX, 1994.

[16]   Tuve, G.L. Air Velocities in Ventilating Jets, ASHVE (predecessor society to ASHRAE) Transactions, Vol 59, 1953, pp 261-282.

Table C1.　　　　Design Guidelines for HVAC System Noise[a]

Space	RC(N) Level[b,c]	Space	RC(N) Level[b,c]
Private residences	25-35	Performing arts spaces	
Hotels/Motels		Drama theaters	25 (max) [d]
Individual rooms or suits	25-35	Concert and recital halls	
Meeting/banquet rooms	25-35	Music teaching studios	25 (max)
Halls, corridors, lobbies	35-45	Music practice rooms	35 (max)
Service support areas	35-45	Laboratories (with fume hoods)	
Office buildings		Testing/research, minimum speech	45-55
Executive and private offices	25-35	Research, extensive speech	40-50
Conference rooms	25-35	Group teaching	35-45
Teleconference rooms	25-35	Churches, mosques, synagogues	25-35 [d]
Open plan offices	25 (max)	With critical music programs	
Circulation and public lobbies	30-40	Schools	
Hospitals and clinics		Classrooms up to 70 m^2 (750 ft^2)	40 (max)
Private rooms	25-35	Classrooms over 70 m^2 (750 ft^2)	35 (max)
Wards	30-40	Lecture rooms for more than 50	35 (max)
Operating rooms	25-35	Libraries	30-40
Corridors	30-40	Indoor stadiums and gymnasiums	
Public areas	30-40	School and collage gymnasiums and auditoriums	40-50[e]
Courtrooms		Large seating capacity spaces (with amplified speech)	45-55[e]
Unamplified speech	25-35		
Amplified speech	30-40		

[a]This table was adapted from table 2, chapter 43 of the 1995 ASHRAE Application Handbook.
[b]The values and ranges are based on judgement and experience, not on quantitative evaluations of human reactions. They represent general limits of acceptability for typical building occupancies.
[c]When the quality of sound in a space is important, criteria should be specified in terms of RC(N). If the quality of sound in a space is of secondary concern, criteria should be specified in terms of RC.
[d]An experienced acoustical consultant should be retained for guidance on these acoustically critical spaces.
[e]Spectrum levels and sound are of lesser importance in these spaces than overall sound levels.

Table C2.   Maximum Recommended "Free" Supply Outlet and Return Air Opening Velocities Needed to Achieve Specified Acoustic Design Criteria

Type of Opening	Design RC(N)	"Free" Opening Airflow Velocity	
		m/s	fpm
Supply Air Outlet	45	3.2	625
	40	2.8	560
	35	2.5	500
	30	2.2	425
	25	1.8	350
Return Air Opening	45	3.8	750
	40	3.4	675
	35	3.0	600
	30	2.5	500
	25	2.2	425

Notes:
1. This table was adapted from table 7, chapter 43 of the 1995 ASHRAE Application Handbook.
2. The presence of diffusers or grills can increase sound levels a little or a lot, depending on how many diffusers or grills and on their design, construction, installation, etc. Thus, allowable outlet or opening velocities should be reduced accordingly.

Table C3.   Comparison of throws for commercial and idealized slot and troffer diffusers

Diffuser Type[*]	Throw to 0.75 m/s (150 fpm), $L_{.75}$			Throw to 0.5 m/s (100 fpm), $L_{.5}$		
	m	ft	Difference[‡]	m	ft	Difference[‡]
Commercial Slot A	1.4	4.6	-7%	2.9	9.5	-27%
Commercial Slot B	1.6	5.2	6%	3.5	11.5	-5%
Idealized Slot	1.5	4.9	NA	3.7	12.1	NA
Commercial Troffer	0.6	2.0	33%	0.9	3.0	-55%
Idealized Troffer	0.4	1.3	NA	1.4	4.6	NA

[*]Throw data for the commercial diffusers is from manufacturers catalogs and from CFD simulations for the idealized diffusers.
[‡]The difference is the throw of idealized from that of the commercial damper, which is
$(L_{vc} - L_{vi})/L_{vc}$ where subscripts c, I and v represent commercial, idealized and velocity respectively.

Table C3. Comparison of throws for commercial and idealized diffusers

Diffuser Type[*]	Throw to 0.75 m/s (150 fpm), $L_{.75}$			Throw to 0.5 m/s (100 fpm), $L_{.5}$		
	m	ft	Difference[‡]	m	ft	Difference[‡]
Commercial Slot A	1.4	4.6	-7%	2.9	9.5	-27%
Commercial Slot B	1.6	5.2	6%	3.5	11.5	-5%
Idealized Slot	1.5	4.9	NA	3.7	12.1	NA
Commercial Troffer	0.6	2.0	33%	0.9	3.0	-55%
Idealized Troffer	0.4	1.3	NA	1.4	4.6	NA

[*]Throw data for the commercial diffusers is from manufacturers catalogs and from CFD simulations for the idealized diffusers.
[‡]The difference is the throw of idealized from that of the commercial damper, which is
$(L_{vc} - L_{vi})/L_{vc}$ where subscripts c, I and v represent commercial, idealized and velocity respectively.